Geological Magazine

www.cambridge.org/geo

Provenance of the early Palaeozoic volcano-sedimentary successions from eastern part of the Central Sudetes: implications for the tectonic evolution of the NE Bohemian Massif

Jacek Szczepański[1], Gabriela Kaszuba[1,2], Robert Anczkiewicz[2] and Sławomir Ilnicki[3]

[1]Faculty of Earth Science and Environmental Management, Institute of Geological Sciences, University of Wrocław, Wrocław, Poland; [2]Polish Academy of Sciences, Research Centre in Cracow, Institute of Geological Sciences, Kraków, Poland and [3]Department of Geochemistry, Mineralogy and Petrology, Faculty of Geology, University of Warsaw, Warsaw, Poland

Original Article

Cite this article: Szczepański J, Kaszuba G, Anczkiewicz R, and Ilnicki S (2023) Provenance of the early Palaeozoic volcano-sedimentary successions from eastern part of the Central Sudetes: implications for the tectonic evolution of the NE Bohemian Massif. *Geological Magazine* **160**: 1498–1534. https://doi.org/10.1017/S0016756823000523

Received: 15 February 2022
Revised: 14 August 2023
Accepted: 20 August 2023
First published online: 2 October 2023

Keywords:
Detrital zircon; Laser ablation ICP-MS; provenance; Gondwana-derived terranes; Fore-Sudetic Block; Bohemian Massif; Variscan metamorphism

Corresponding author:
Jacek Szczepański;
Email: jacek.szczepanski@uwr.edu.pl

Abstract

The Kamieniec Metamorphic Belt (KMB) and the Doboszowice Metamorphic Complex (DMC) expose a fragment of the pre-Variscan volcano-sedimentary cover preserved in the Fore-Sudetic Block in the NE part of the Bohemian Massif. We present the age of detrital and magmatic zircon grains and the bulk rock chemical composition of rock samples from the KMB and the DMC to better understand the evolution of the early Palaeozoic Gondwana margin. The zircon age spectra were acquired by U–Pb LA–ICP–MS dating and represent two groups that differ by maximum depositional age (MDA). The paragneiss from the DMC displays the MDA at 456 Ma, whereas the mica shist from the KMB displays the MDA at 529 Ma. Older age peaks in both groups of samples are represented by the Neoproterozoic and less frequent the Paleoproterozoic and Archean. The data presented indicate that the rock successions were sourced from the Cadomian orogen and deposited in the basins that developed on the Gondwana margin. Our results support the suggestion that the crystalline basement in the eastern part of the Fore-Sudetic Block has an affinity to the Trans-Saharan Belt or West African Craton and was part of a Gondwana shelf. The final stage of evolution of the studied successions was related to the Variscan thermal overprint. Based on presented data, we support the idea that the suture separating the Brunovistulian domain from the rest of the Gondwana-derived terranes is not related to the closure of the Rheic Ocean and represents a local feature.

1. Introduction

Several crustal fragments of the Bohemian Massif comprise Neoproterozoic-Early Ordovician volcano-sedimentary successions formed at the northern Gondwana margin. In the Neoproterozoic and early Cambrian, northern part of Gondwana was a long volcano-magmatic arc formed in response to subduction of oceanic domains identified in the literature as the Iapetus and Tornquist Oceans (e.g. Linnemann *et al.* 2007; Nance *et al.* 2012; Domeier, 2016; Boris, Domeier & Jakob, 2021; Oriolo *et al.* 2021) or the Paleo-Pacific Ocean (Merdith *et al.* 2021). During the late Cambrian and Early Ordovician, the arc was split into two parts called Avalonia and Cadomia, and separated by the newly opened Rheic Ocean (e.g. Linnemann *et al.* 2004; Linnemann *et al.* 2008; Nance & Linnemann, 2008; Oriolo *et al.* 2021). This resulted in the late Cambrian-Early Ordovician times in transformation of the Gondwana active margin into a passive margin, although the mechanism responsible for this transformation is still debated (e.g. Winchester *et al.* 2006; Linnemann *et al.* 2008; Sláma *et al.* 2008b; Nance *et al.* 2010; Díez Fernández *et al.* 2012; Hajná *et al.* 2018). Subsequently, during the closure of the Rheic Ocean, remnants of the Neoproterozoic basement were trapped between the colliding continents of Gondwana and Laurussia and recycled in the Variscan belt of Europe. Subsequently, remnants of the Avalonian and Cadomian basement were dispersed throughout the Variscan belt of Europe and juxtaposed along the Rheic suture (Fig. 1). The suture is relatively well documented in the western and central sectors of the Variscan belt of Europe (e.g. Linnemann *et al.* 2007; Pérez-Cáceres *et al.* 2015; Kirchner & Albert, 2020). However, in its eastern part, that is, in the Sudetes, the location of the suture is still poorly recognized. Some authors discussed the presence of the Rheic suture between the Central and East Sudetes (e.g. Mazur *et al.* 2012; Jastrzębski *et al.* 2013; Jastrzębski *et al.* 2015; Oberc-Dziedzic *et al.* 2018; Jastrzębski *et al.* 2020; Śliwiński *et al.* 2022), while others questioned its existence in this fragment of the Variscan belt of Europe (Soejono *et al.* 2010; Collett *et al.* 2021, 2022). Unfortunately, this fragment of the Variscan orogen is partly located on the Fore-Sudetic Block, where the metamorphic basement is mostly

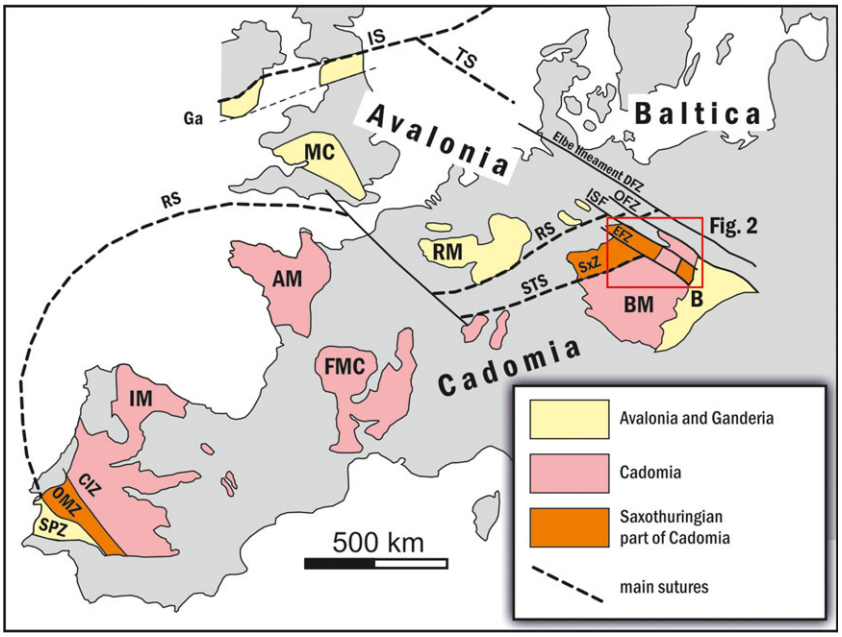

Figure 1. (Colour online) Peri-Gondwanan terranes of Southern and Central Europe (modified from Franke, 1989; Linnemann *et al.* 2007; Nance *et al.* 2008). AM – Armorican Massif, IM – Iberian Massif, FMC – French Massif Central, BM – Bohemian Massif, RM – Rhenish Massif, MC – Midland Craton, B – Brunovistulicum, Ga- Ganderia, SPZ – South Portuguese Zone, OMZ – Ossa-Morena Zone, CIZ- Central Iberian Zone, SxZ – Saxothuringian Zone, EFZ – Elbe Fault Zone, ISF – Intra Sudetic Fault, DFZ – Dolsk Fault Zone, OFZ – Odra Fault Zone, IS – Iapetus Suture, RS – Rheic Suture STS – Saxothuringian Suture, TS – Thor Suture.

covered by Cenozoic sediments. Therefore, unravelling the location of the suture in this portion of the Sudetes and the nature of the exposed basement is disputable, and every new piece of evidence becomes important.

In this paper, we present new LA–ICP–MS U–Pb data on zircons and bulk chemical composition of the volcano-sedimentary successions from the Kamieniec Metamorphic Belt (KMB) and the Doboszowice Metamorphic Complex (DMC) exposed in the eastern part of the Fore-Sudetic Block (Fig. 2). The data are used to describe the provenance of the detrital material, the time of deposition and the tectonic setting of the formation of the volcano-sedimentary successions in the eastern part of the Fore-Sudetic Block. This allows us to propose a new model for the development of the Cambro-Ordovician rocks cropping out in the eastern part of the Fore-Sudetic Block from the early Palaeozoic to the Carboniferous. The model is generally consistent with those proposed for other Late Neoproterozoic and Cambro-Ordovician sequences exposed in the Bohemian Massif (Jastrzębski *et al.* 2017; Hajná *et al.* 2018; Collett *et al.* 2020; Soejono *et al.* 2020; Collett *et al.* 2022; Soejono *et al.* 2022). Our data combined with already published results shed new light on the development of the passive Gondwana margin and the nature of the tectonic suture separating the Central and East Sudetes. Furthermore, the presented data provide important time limitations on the Variscan tectonothermal event responsible for recycling of the Cadomian crust.

2. Geological setting

The KMB and the DMC are fragments of the crystalline basement, emerging from below the younger Cenozoic cover of the Fore-Sudetic Block (Fig. 2). The KMB forms c. 25 km long and 5 km wide longitudinal belt between the Góry Sowie Massif and the Niemcza Shear Zone in the west and the Strzelin Crystalline Massif (including the Lipowe Hills) in the east (Fig. 2). A volcano-sedimentary succession exposed in the KMB is dominated by mica schists intercalated with scarce paragneisses, marbles, quartz-graphite schists, eclogites, and felsic volcanics (Fig. 3). The latter are interpreted as tuffs or lava flows (Dziedzicowa, 1966). On the contrary, the DMC is a c. 6 km long exposure of crystalline basement located south-east of the KMB and directly west of the Niedźwiedź Amphibolite Massif (NAM, Fig. 2). The DMC may be divided into a western and an eastern parts. The western part exposes the Doboszowice orthogneiss with protolith age dated on zircons using U–Pb SHRIMP at 488 ± 6 Ma (Mazur *et al.* 2010) or at 494 ± 5 Ma using U–Pb ICP–MS (Jastrzębski *et al.* 2023). The eastern part is mainly composed of the migmatic Chałupki paragneiss interleaved with scarce mica schists and metabasalts of unknown age (Fig. 3). The protolith age of the volcano-sedimentary successions exposed in the KMB and DMC is poorly known. Available data suggest that the maximum depositional age (MDA) of the KMB and the adjacent Lipowe Hills mica schists is in the range of c. 560–570 Ma (Oberc-Dziedzic *et al.* 2018; Jastrzębski *et al.* 2020), while the Chałupki paragneiss from the DMC has a late Cambrian MDA (Jastrzębski *et al.* 2023).

The volcano-sedimentary successions comprised in the KMB and DMC suffered a Variscan metamorphism. According to several authors, it was related to continental collision between two Gondwana-derived crustal domains represented by the Saxothuringian and Brunovistulian (e.g. Schulmann *et al.* 2009; Chopin *et al.* 2012; Jastrzębski *et al.* 2020; Szczepański *et al.* 2022; Szczepański & Goleń, 2022). However, the metamorphic records preserved in the KMB and DMC are strikingly different. The mica schists of the KMB underwent HP-LT metamorphism at c. 490°C and 18 kbar which was overprinted by LP-HT episode at c. 530–580°C and 3–7 kbar (Szczepański *et al.* 2022; Szczepański & Goleń, 2022). On the other hand, the migmatized Chałupki paragneiss bears record of HT metamorphism at max. 670°C and 8 kbar (Puziewicz *et al.* 1999; Szczepański & Marciniak, 2018). The age of the tectonothermal event recorded in the KMB has recently been estimated at c. 330 Ma (Jastrzębski *et al.* 2020) and in the DMC at c. 346–341 Ma based on ICP–MS U–Th–Pb dating of monazite (Jastrzębski *et al.* 2023). This is in agreement with Lu-–Hf and Sm–Nd garnet dating of the Chałupki paragneiss, which shows that these rocks were metamorphosed between 347 ± 3.6 Ma and 337.3 ± 6.6 Ma (Szczepanski *et al.* 2022).

https://doi.org/10.1017/S0016756823000523 Published online by Cambridge University Press

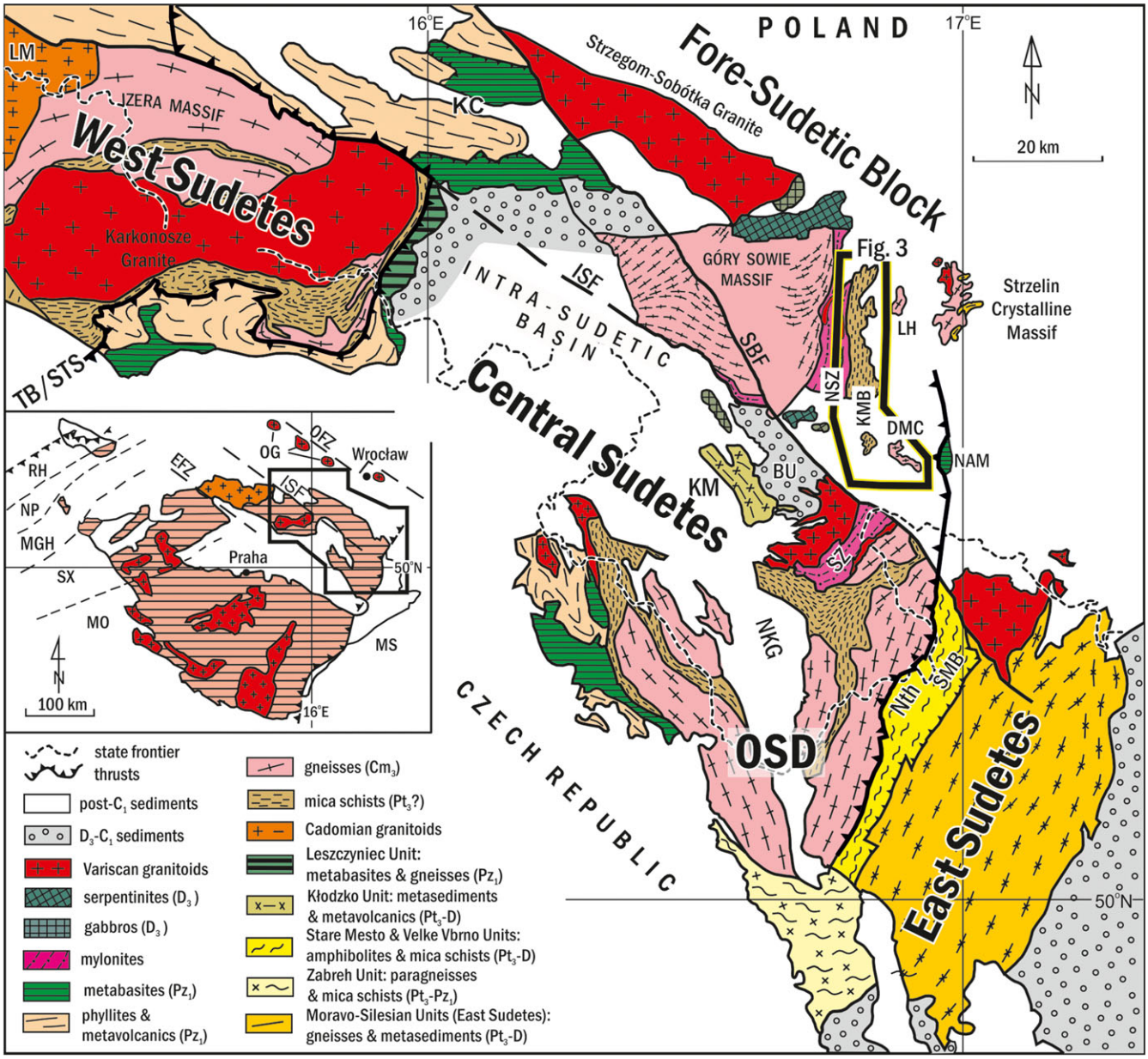

Figure 2. (Colour online) Geological sketch map of the Sudetes after Mazur *et al.* (2006). Abbreviations: BU – Bardo Sedimentary unit; OSD – Orlica-Śnieżnik Dome, ISF – Intra-Sudetic fault; KM – Kłodzko massif; KMB – Kamieniec Metamorphic Belt; DMC – Doboszowice Metamorphic Complex; LM – Lusatian massif; NKG – Nysa Kłodzka Graben, NAM – Niedźwiedź amphibolite massif; LH – Lipowe Hills Massif; SBF – Sudetic boundary fault; SMB – Staré Město Belt; TB/STS – Teplá-Barrandian/Saxothuringian suture; Nth – Nyznerov thrust. Abbreviations inset: EFZ – Elbe Fault Zone, MGH – Mid-German Crystalline High; MO – Moldanubian zone; MS – Moravo-Silesian zone; NP – Northern Phyllite zone; OG – Odra granitoids, OFZ – Odra Fault Zone, RH – Rhenohercynian zone; SX – Saxothuringian zone. Age assignments: Pt – Proterozoic; Pz – Palaeozoic; Cm – Cambrian; Or – Ordovician; D – Devonian; C – Carboniferous; 1 – Early; 2 – Middle.

3. Analytical methods

Bulk rock chemical analyses of 53 mica schists, 10 paragneisses and 17 quartz-feldspathic rocks (interpreted as metarhyolites, see below) were performed at Acme Analytical Laboratories Ltd. (Vancouver, Canada) and are summarized in Supplementary Table 1. The location of all the samples used in this study is shown in Fig. 3. The location and a brief petrological description of the geochronological samples from the studied units are given in Table 1. Major and trace element abundances were determined using ICP-MS following lithium metaborate fusion and nitric acid digestion of 0.2 g of representative whole-rock powder. Loss on ignition (LOI) was measured by weight difference after ignition at 1000°C. The detection limits are within 0.01% for major elements, between 0.05 and 0.5 ppm for most trace elements. The detection limits for all analysed elements are given in Supplementary Table 1. Geochemical diagrams were designed using the R software environment (R Core Team, 2021).

Mineral separation was carried out at the Kraków Research Centre, Institute of Geological Sciences, Polish Academy of Sciences following conventional techniques involving crushing, sieving, heavy liquids and Frantz magnetic separator. Zircon grains were hand-picked under a binocular so that representative population was achieved. Cathodoluminescent images of zircons were obtained using a JEOL electron microscope (15 kV and 1 nA)

https://doi.org/10.1017/S0016756823000523 Published online by Cambridge University Press

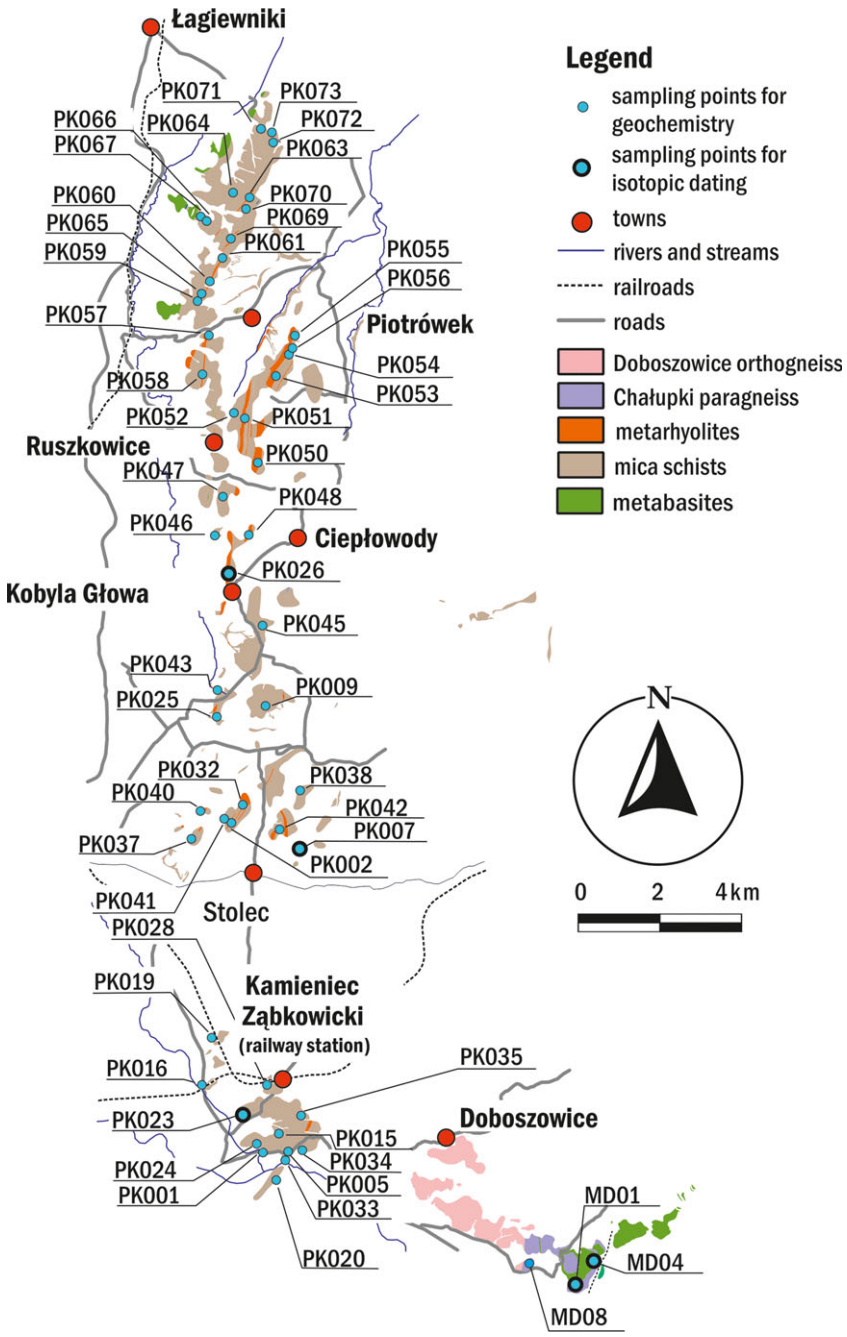

Figure 3. (Colour online) Geological sketch map of the Kamieniec Metamorphic Belt and the Doboszowice Metamorphic Complex.

at the Institute of Geological Sciences, University of Wroclaw, Poland.

In situ U-Pb detrital zircon dating of five samples by laser ablation inductively coupled plasma mass spectrometry (LA ICP-MS) was conducted at the Kraków Research Centre, Institute of Geological Sciences, Polish Academy of Sciences. The analyses were carried out using an excimer laser (ArF) RESOlution by Resonetics (now Applied Spectra) equipped with S155 dual-volume, large format sample cell. Laser ablation was coupled with ICP-MS XseriesII by ThermoFisher Scientific. Ablation took place in He which was mixed downstream with Ar and small amount of nitrogen to enhance sensitivity of ICP-MS. Before reaching the plasma, the carrier gas passes through a signal smoothing manifold. We applied a 32 μm diameter laser spot of about 3 J/cm^2 energy fired with 5 Hz frequency (analytical parameters are summarized in Supplementary Table 2). The main ablation is preceded by two surface cleaning shots and gas blank measurement. Zircon Z91500 (Wiedenbeck *et al.* 1995) was used as a primary standard, and zircons GJ-1 (Jackson *et al.* 2004) and/or Plešovice (Sláma *et al.* 2008a) were frequently measured for quality control. Typically, two primary standards were measured every six or seven unknowns (Supplementary Table 3). For each analytical session, the secondary standards yielded Concordia ages accurate within ≤ 1% precision (two relative standard deviations).

The data were reduced using Iolite 3 software (Paton *et al.* 2011). The data treatment along with the error propagation method are presented in Paton *et al.* (2010). No common Pb correction was applied. All analyses are presented on the Concordia plots using Isoplot/Ex 4.15 (Ludwig, 2008), whereas the KDE diagrams contain only zircons with ≤ 10% discordance

https://doi.org/10.1017/S0016756823000523 Published online by Cambridge University Press

Table 1. Location and brief petrological description of geochronological samples from the studied area. The abbreviations of mineral names are after Whitney and Evans (2010)

Sample	rock type	Longitude (E)	Latitude (N)	Mineral composition
Kamieniec Metamorphic Belt				
PK007	Mica schist	16.90066	50.59137	Qz, Ms, Bt, Pl, Grt, Chl, Cld, Pg, Rt, Ilm
PK023	Mica schist	16.87931	50.5275	Qz, Wm, Bt, Pl, St, Chl, And, Rt, Ilm, Mrg, Pg, Cld, Ep
PK026	Metarhyolite	16.87396	50.65736	Qz, Kfs, Pl, Ms, Bt, Opq
Doboszowice Metamorphic Complex				
MD01	Paragneiss	17.00434	50.48672	Qz, Ms, Bt, Pl, Grt, Chl, Ilm
MD04	Paragneiss	17.01103	50.4936	Qz, Ms, Bt, Pl, Chl, Ilm

(% discordance = $[1 - (^{206}Pb/^{238}U \text{ age})/(^{207}Pb/^{235}U \text{ age})] \times 100\%$). For KDE, we used $^{206}Pb/^{238}U$ ages except for zircons older than 1 Ga, for which we used $^{207}Pb/^{206}Pb$ ages. The diagrams were constructed using the R software environment (R Core Team, 2021). The MDA of the sedimentary protolith was defined according to Dickinson and Gehrels (2009) using the youngest graphical detrital zircon age peak on an age probability plot and the mean age of the youngest two or more grains that overlap in age at 1σ. In our interpretation of MDA, we ignored single-grain age peaks. All mineral abbreviations are after Whitney and Evans (2010).

3.a. Petrography of geochronological samples

Two mica schist samples (PK007and PK023) and quartz-feldspathic schist (metarhyolite PK026) from the KMB, and two samples of migmatitic paragneiss from the DMC (MD01-32 and MD04-01) were subjected to LA ICP-MS U-Pb zircon dating (Fig. 4, Tables 2–6). Petrography, mineral assemblages and the P-T history of mica schists from the KMB were described in detail by Szczepański *et al.* (2022) and Szczepański and Goleń (2022). In this study, we used the same set of samples, and therefore here only a brief description of the mica schist from the KMB used for the geochronological study is given. The mica schist PK007 (Fig. 4a) is a fine-grained rock that contains two mineral assemblages. The M1 assemblage consists of the first generation of garnet – Grt1 forming the cores of the garnet grains and Cld + Ph + Pg + Chl + Rt + Qz forming inclusions predominantly in Grt1. Quartz, phengitic white mica, chlorite and rutile are also present in the rock matrix of the examined sample. The M2 assemblage is represented by the second garnet generation – Grt2, which defines narrow rims growing on the first garnet generation (Grt1) and Ms + Bt + Pl + Chl + Ilm + Qz. The mineral assemblage M2 is observed as inclusions in the Grt2 as well as in the rock matrix. Sample PK023 (Fig. 4b) is a medium- to coarse-grained mica schist that contains two mineral assemblages. The M1 assemblage represented by Cld + Ph + Pg + Ep + Chl + Rt + Qz is mostly observed as inclusions in garnet porpyroblasts. The M2 assemblage represented by Ms + Bt + Mrg + Pl + St + Ilm + And + Qz is partly observed as inclusions in garnet grains and also occurs in the rock matrix.

Quartz-feldspathic (metarhyolite) PK026 sample (Fig. 4c) is a fine-grained rock containing a mineral assemblage composed of Qz + Kfs + Ms + Bt + Opq. The sample contains K-feldspar porphyroblasts reaching up to 2 mm in diameter that are dispersed in a very fine-grained matrix consisting mainly of a mixture of recrystallized K-feldspar, quartz and rare white mica flakes. Due to this petrographic and mineral evidence coupled with geochemical features (see section 3.c.), we identify sample PK026 (together with the whole group of quartz-feldspathic rocks) as a metarhyolite.

A detailed description of the paragneisses from the DMC has already been published (Puziewicz *et al.* 1999), and therefore only a brief petrographic description of the analysed samples is presented here. Sample MD01-32 (Fig. 4d) is a medium-grained garnet-bearing paragneiss containing two mineral assemblages. The M1 assemblage consists of rare high Si white mica grains (Ms1) together with rutile needles, and the M2 assemblage consists of Grt and low Si white mica (Ms2) accompanied by Pl + Bt + Ilm. Sample MD04-01 (Fig. 4e) is a medium-grained paragneiss that contains one mineral assemblage comprising low Si white mica (Ms2) and Pl + Bt + Rt + Ilm. Both paragneiss samples show elongated quartz-feldspathic patches of variable size (up to 2–3 cm in length) that are aligned parallel to the penetrative foliation (Fig. 4d, e).

3.b. Whole-rock geochemistry of metasedimentary rocks

Fifty-three mica schist samples and ten paragneiss samples from the KMB and the DMC were analysed for major and trace element composition (Fig. 3, Supplementary Table 1). The two rock suites differ in the chemical composition of the major elements. This is expressed by a higher average SiO_2 value (72.5 wt%) in the analysed paragneisses compared to mica schists (64.4 wt%). On the contrary, the mica schists have a higher Al_2O_3 content (17.15 wt %) compared to the paragneisses (14.25 wt%). Similarly, the average sum of MgO and FeO (7.8 in the mica schists and 4.0 in the paragneisses) and the average sum of Na_2O, K_2O and CaO (4.3 in the mica schists and 1.7 in the paragneisses) are different.

Major element data can be used to distinguish carbonates and soils from more clastic sediments and to classify greywacke along with arkose and quartz-rich sandstones using binary plots. A ternary plot utilizing SiO_2, Al_2O_3+Fe_2O_3 and CaO+MgO (Hasterok *et al.* 2018) shows that all the samples fall into the pelite field close to the psammite field (Fig. 5a). On the classification diagram of Wimmenauer (1984), the studied samples show a rather limited range of SiO_2/Al_2O_3 ratio and are scattered between the greywacke and pelite fields, while a minority of samples show a composition typical of pelitic greywacke and arkoses (Fig. 5b). The diagram proposed by Herron (1988) shows that in terms of chemical composition the analysed rocks resemble mostly shales and wackes, while minority of samples are chemically similar to arkoses (Fig. 5c). On the other hand, the diagram proposed by Pettijohn *et al.* (1987) shows that inspected rocks are scattered in the fields of greywacke, litharenite and arkose (Fig. 5d). In terms of trace element abundances when normalized to the

https://doi.org/10.1017/S0016756823000523 Published online by Cambridge University Press

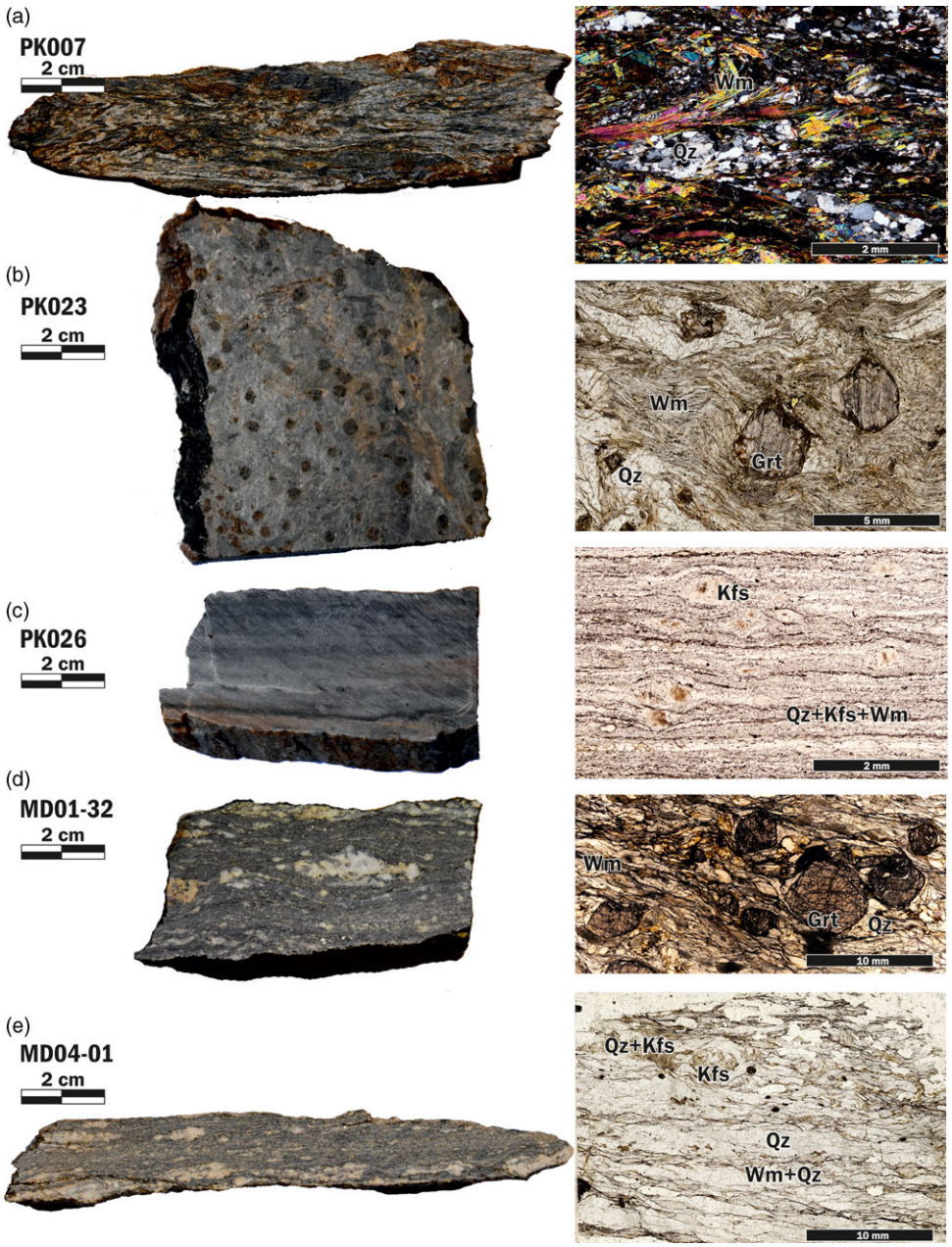

Figure 4. (Colour online) Macro- and micro-photographs of representative lithologies from the Kamieniec Metamorphic Belt and the Doboszowice Metamorphic Complex: (a) fine-grained mica schist sPK007, (b) coarse-grained mica schist PK023, (c) fine-grained metarhyolite PK026, (c) medium-grained migmatic Chałupki paragneiss MD01 and (d) medium-grained migmatic Chałupki paragneiss MD04.

composition of the upper continental crust, the studied mica schist and paragneiss samples show quite consistent patterns (Fig. 5e, f). All samples studied display strong Sr-negative anomaly and, in the case of the mica schists, variously developed U-negative and Nb-positive anomalies. In addition, the paragneiss samples show variously developed Zr and Hf negative anomalies and variously developed Sc negative anomalies. The DMC paragneisses also exhibit variable Cs content.

3.c. Whole-rock geochemistry of metarhyolites from the KMB

Metarhyolites were analysed for major and trace element composition (Fig. 3, Supplementary Table 1). They have 73.3–81.8 wt% of SiO_2, 9.8–14.9 wt% of Al_2O_3, 0.39–2.73 wt% of $Fe_2O_3^{tot}$, 0.08–1.53 wt% of MgO and 5.11–9.89 wt% Na_2O+K_2O.

The total alkali versus SiO_2 plot (TAS diagram, not shown) reveals that these rocks are rhyolites of subalkaline affinity, which is consistent with petrographic evidence (Fig. 4c). Diagrams based on immobile trace element ratios confirm that these rocks have the composition corresponding to that of rhyolites (Fig. 6b), while on the Co versus Th plot (Hastie *et al.* 2007) they fall in the field of high-K calc-alkaline and shoshonitic series but near the borderline with calc-alkaline series (Fig. 6c). The A/CNK (molar $Al_2O_3/(CaO + Na_2O + K_2O)$) and A/NK (molar $Al_2O_3/(Na_2O + K_2O)$) values (both 1.1–2.3) indicate that they are peraluminous (Fig. 6a), whilst in terms of CIPW norms are corundum-normative (1.1–7.6%).

The investigated rocks show negative correlations of SiO_2: well defined with Al_2O_3 and $Fe_2O_3^{tot}$, and less distinct with TiO_2, MgO and CaO (Fig. S01), which may indicate a fractionation and removal of plagioclase, biotite, apatite, and ilmenite. Given the peraluminous composition, it could be conjectured that the negative correlations of Al_2O_3, FeO^{tot} and MgO against SiO_2 imply cordierite-crystallizing magmas.

https://doi.org/10.1017/S0016756823000523 Published online by Cambridge University Press

Table 2. Laser ablation ICP-MS U–Pb isotopic data of detrital zircons from sample PK007

		Isotopic ratios							Ages [Ma]						Approximate	
Sample	^{238}U cps*1000	^{206}Pb/^{238}U	2SE	^{207}Pb/^{235}U	2SE	Rho	^{207}Pb/^{206}Pb	2SE	^{206}Pb/^{238}U	2SE	^{207}Pb/^{235}U	2SE	^{207}Pb/^{206}Pb	2SE	Th/U	Disc.%
PK007_2 – 1	76	0.1014	0.0036	0.846	0.052	0.02	0.0603	0.0034	623	21	615	28	520	120	0.7	1.2
PK007_2 – 2	257	0.0988	0.0035	0.853	0.048	0.27	0.0613	0.0030	607	21	623	27	660	100	1.7	2.5
PK007_2 – 3	974	0.0802	0.003	0.679	0.032	0.56	0.0608	0.0019	497	18	525	20	622	68	0.6	5.3
PK007_2 – 4	112	0.0943	0.0032	1.160	0.063	0.20	0.0894	0.0046	581	19	776	32	1360	110	0.8	25.1
PK007_2 – 5	75	0.0877	0.0031	0.784	0.047	0.07	0.0655	0.0037	542	19	587	28	710	120	0.4	7.7
PK007_2 – 6	78	0.0716	0.0032	1.160	0.067	0.12	0.1170	0.0062	445	19	770	32	1810	110	0.4	42.2
PK007_2 – 7	25	0.1044	0.0042	0.999	0.088	0.04	0.0704	0.0058	640	25	685	47	730	190	2.3	6.6
PK007_2 – 8	170	0.1088	0.0038	0.922	0.045	0.04	0.0617	0.0025	666	22	666	25	639	90	1.9	0.1
PK007_2 – 9	217	0.1027	0.0035	0.827	0.042	0.05	0.0578	0.0024	630	20	608	23	485	90	1.0	3.7
PK007_2 – 10	169	0.1501	0.0051	1.480	0.068	0.07	0.0710	0.0025	901	28	919	28	927	74	0.4	1.9
PK007_2 – 11	72	0.368	0.013	6.520	0.290	0.12	0.1274	0.0042	2020	59	2044	39	2047	59	1.0	1.2
PK007_2 – 12	52	0.1068	0.0042	0.873	0.065	0.37	0.0587	0.0040	654	24	622	36	440	140	1.1	5.1
PK007_2 – 13	97	0.1638	0.0057	1.680	0.110	0.33	0.0741	0.0052	977	32	997	38	1020	110	0.7	2.0
PK007_2 – 14	59	0.0938	0.0034	0.835	0.055	0.18	0.0642	0.0039	578	20	610	32	660	130	0.4	5.3
PK007_2 – 15	429	0.0984	0.0045	0.831	0.055	0.10	0.0615	0.0024	605	26	613	27	630	80	0.0	1.3
PK007_2 – 16	187	0.3716	0.012	7.490	0.290	0.34	0.1455	0.0042	2037	58	2171	38	2289	52	0.3	6.2
PK007_2 – 17	108	0.1028	0.0036	0.880	0.048	0.04	0.0615	0.0029	631	21	638	25	612	100	0.6	1.1
PK007_2 – 18	170	0.0899	0.0032	0.734	0.037	0.25	0.0594	0.0025	555	19	559	23	535	89	0.4	0.8
PK007_2 – 19	139	0.4959	0.016	13.050	0.540	0.33	0.1904	0.0059	2596	72	2682	39	2741	52	0.4	3.2
PK007_2 – 20	360	0.0859	0.0029	0.707	0.033	0.17	0.0590	0.0021	531	17	541	19	543	77	0.5	1.8
PK007_2 – 21	142	0.09539	0.0033	0.785	0.042	0.31	0.0592	0.0025	587	20	584	23	531	92	1.2	0.6
PK007_2 – 22a	136	0.4334	0.018	11.450	0.540	0.59	0.1915	0.0054	2320	88	2559	67	2751	52	0.9	9.3
PK007_2 – 23	89	0.1311	0.0046	1.636	0.086	0.06	0.0905	0.0040	794	27	977	36	1380	92	0.2	18.7
PK007_2 – 24	430	0.09877	0.0039	0.833	0.049	0.11	0.0609	0.0025	607	22	614	25	612	82	0.2	1.1
PK007_2 – 25	156	0.6086	0.021	19.260	0.840	0.45	0.2286	0.0065	3064	85	3054	41	3040	45	0.2	0.3
PK007_2 – 26	63	0.093	0.0033	0.784	0.056	0.19	0.0607	0.0039	573	20	577	32	510	140	0.6	0.7
PK007_2 – 27	272	0.08692	0.003	0.739	0.037	0.07	0.0613	0.0026	537	18	560	22	621	84	0.3	4.1
PK007_2 – 28	59	0.3733	0.012	6.470	0.270	0.22	0.1252	0.0047	2044	59	2034	41	2010	67	0.6	0.5
PK007_2 – 29	68	0.5495	0.019	14.140	0.600	0.20	0.1851	0.0056	2822	78	2756	40	2695	52	0.8	2.4
PK007_2 – 31	186	0.09735	0.0034	0.794	0.039	0.09	0.0590	0.0025	599	20	590	23	520	92	1.3	1.5

(*Continued*)

Table 2. (*Continued*)

PK007_2 – 32	82	0.0969	0.0034	0.794	0.052	0.02	0.0593	0.0035	596	20	586	29	480	120	0.7	1.7
PK007_2 – 33	617	0.08458	0.0028	0.681	0.030	0.10	0.0581	0.0020	523	17	526	18	520	72	0.8	0.5
PK007_2 – 34	684	0.07348	0.0026	0.728	0.034	0.37	0.0715	0.0026	457	15	554	20	956	68	0.5	17.5
PK007_2 – 35	475	0.08674	0.0029	0.731	0.032	0.02	0.0609	0.0023	536	17	556	19	614	77	0.3	3.6
PK007_2 – 36	396	0.0976	0.0033	0.867	0.049	0.08	0.0642	0.0033	601	19	632	27	718	93	0.7	5.0
PK007_2 – 37	303	0.10243	0.004	0.832	0.046	0.13	0.0588	0.0024	629	23	612	24	520	84	0.5	2.7
PK007_2 – 38	94	0.0767	0.0028	0.695	0.046	0.15	0.0653	0.0038	476	17	533	28	700	130	0.5	10.7
PK007_2 – 39	84	0.1446	0.0067	1.316	0.064	0.10	0.0660	0.0035	870	39	848	29	760	95	0.8	2.6
PK007_2 – 40	107	0.1065	0.0036	0.849	0.046	0.17	0.0573	0.0027	653	21	619	26	470	100	0.4	5.5
PK007_2 – 42	49	0.2042	0.0072	2.420	0.130	0.08	0.0856	0.0035	1197	38	1245	36	1314	74	0.2	3.9
PK007_2 – 43	367	0.13	0.0046	1.601	0.074	0.69	0.0887	0.0027	787	27	967	30	1391	62	0.1	18.6
PK007_2 – 44	206	0.09176	0.0031	0.730	0.036	0.02	0.0574	0.0023	566	19	555	21	482	88	0.5	2.0
PK007_2 – 45	41	0.1657	0.006	1.638	0.095	0.12	0.0715	0.0036	988	33	976	36	927	97	1.1	1.2
PK007_2 – 46	137	0.0923	0.0031	0.759	0.038	0.19	0.0593	0.0026	569	18	574	22	540	95	0.6	0.9
PK007_2 – 47	86	0.098	0.0035	0.828	0.046	0.08	0.0609	0.0029	602	21	607	26	571	110	0.6	0.8
PK007_2 – 48	117	0.2618	0.0091	3.900	0.170	0.29	0.1074	0.0035	1499	47	1609	37	1739	60	0.4	6.8
PK007_2 – 49	186	0.09698	0.0033	0.792	0.040	0.04	0.0590	0.0024	597	19	589	22	520	89	0.6	1.3
PK007_2 – 50	340	0.2185	0.0073	3.164	0.130	0.36	0.1043	0.0030	1274	39	1447	32	1696	53	0.8	12.0
PK007_2 – 51	253	0.09513	0.0033	0.796	0.037	0.03	0.0603	0.0023	586	19	592	22	582	83	1.2	1.1
PK007_2 – 52	414	0.1489	0.005	2.426	0.100	0.37	0.1167	0.0034	895	28	1249	32	1906	56	0.2	28.4
PK007_2 – 53	133	0.08976	0.0031	0.887	0.045	0.15	0.0715	0.0030	554	18	641	24	942	82	0.6	13.6
PK007_2 – 54	138	0.0877	0.0031	0.695	0.049	0.23	0.0566	0.0038	542	18	530	29	430	130	0.6	2.2
PK007_2 – 55	128	0.0874	0.003	0.723	0.042	0.01	0.0600	0.0031	540	18	547	25	520	110	0.3	1.3
PK007_2 – 56	116	0.0992	0.0034	0.839	0.043	0.03	0.0614	0.0028	610	19	612	24	570	97	1.9	0.3
PK007_2 – 57	59	0.1047	0.0038	0.872	0.055	0.05	0.0600	0.0033	642	22	627	30	520	120	1.4	2.3
PK007_2 – 58	157	0.0837	0.0035	0.664	0.086	0.09	0.0575	0.0052	518	21	513	42	440	140	0.2	1.0
PK007_2 – 59	120	0.0955	0.0033	0.758	0.041	0.37	0.0571	0.0025	588	20	568	24	444	100	1.4	3.5
PK007_2 – 60	668	0.0965	0.0036	1.457	0.075	0.90	0.1086	0.0036	594	21	909	31	1760	60	0.1	34.7
PK007_2 – 61	137	0.1654	0.0056	1.718	0.080	0.06	0.0750	0.0027	987	31	1011	30	1038	73	0.6	2.4
PK007_2 – 62	132	0.1	0.0034	0.828	0.041	0.03	0.0597	0.0026	614	20	613	23	540	93	2.1	0.2
PK007_2 – 63	203	0.2097	0.0086	3.281	0.170	0.34	0.1137	0.0037	1227	47	1475	50	1850	68	0.4	16.8
PK007_2 – 64	393	0.09308	0.0031	0.776	0.035	0.08	0.0601	0.0021	574	19	582	20	583	77	1.1	1.4

(*Continued*)

Table 2. (*Continued*)

Sample	^{238}U cps*1000	Isotopic ratios							Ages [Ma]				Approximate	Disc.%
		^{206}Pb/^{238}U	2SE	^{207}Pb/^{235}U	2SE	Rho	^{207}Pb/^{206}Pb	2SE	^{206}Pb/^{238}U	2SE	^{207}Pb/^{235}U	2SE	^{207}Pb/^{206}Pb	2SE	Th/U	
PK007_2 – 65	139	0.0916	0.0032	0.881	0.049	0.07	0.0696	0.0033	565	19	636	26	851	93	1.8	11.2
PK007_2 – 66	127	0.2528	0.011	5.780	0.290	0.88	0.1656	0.0050	1449	56	1934	44	2505	51	0.4	25.1
PK007_2 – 67	56	0.1003	0.0037	0.843	0.059	0.04	0.0610	0.0039	616	22	609	32	510	140	0.9	1.1
PK007_2 – 68	153	0.0946	0.004	0.773	0.043	0.02	0.0591	0.0025	583	23	578	24	526	91	0.5	0.8
PK007_2 – 69	548	0.1218	0.0074	1.484	0.150	0.48	0.0880	0.0038	741	41	922	48	1374	69	0.7	19.6
PK007_2 – 70	256	0.1032	0.0035	0.873	0.041	0.04	0.0614	0.0023	633	20	635	23	620	85	0.4	0.3
PK007_2 – 72	107	0.0989	0.0034	0.794	0.042	0.10	0.0581	0.0027	608	20	589	24	470	100	0.3	3.2
PK007_2 – 73	237	0.1901	0.0065	2.281	0.110	0.56	0.0862	0.0031	1122	35	1202	33	1324	66	0.3	6.7
PK007_2 – 74	7	0.1	0.0046	0.830	0.140	0.10	0.0591	0.0094	616	28	535	75	110	290	1.0	15.1
PK007_2 – 75a	283	0.0975	0.003	0.821	0.038	0.05	0.0615	0.0024	600	18	607	21	630	77	0.7	1.2
PK007_2 – 76	472	0.0927	0.003	0.789	0.032	0.00	0.0621	0.0020	572	18	590	19	664	71	0.4	3.1

The concentrations of compatible trace elements are low, for example, Co (0.3–2.2 ppm), V (8–20 ppm) Sc (2–11 ppm) or below detection limit (Cr, Ni). The rocks have variable concentrations of incompatible trace elements (e.g. Zr: 57–160 ppm, Ba: 353–1707 ppm, Y: 24–50 ppm, Th: 9.6–20 ppm and ΣREE: 99–212 ppm), and among them only a few show but weak trend with increasing SiO_2 (Zr and Nb negative, Th positive; Fig. S02). In the case of large ion lithophile elements (LILE), this lack of correlation most probably indicates element mobility under metamorphic conditions. The rare earth elements (REE) chondrite-normalized (CN, Sun & McDonough, 1989) profiles show enrichment of light rare earth elements (LREE) over mid rare earth elements (MREE) and heavy rare earth elements (HREE) ($[La/Sm]_{CN} = 2.81–5.47$, $[La/Yb]_{CN} = 3.80–13.6$). The resulting REE patterns have a negative slope for LREE and are flat for MREE–HREE (Fig. 7a). The fractionation of MREE from HREE is weak as $[Gd/Yb]_{CN}$ ranges from 1.0 to 1.5. The rocks show a pronounced Eu anomaly ($Eu/Eu^* = 0.11–0.36$, Fig. 7a), and assuming a divalent oxidation state of Eu, it may indicate either fractional crystallization of plagioclase or that during partial melting this mineral was present in the source. On upper continental crust-normalized variation diagrams (Fig. 7b), meta-rhyolites show variable enrichment in LILE and Th but strong depletion in high-field-strength elements (HFSE, i.e. Nb, Ta, Ti, P, Zr, Hf) and in Sr; the latter negative anomaly is probably related to the Eu anomaly. These significant and negative anomalies support the fractionation of the Pl + Bt + Ap + Ilm mineral assemblage, presumably joined by some zircon and perhaps monazite, as shown by negative trends of Zr versus SiO_2 (Fig. S02) and $[La/Yb]_{CN}$ versus Ce_{CN} (not shown). However, these anomalies may also characterize the melt source, as upper and/or middle crust have developed depletion in high-field-strength elements (Taylor & McLennan, 1985).

3.d. Internal structure of analysed zircon grains

3.d.1. Sample PK007

The zircon population of sample PK007 ranges from 40 to 152 μm with a mean length of 80 μm. It is dominated by grains with an elongation of less than 2 (84%), while zircons with an elongation in the range of 2 to 3 are much less frequent (16%). The zircon grains examined are often ovoid (32%) to well-rounded (38%). However, euhedral crystals are an important group (30%). Most of the grains in the examined sample are homogeneous (60%), while 40% of them show inherited cores. The very small group of grains (4%) have dark, thin rims.

3.d.2. Sample PK023

Sample PK023 contains grains ranging in length from 51 to 149 μm with a mean length of 83 μm. Most of the zircons analysed have an elongation of less than 2 (64%), while grains with an elongation greater than 2 form a much smaller group (36%). A large group of zircons are rounded to euhedral crystals (66%), while ovoid to well-rounded grains are less common (34%). Most grains are homogeneous (74%), and only a small group of zircons (18%) show inherited cores. Examined zircons often show dark, thin rims (44%) or represent dark, homogeneous grains (8%).

3.d.3. Sample MD01-31

The zircons in sample MD01-32 range in length from 56 to 121 μm with a mean length of 85 μm. Half of the grains analysed have an elongation of less than 2. The sample is dominated by euhedral crystals (55% of the population). However, well-rounded grains are

https://doi.org/10.1017/S0016756823000523 Published online by Cambridge University Press

Table 3. Laser ablation ICP-MS U–Pb isotopic data of detrital zircons from sample PK023

		Isotopic ratios							Ages [Ma]						Approximate	
Sample	^{238}U cps*1000	^{206}Pb/^{238}U	2SE	^{207}Pb/^{235}U	2SE	Rho	^{207}Pb/^{206}Pb	2SE	^{206}Pb/^{238}U	2SE	^{207}Pb/^{235}U	2SE	^{207}Pb/^{206}Pb	2SE	Th/U	Disc.%
PK023 – 1a	116	0.0895	0.0029	0.927	0.052	0.38	0.0777	0.0038	552	17	661	28	1090	120	0.5	16.5
PK023 – 2	745	0.0859	0.0021	0.700	0.028	0.03	0.0596	0.0023	531	12	538	16	588	87	0.0	1.3
PK023 – 3	677	0.09154	0.0018	0.760	0.032	0.03	0.0609	0.0028	565	11	575	18	618	97	0.2	1.8
PK023 – 4	132	0.083	0.0034	0.699	0.056	0.37	0.0622	0.0052	514	20	536	34	620	170	0.4	4.1
PK023 – 5	126	0.107	0.0042	0.874	0.042	0.15	0.0607	0.0031	655	25	631	25	560	110	0.2	3.8
PK023 – 6	494	0.06067	0.0014	0.489	0.026	0.08	0.0590	0.0033	380	8	403	18	551	130	0.1	5.8
PK023 – 7	20	0.3733	0.012	6.620	0.370	0.27	0.1311	0.0073	2043	56	2048	48	2103	95	1.8	0.2
PK023 – 8a	26	0.3358	0.0054	4.760	0.078	0.36	0.1061	0.0042	1866	32	1767	39	1700	110	1.3	5.6
PK023 – 9	570	0.0662	0.0019	0.509	0.035	0.11	0.0563	0.0035	413	12	416	22	420	120	0.1	0.7
PK023 – 10	126	0.096	0.0031	0.824	0.068	0.19	0.0641	0.0052	591	18	614	37	670	180	0.5	3.7
PK023 – 11	159	0.0924	0.0026	0.876	0.066	0.21	0.0692	0.0053	570	15	632	34	810	140	0.7	9.8
PK023 – 12	173	0.1145	0.0029	0.949	0.059	0.21	0.0599	0.0041	699	17	673	30	550	140	0.6	3.9
PK023 – 13	103	0.1086	0.0057	1.017	0.071	0.05	0.0679	0.0037	665	34	705	40	780	140	0.9	5.7
PK023 – 14	82	0.0994	0.0031	0.853	0.064	0.08	0.0614	0.0049	611	18	620	35	570	170	1.6	1.5
PK023 – 15	524	0.06518	0.0015	0.590	0.027	0.45	0.0644	0.0029	407	9	472	17	742	98	0.1	13.8
PK023 – 16	172	0.0917	0.0034	1.053	0.081	0.07	0.0823	0.0091	566	20	725	37	1190	150	2.2	21.9
PK023 – 18	3417	0.04896	0.00098	0.386	0.013	0.44	0.0562	0.0020	308	6	331.4	9.3	455	82	12.7	7.0
PK023 – 19	134	0.1027	0.003	0.932	0.042	0.02	0.0644	0.0036	630	18	663	24	710	130	1.0	5.0
PK023 – 20a	423	0.0985	0.0024	0.832	0.039	0.05	0.0609	0.0043	605	15	611	27	550	140	0.6	0.9
PK023 – 21	68	0.06289	0.0011	0.519	0.019	0.24	0.0592	0.0025	393	7	422	14	530	110	0.0	6.8
PK023 – 22	445	0.0941	0.0027	0.779	0.079	0.04	0.0583	0.0061	580	16	574	46	430	220	1.0	1.0
PK023 – 23	73	0.0912	0.0021	0.894	0.053	0.09	0.0687	0.0042	563	13	644	29	840	140	0.9	12.6
PK023 – 24	192	0.1129	0.0029	0.989	0.073	0.27	0.0624	0.0048	690	17	696	38	620	170	0.8	0.9
PK023 – 25	102	0.0737	0.0017	0.696	0.036	0.07	0.0673	0.0038	459	10	534	21	808	120	0.6	14.1
PK023 – 26	354	0.06938	0.0014	0.735	0.028	0.06	0.0757	0.0033	432	8	559	17	1073	87	0.9	22.6
PK023 – 27	816	0.07359	0.0018	0.643	0.037	0.16	0.0635	0.0040	458	11	501	25	675	150	0.2	8.6
PK023 – 28	182	0.07424	0.0015	0.693	0.031	0.01	0.0677	0.0032	462	9	535	19	838	100	0.3	13.7
PK023 – 29	874	0.195	0.0046	3.340	0.140	0.32	0.1238	0.0055	1148	25	1486	33	1998	79	0.6	22.7
PK023 – 31	96	0.0929	0.002	0.772	0.034	0.09	0.0615	0.0031	573	12	579	20	628	110	0.4	1.1
PK023 – 32	398	0.3096	0.0063	4.869	0.160	0.18	0.1161	0.0042	1739	31	1796	27	1892	66	0.9	3.2

(*Continued*)

Table 3. (*Continued*)

		Isotopic ratios							Ages [Ma]						Approximate	
Sample	^{238}U cps*1000	^{206}Pb/^{238}U	2SE	^{207}Pb/^{235}U	2SE	Rho	^{207}Pb/^{206}Pb	2SE	^{206}Pb/^{238}U	2SE	^{207}Pb/^{235}U	2SE	^{207}Pb/^{206}Pb	2SE	Th/U	Disc.%
PK023 – 33	402	0.0943	0.0025	0.984	0.065	0.11	0.0793	0.0069	581	15	687	26	1070	91	0.4	15.4
PK023 – 34	104	0.0861	0.0019	0.702	0.032	0.08	0.0607	0.0031	533	11	541	21	613	120	0.7	1.6
PK023 – 35	229	0.1105	0.0026	0.907	0.054	0.03	0.0614	0.0039	675	15	651	29	620	140	0.9	3.7
PK023 – 36	244	0.1001	0.0024	0.798	0.048	0.06	0.0595	0.0038	615	14	594	27	550	140	1.5	3.5
PK023 – 37	727	0.0743	0.0019	2.150	0.200	0.29	0.2180	0.0180	462	11	1149	58	2890	110	0.1	59.8
PK023 – 38	155	0.0986	0.0023	0.808	0.053	0.07	0.0603	0.0041	606	13	597	29	550	150	0.6	1.6
PK023 – 39	80	0.0809	0.0022	0.583	0.057	0.12	0.0535	0.0052	501	13	460	36	280	200	0.5	9.0
PK023 – 40	155	0.3003	0.0071	5.290	0.200	0.54	0.1290	0.0050	1692	35	1864	32	2076	69	0.3	9.2
PK023 – 41	453	0.05853	0.0013	0.524	0.028	0.17	0.0662	0.0040	367	8	426	17	766	98	0.0	13.9
PK023 – 42	230	0.05523	0.0014	0.528	0.033	0.12	0.0700	0.0046	347	9	428	22	895	130	0.5	19.0
PK023 – 43	89	0.1593	0.0053	2.100	0.110	0.20	0.0953	0.0050	953	30	1143	40	1518	100	0.6	16.6
PK023 – 44	274	0.09864	0.002	0.840	0.040	0.08	0.0629	0.0034	606	12	617	22	687	100	1.4	1.7
PK023 – 45	510	0.04888	0.0011	0.509	0.023	0.45	0.0754	0.0034	308	7	417	15	1063	91	0.1	26.2
PK023 – 46	35	0.1072	0.0041	0.868	0.066	0.15	0.0601	0.0055	656	24	621	38	480	190	0.6	5.6
PK023 – 47	76	0.1005	0.0033	0.811	0.062	0.02	0.0591	0.0046	617	20	595	35	480	160	1.5	3.7
PK023 – 48	442	0.0908	0.0021	0.911	0.038	0.25	0.0727	0.0031	560	12	656	20	989	92	0.4	14.6
PK023 – 49	302	0.1049	0.0023	1.385	0.076	0.09	0.0942	0.0054	643	13	875	34	1450	120	0.7	26.5
PK023 – 50	45	0.1324	0.0038	1.229	0.110	0.07	0.0666	0.0058	801	22	804	48	730	190	0.7	0.4
PK023 – 51	479	0.06578	0.0017	0.529	0.026	0.03	0.0577	0.0029	411	10	433	18	480	120	0.2	5.2
PK023 – 52	112	0.2708	0.0065	4.150	0.190	0.27	0.1076	0.0049	1544	33	1659	37	1756	88	0.4	6.9
PK023 – 53	27	0.1073	0.004	0.790	0.110	0.08	0.0530	0.0076	657	23	570	62	170	280	0.3	15.3
PK023 – 54	73	0.1354	0.0032	2.476	0.100	0.39	0.1292	0.0054	818	18	1267	27	2077	73	0.6	35.4
PK023 – 55	500	0.0582	0.0012	0.765	0.033	0.20	0.0930	0.0043	365	8	575	19	1472	86	0.2	36.6
PK023 – 56	429	0.05402	0.0013	0.508	0.023	0.16	0.0675	0.0035	339	8	416	16	822	110	0.1	18.5
PK023 – 57	215	0.0521	0.0014	0.427	0.031	0.12	0.0583	0.0045	328	9	363	24	490	170	0.1	9.8
PK023 – 58	578	0.06297	0.0013	0.517	0.021	0.19	0.0586	0.0027	394	8	422	14	530	100	0.2	6.7
PK023 – 59	137	0.0979	0.0024	0.798	0.059	0.04	0.0584	0.0045	602	14	590	33	470	160	0.7	2.1
PK023 – 60	45	0.1	0.0031	0.903	0.083	0.17	0.0655	0.0065	614	18	642	47	660	220	0.4	4.4
PK023 – 61	165	0.075	0.0021	0.702	0.042	0.15	0.0689	0.0043	466	13	537	25	840	130	0.1	13.2
PK023 – 62	343	0.0712	0.0027	1.142	0.054	0.33	0.1202	0.0079	443	16	771	26	1910	120	0.5	42.5

(*Continued*)

Table 3. (*Continued*)

PK023 – 63	284	0.0695	0.0042	0.810	0.160	0.90	0.0800	0.0110	433	25	564	78	950	250	0.1	23.2
PK023 – 64	508	0.0665	0.0015	0.496	0.021	0.17	0.0551	0.0026	415	9	408	14	394	100	0.1	1.7
PK023 – 65	360	0.0964	0.0044	0.809	0.051	0.69	0.0622	0.0032	592	26	598	28	648	110	0.3	1.0
PK023 – 66	840	0.04263	0.00097	0.646	0.024	0.21	0.1115	0.0047	269	6	505.6	15	1825	71	0.6	46.8
PK023 – 67	332	0.075	0.0018	3.990	0.210	0.64	0.3930	0.0190	467	11	1624	42	3868	75	2.0	71.3
PK023 – 68	150	0.0577	0.0015	0.423	0.035	0.02	0.0545	0.0047	361	9	355	24	310	170	0.1	1.8
PK023 – 69	399	0.0649	0.0023	0.515	0.030	0.58	0.0587	0.0031	405	14	420	20	523	120	0.1	3.6
PK023 – 70	369	0.0729	0.0022	0.570	0.033	0.36	0.0578	0.0033	454	13	456	21	480	130	0.0	0.4
PK023 – 71	93	0.1115	0.0042	0.815	0.068	0.33	0.0552	0.0047	681	24	598	37	340	180	0.3	13.9

also common (45%). Most zircon crystals are homogeneous (75%), while grains with inherited cores are much less frequent (25%). Zircons with dark, thin rims make up 40% of the population.

3.d.4. MD04-01

Zircon grains in sample MD04-01 range in length from 57 to 166 μm with a mean length of 92 μm and an elongation mostly below 2 (73%). Most grains are euhedral (78%), while rounded and well-rounded zircons are common (22% of the population). A relatively large group of grains have dark and thin rims (57%).

3.d.5. Sample PK026

The zircon population of sample PK026 ranges from 54 to 164 μm with a mean length of 121 μm. The population of grains with elongation greater than 2 is relatively abundant (40%). The zircon grains examined are predominantly euhedral (95%) and homogenous (83%) crystals. A small group of zircons (17%) show inherited cores.

In summary, cathodoluminescence images of the investigated zircon population show that within the metasedimentary samples most of the investigated grains show similar characteristics in terms of brightness, internal texture and elongation. Most of the grains are euhedral with locally corroded faces and show moderate cathodoluminescence and fine oscillatory zoning of clearly magmatic origin (e.g. PK007-2-36, Fig. 8) of which some are well rounded (e.g. PK023-40, Fig. 8). Some zircons have textures indicative of metasomatic alterations (e.g. MD04-1-12, Fig. 8). Some zircons from both groups contain xenocrystic cores (e.g. PK026-26, Fig. 8). Interestingly, especially in samples PK023, MD01-32 and MD04-01, a number of grains show thin and dark rims (e.g. PK023-21, MD04-1-91, MD04-1-116, Fig. 8 and S03) or represent dark, homogeneous grains with patchy or no internal zoning pattern (PK023-18. Fig. 8) probably related to metamorphic growth. It is worth noting that the population of zircon grains documented in the sample PK026 differs slightly from the remaining samples. The majority of grains in this sample are characterized by long euhedral grains with high elongation of greater than 2 and with oscillatory zoning of clearly magmatic origin supporting our interpretation that this sample represents metarhyolite (Fig. 8).

3.e. U-Pb zircon dating

Laser ablation ICP–MS U–Pb dating identified more than 80 % of zircons as younger than 1 Ga (Figs. 9 and 10, Tables 2–6). Although the samples show significant differences in their KDE age spectra, they all share the presence of the prominent 590–600 Ma peak (Fig. 10). In the case of sample PK007, this peak dominates the entire spectrum but is additionally accompanied by a significant small group of zircons of about 1.0 Ga (Fig. 10a). Sample PK023 contains, in addition to the common Ediacaran peak mentioned above, a prominent younger peak of 400 Ma tailing to about 320 Ma representing the youngest age component in the latter sample (Fig. 10b). The paragneisses contain a very pronounced peak of 480–510 Ma, which is dominant in sample MD01-32 (Fig. 10c, d). The two paragneisses also contain several smaller peaks ranging from about 770 to 1000 Ma (Fig. 10c, d). All samples contain several minor groups of grains of Proterozoic and Archean age (Fig. 10).

Except for the four metamorphosed sedimentary rocks presented above, we additionally analysed the quartz-feldspathic schist PK026, which we interpreted on account of its mineral

https://doi.org/10.1017/S0016756823000523 Published online by Cambridge University Press

Table 4. Laser ablation ICP-MS U–Pb isotopic data of detrital zircons from sample PK026

		Isotopic ratios							Ages [Ma]						Approximate	
Sample	^{238}U cps *1000	^{206}Pb/^{238}U	2SE	^{207}Pb/^{235}U	2SE	Rho	^{207}Pb/^{206}Pb	2SE	^{206}Pb/^{238}U	2SE	^{207}Pb/^{235}U	2SE	^{207}Pb/^{206}Pb	2SE	Th/U	Disc.%
PK026 – 1a	270	0.07418	0.0017	1.323	0.060	0.29	0.1290	0.0051	461	10	854	27	2073	59	0.5	46.0
PK026 – 2	259	0.08171	0.0019	0.646	0.034	0.19	0.0570	0.0017	506	11	504	21	448	75	0.2	0.5
PK026 s- 3	162	0.1022	0.0023	0.843	0.045	0.07	0.0596	0.0026	627	13	621	24	561	79	3.0	1.0
PK026 – 4	637	0.0751	0.0019	0.610	0.078	0.03	0.0582	0.0015	467	12	483	39	538	120	0.2	3.4
PK026 – 5	340	0.08167	0.0018	0.658	0.047	0.09	0.0582	0.0019	506	11	512	26	510	92	0.2	1.2
PK026 – 6	625	0.07882	0.0018	0.613	0.030	0.07	0.0562	0.0013	489	11	484.8	19	450	57	0.1	0.9
PK026 – 7	297	0.08302	0.0018	0.677	0.033	0.13	0.0590	0.0026	514	11	523	20	523	74	0.3	1.7
PK026 – 8	193	0.0812	0.0018	0.663	0.037	0.02	0.0591	0.0028	503	11	513	23	510	87	0.1	1.9
PK026 – 9	252	0.0864	0.002	0.811	0.100	0.15	0.0682	0.0027	534	12	603	44	830	130	0.2	11.4
PK026 – 10	472	0.08106	0.0018	0.747	0.041	0.04	0.0665	0.0021	502	11	565	23	801	77	0.2	11.1
PK026 – 11	456	0.08238	0.0018	0.655	0.032	0.09	0.0572	0.0014	510	11	510.9	20	485	62	0.2	0.1
PK026 – 13a	547	0.0729	0.0017	0.581	0.029	0.19	0.0576	0.0025	454	10	464	19	491	59	0.3	2.2
PK026 – 14	344	0.0846	0.0023	0.671	0.035	0.26	0.0566	0.0028	524	14	519	21	440	74	0.2	0.9
PK026 – 15	108	0.0834	0.0022	0.655	0.047	0.08	0.0568	0.0039	516	13	509	28	410	120	0.2	1.5
PK026 – 16	191	0.08233	0.0018	0.647	0.034	0.05	0.0567	0.0019	510	11	504	21	444	82	0.2	1.2
PK026 – 17	335	0.08127	0.0022	0.630	0.180	0.04	0.0559	0.0022	504	13	494	69	412	200	0.2	2.0
PK026 – 18	403	0.4558	0.0098	10.962	0.470	0.62	0.1733	0.0012	2420	43	2518.8	40	2588	27	0.1	3.9
PK026 – 19	611	0.08129	0.0017	0.678	0.047	0.03	0.0602	0.0023	504	10	524	26	587	85	0.2	3.9
PK026 – 20	318	0.0819	0.0021	0.624	0.038	0.06	0.0551	0.0026	507	13	491	23	400	90	0.6	3.3
PK026 – 21	123	0.1869	0.0042	2.519	0.120	0.20	0.0974	0.0026	1104	23	1273	35	1563	55	0.1	13.3
PK026 – 22	280	0.07894	0.0018	0.621	0.031	0.10	0.0571	0.0017	490	10	490	20	453	72	0.3	0.1
PK026 – 23	444	0.08276	0.002	0.660	0.050	0.24	0.0576	0.0015	513	12	513	28	493	110	0.2	0.1
PK026 – 24	295	0.0846	0.0019	0.671	0.033	0.07	0.0572	0.0015	524	11	521	21	470	68	0.3	0.5
PK026 – 25	310	0.103	0.0022	0.874	0.041	0.10	0.0614	0.0019	632	13	636	23	624	61	0.6	0.7
PK026 – 26	291	0.07863	0.0017	0.622	0.035	0.23	0.0571	0.0021	488	10	491	22	465	81	0.1	0.6
PK026 – 27	410	0.082	0.0018	0.645	0.031	0.01	0.0568	0.0015	508	11	504	19	452	63	0.4	0.8
PK026 – 28	191	0.08423	0.002	0.666	0.037	0.11	0.0570	0.0022	521	12	515	23	443	89	0.2	1.2
PK026 – 29	322	0.08312	0.0021	0.659	0.150	0.05	0.0572	0.0024	515	13	512	62	461	190	0.2	0.5
PK026 – 30	894	0.0819	0.0019	1.260	0.140	0.20	0.1114	0.0089	507	11	811	54	1680	150	0.3	37.4
PK026 – 31	268	0.10504	0.0023	0.905	0.047	0.03	0.0622	0.0020	644	14	651	25	648	76	0.4	1.1

(*Continued*)

Table 4. (*Continued*)

PK026 – 32	452	0.07889	0.0017	0.649	0.037	0.06	0.0593	0.0022	490	10	506	22	547	78	0.2	3.3
PK026 – 33	388	0.07417	0.0016	0.812	0.044	0.22	0.0792	0.0036	461	10	600	24	1124	81	0.8	23.1
PK026 – 34	546	0.09133	0.0021	0.739	0.033	0.16	0.0584	0.0018	563	13	561	20	546	60	0.5	0.4
PK026 – 35	347	0.0825	0.0018	0.663	0.032	0.08	0.0581	0.0018	511	11	515	19	520	64	0.2	0.8
PK026 – 36	139	0.0824	0.0033	0.910	0.110	0.32	0.0760	0.0110	510	20	622	52	870	160	0.1	18.0
PK026 – 37	221	0.0834	0.0019	0.656	0.032	0.04	0.0570	0.0024	516	11	511	20	459	67	0.1	1.0
PK026 – 38	294	0.0798	0.0033	0.698	0.110	0.22	0.0626	0.0049	495	20	532	48	610	220	0.2	7.0

composition, zircon morphology and bulk geochemical features as a metarhyolite (see sections 3a, 3c and 3d). The vast majority of analyses plot between 450 and 550 Ma ($^{206}Pb/^{238}U$ ages). The most common group of analyses defines a clear cluster around 510 Ma, which we interpret as the time of rhyolite emplacement (Fig. 9c, d). Some younger ages we interpret as the result of Pb loss due to a Variscan event. A group of three concordant analyses reflects inherited domains of 630–645 Ma, and $^{207}Pb/^{206}Pb$ ages define the minimum zircon crystallization ages of the two oldest domains defined by single analyses as 2593 ± 21 and 1536 ± 76 Ma (Fig. 9c, d).

4. Discussion

4.a. Potential influence of metamorphism on whole-rock geochemistry

Both metasediments and metaryolites have undergone a medium- to high-temperature metamorphism, which could have mobilized the large-ion lithophile elements (e.g. Na, K, Ba, Rb and Cs). However, any large-scale remobilization of REEs, Th, Zr, Sc, Cr and Co seems unlikely as the patterns observed on the spider plots are quite uniform in the examined samples suite (Figs. 5 and 7). Furthermore, these elements are thought to be largely transferred to clastic sediments during weathering and transport, thus reflecting the signature of the parent material (Bhatia & Crook, 1986; McLennan, 1989).

4.b. Provenance signature based on chemical composition of metasediments

The La/Sc and Th/Co ratios are commonly considered useful provenance indicators (Cullers, 2002). The samples used in this study show La/Sc (1.02 to 10.57) and Th/Co (0.48 to 30.7) ratios typical of felsic rocks (Fig. 11a). Similarly, TiO_2 (0.04 to 1.08) and Ni (2 to 82.8) concentrations, as well as Hf/Yb and La/Th ratios, are mostly characteristic of the felsic source in the examined samples (Floyd *et al.* 1990; Fig. 11b, c). These conclusions are confirmed by the Th/Sc versus Zr/Sc diagram (Fig. 11d). Since these elements are transferred quantitatively from source to sink sediment, their ratio can be used to infer the composition of the source rock and the sedimentary processes it suffered (McLennan *et al.* 1993). Zirconium is mainly retained in zircon, and thus the Zr/Sc ratio is a useful index of zircon enrichment in sedimentary rocks. However, the Th/Sc ratio is a good index of igneous differentiation processes because Th is typically an incompatible element, whereas Sc is compatible in igneous rocks. Therefore, the Zr/Sc ratio is considered a proxy for the degree of recycling, whereas the Th/Sc ratio reflects the average composition of the source rocks (McLennan *et al.* 1993). Consequently, igneous differentiation results in a positive linear correlation of the Th/Sc versus Zr/Sc ratios. Interestingly, the analysed samples show Zr/Sc (7.8 to 53.4) and Th/Sc (0.6 to 7.0) ratios intermediate between rhyolite and granite source rocks (Fig. 11d). Furthermore, relatively low values of the Zr/Sc ratio and low Zr concentration (0.47 to 0.78) suggest that sediment recycling and reworking did not influence the final composition of the studied metasediments (Floyd *et al.* 1990; McLennan *et al.* 1993).

The REE pattern of the source rocks is preserved in clastic sediments and can therefore be used to distinguish between a felsic and a mafic dominated source of clastic sediments (Taylor & McLennan, 1985). Felsic rocks are characterized by higher LREE/HREE ratios and negative Eu anomalies, whereas mafic rocks

https://doi.org/10.1017/S0016756823000523 Published online by Cambridge University Press

Table 5. Laser ablation ICP-MS U–Pb isotopic data of detrital zircons from sample MD01-32

		Isotopic ratios							Ages [Ma]						Approximate	
Sample	^{238}U cps*1000	^{206}Pb/^{238}U	2SE	^{207}Pb/^{235}U	2SE	Rho	^{207}Pb/^{206}Pb	2SE	^{206}Pb/^{238}U	2SE	^{207}Pb/^{235}U	2SE	^{207}Pb/^{206}Pb	2SE	Th/U	Disc.%
MD01-32_2 – 1	189	0.06489	0.0021	0.565	0.030	0.03	0.0638	0.0035	405	13	451	19	660	110	0.1	10.1
MD01-32_2 – 2	168	0.0756	0.0023	0.610	0.030	0.09	0.0589	0.0028	470	14	480	19	511	110	0.1	2.2
MD01-32_2 – 3	77	0.076	0.0025	0.591	0.043	0.24	0.0564	0.0038	472	15	464	26	360	140	0.3	1.8
MD01-32_2 – 4	207	0.0954	0.0027	0.828	0.037	0.30	0.0628	0.0026	587	16	609	21	654	90	0.6	3.5
MD01-32_2 – 5	579	0.07355	0.0021	0.575	0.022	0.16	0.0571	0.0021	458	12	460	14	470	81	0.4	0.5
MD01-32_2 – 6	380	0.06097	0.0019	0.543	0.032	0.08	0.0646	0.0030	382	12	439	20	735	96	0.1	13.1
MD01-32_2 – 7	237	0.0965	0.0027	0.818	0.030	0.05	0.0608	0.0022	594	16	605	18	615	82	0.0	1.8
MD01-32_2 – 8	51	0.1085	0.0034	1.079	0.071	0.10	0.0726	0.0048	664	20	727	36	880	140	0.5	8.7
MD01-32_2 – 9	44	0.1461	0.0046	1.310	0.074	0.23	0.0657	0.0042	879	26	841	36	690	130	1.0	4.5
MD01-32_2 – 10	215	0.083	0.0024	0.616	0.028	0.02	0.0542	0.0024	514	14	485	18	340	95	0.4	6.0
MD01-32_2 – 11	546	0.2118	0.015	4.350	0.330	0.54	0.1458	0.0041	1239	74	1701	44	2295	51	0.1	27.2
MD01-32_2 – 12	112	0.0762	0.0022	0.612	0.032	0.03	0.0589	0.0031	473	13	481	21	490	120	0.5	1.6
MD01-32_2 – 13	292	0.0726	0.0021	0.572	0.027	0.15	0.0573	0.0027	452	13	457	17	460	100	1.6	1.1
MD01-32_2 – 14	104	0.0769	0.0023	0.747	0.081	0.04	0.0709	0.0074	478	14	566	39	900	140	0.4	15.6
MD01-32_2 – 15	133	0.0904	0.0027	0.937	0.059	0.28	0.0751	0.0045	558	16	672	32	1010	120	0.7	17.0
MD01-32_2 – 16	248	0.1899	0.0067	3.006	0.320	0.30	0.1157	0.0100	1121	35	1407	54	1883	100	0.4	20.3
MD01-32_2 – 17	37	0.3517	0.01	6.010	0.220	0.22	0.1230	0.0042	1942	49	1970	34	1989	65	1.2	1.4
MD01-32_2 – 18	157	0.079	0.0023	0.627	0.030	0.17	0.0565	0.0028	490	14	491	18	420	100	0.1	0.2
MD01-32_2 – 19	133	0.1011	0.003	0.858	0.040	0.06	0.0612	0.0028	621	18	627	22	613	100	0.9	1.0
MD01-32_2 – 20	104	0.0807	0.0023	0.644	0.034	0.21	0.0580	0.0031	501	14	501	22	490	120	0.1	0.1
MD01-32_2 – 21	109	0.0904	0.0027	0.831	0.110	0.01	0.0668	0.0077	558	16	607	47	740	160	0.4	8.1
MD01-32_2 – 22	171	0.07456	0.0022	0.594	0.029	0.05	0.0575	0.0028	464	13	470	18	453	100	0.2	1.4
MD01-32_2 – 23	231	0.0858	0.0024	0.795	0.046	0.12	0.0669	0.0037	531	14	594	24	811	100	0.7	10.7
MD01-32_2 – 24	82	0.1662	0.005	1.597	0.072	0.06	0.0700	0.0031	991	28	964	28	880	88	1.4	2.8
MD01-32_2 – 25	262	0.173	0.0055	2.595	0.100	0.34	0.1066	0.0032	1029	31	1297	34	1734	61	0.9	20.7
MD01-32_2 – 26	441	0.1748	0.0049	1.868	0.059	0.10	0.0777	0.0023	1038	27	1068	21	1131	58	0.9	2.8
MD01-32_2 – 27	91	0.0803	0.0024	0.654	0.038	0.22	0.0587	0.0033	498	14	504	23	470	120	0.4	1.3
MD01-32_2 – 28	74	0.1111	0.0037	0.913	0.060	0.09	0.0602	0.0034	679	21	651	31	530	120	0.0	4.3
MD01-32_2 – 29	309	0.07463	0.0021	0.598	0.025	0.22	0.0580	0.0022	464	13	474	16	503	86	0.8	2.1
MD01-32_2 – 30	112	0.0752	0.0023	0.591	0.035	0.00	0.0574	0.0034	467	14	466	23	410	130	0.6	0.3
MD01-32_2 – 31	112	0.4744	0.014	11.680	0.390	0.70	0.1780	0.0050	2501	62	2578	32	2630	47	0.9	3.0

(*Continued*)

Table 5. (*Continued*)

MD01-32_2 – 32	136	0.0833	0.0024	0.687	0.031	0.20	0.0599	0.0027	516	14	528	19	540	99	0.3	2.3
MD01-32_2 – 33	82	0.0947	0.0028	0.819	0.035	0.25	0.0620	0.0026	583	17	599	20	580	97	0.9	2.7
MD01-32_2 – 34	20	0.5104	0.016	12.760	0.480	0.29	0.1815	0.0063	2656	67	2654	36	2648	61	0.3	0.1
MD01-32_2 – 35	229	0.07454	0.0022	1.281	0.058	0.01	0.1242	0.0055	463	13	832	28	1975	92	0.6	44.3
MD01-32_2 – 36	89	0.0736	0.0025	0.559	0.049	0.22	0.0545	0.0043	458	15	447	30	330	140	0.2	2.5
MD01-32_2 – 37	262	0.0945	0.0028	0.787	0.031	0.18	0.0603	0.0023	582	16	587	18	597	80	1.1	0.9
MD01-32_2 – 38	273	0.1538	0.0043	1.486	0.051	0.10	0.0701	0.0024	922	24	923	21	915	66	0.5	0.1
MD01-32_2 – 39	283	0.2255	0.0063	3.504	0.110	0.39	0.1131	0.0032	1311	34	1527	28	1845	54	0.2	14.1
MD01-32_2 – 40	95	0.132	0.0039	1.201	0.053	0.33	0.0657	0.0029	799	22	796	25	750	95	1.1	0.4
MD01-32_2 – 41	468	0.07961	0.0025	0.892	0.038	0.21	0.0819	0.0039	494	15	646	20	1215	83	0.5	23.6
MD01-32_2 – 42	175	0.0766	0.0023	0.625	0.031	0.00	0.0591	0.0029	476	14	490	19	510	100	0.4	2.9
MD01-32_2 – 43	70	0.0812	0.0025	0.651	0.043	0.32	0.0576	0.0036	503	15	500	26	410	130	0.5	0.7
MD01-32_2 – 44	480	0.1074	0.0029	0.924	0.031	0.20	0.0619	0.0020	657	17	663	16	651	67	0.7	0.8
MD01-32_2 – 45	121	0.07711	0.0023	0.601	0.033	0.13	0.0561	0.0030	479	14	473	21	382	110	0.1	1.2
MD01-32_2 – 46	150	0.0967	0.0028	0.811	0.038	0.06	0.0605	0.0027	595	17	599	21	584	93	1.2	0.7
MD01-32_2 – 47	131	0.0772	0.0025	0.615	0.031	0.25	0.0575	0.0025	480	15	481	19	430	97	0.1	0.3
MD01-32_2 – 48	114	0.2925	0.0086	6.350	0.220	0.33	0.1572	0.0048	1654	44	2022	33	2417	52	0.1	18.2
MD01-32_2 – 49	101	0.0771	0.0023	0.646	0.034	0.17	0.0604	0.0032	479	14	503	21	551	110	0.2	4.9
MD01-32_2 – 50	141	0.1041	0.003	0.906	0.040	0.17	0.0626	0.0026	638	18	651	21	645	91	0.6	2.0
MD01-32_2 – 51	173	0.1001	0.0029	0.831	0.037	0.02	0.0600	0.0026	615	17	611	20	553	96	1.2	0.6
MD01-32_2 – 52	42	0.0982	0.0031	0.843	0.052	0.02	0.0619	0.0041	604	18	613	29	580	130	2.1	1.5
MD01-32_2 – 53	140	0.1069	0.0032	0.889	0.040	0.07	0.0604	0.0026	655	19	642	22	563	92	0.0	2.0
MD01-32_2 – 54	123	0.0951	0.0028	0.790	0.043	0.27	0.0598	0.0032	586	17	585	25	527	110	1.0	0.1
MD01-32_2 – 55	79	0.344	0.01	6.470	0.240	0.39	0.1334	0.0041	1905	51	2036	36	2131	55	0.6	6.4
MD01-32_2 – 56	127	0.1013	0.003	0.838	0.042	0.04	0.0595	0.0029	622	18	612	23	517	100	1.5	1.6
MD01-32_2 – 57	162	0.0689	0.0023	1.532	0.080	0.33	0.1592	0.0097	430	14	937	34	2413	110	2.6	54.2
MD01-32_2 – 58	51	0.097	0.0034	0.793	0.070	0.12	0.0596	0.0050	596	20	581	36	460	160	0.6	2.6
MD01-32_2 – 59	84	0.1027	0.003	0.840	0.044	0.25	0.0582	0.0029	630	18	612	24	490	110	0.9	2.9
MD01-32_2 – 60	261	0.0987	0.0032	0.865	0.037	0.23	0.0635	0.0025	607	19	630	21	692	86	0.8	3.7
MD01-32_2 – 61	104	0.0811	0.0025	0.918	0.048	0.01	0.0817	0.0042	503	15	654	26	1180	110	0.4	23.2
MD01-32_2 – 62	1155	0.06935	0.0025	0.574	0.047	0.02	0.0586	0.0036	432	15	460	26	534	97	0.4	6.0
MD01-32_2 – 63	17	0.1349	0.0051	1.230	0.097	0.24	0.0640	0.0051	815	29	787	50	560	170	1.0	3.6
MD01-32_2 – 64	42	0.4027	0.012	7.420	0.270	0.32	0.1323	0.0043	2180	54	2154	34	2106	61	0.6	1.2

(*Continued*)

Table 5. (*Continued*)

Sample	Isotopic ratios							Ages [Ma]				Approximate	
	^{238}U cps*1000	^{206}Pb/^{238}U	2SE	^{207}Pb/^{235}U	2SE	Rho	^{207}Pb/^{206}Pb	2SE	^{206}Pb/^{238}U	2SE	^{207}Pb/^{235}U	2SE	^{207}Pb/^{206}Pb	2SE	Th/U	Disc.%
MD01-32_2 – 65	169	0.0802	0.0035	0.628	0.041	0.11	0.0563	0.0025	497	20	492	23	410	92	0.0	1.1
MD01-32_2 – 66	59	0.1095	0.0035	0.910	0.058	0.04	0.0602	0.0039	670	20	646	31	490	140	1.0	3.7
MD01-32_2 – 67	205	0.1169	0.0047	1.020	0.330	0.36	0.0628	0.0130	713	27	710	87	665	190	0.0	0.4
MD01-32_2 – 68	181	0.07692	0.0022	0.607	0.028	0.02	0.0567	0.0026	478	13	479	18	443	99	0.1	0.3
MD01-32_2 – 69	108	0.0775	0.0022	0.608	0.038	0.09	0.0567	0.0035	481	13	477	23	400	120	0.2	0.9
MD01-32_2 – 70	215	0.0767	0.0024	0.798	0.038	0.31	0.0750	0.0034	476	14	590	24	990	120	0.4	19.3
MD01-32_2 – 71	398	0.0733	0.0039	0.644	0.036	0.48	0.0620	0.0026	456	23	503	20	640	91	1.9	9.3
MD01-32_2 – 72	126	0.0819	0.0028	0.632	0.039	0.32	0.0561	0.0033	507	17	496	25	370	120	0.2	2.2

generally have lower LREE/HREE ratios accompanied by little or no Eu anomalies (Cullers, 1994). The samples examined generally show high $(LREE/HREE)_{CN}$ ratios (0.8 to 14.5 with the mean value of 8.7) and moderate to strong negative Eu_{CN} anomalies (1.34 to 18.94 with the mean value of 2.46, Fig. 7c, d).

In summary, the ratios of La/Sc, Th/Sc, Th/Co, Zr concentration and the REE distribution patterns of the studied sedimentary successions from the KMB and DMC indicate that they were generally derived from a felsic source and, as shown by the Eu anomaly, the Zr/Sc ratio and Zr concentration, they were not significantly affected by alteration during transport (Cullers, 1994; Cullers, 2000).

4.c. Tectonic setting of deposition

Several diagrams allow for the identification of the tectonic setting of a source region (e.g. Bhatia, 1983; Roser &Korsch, 1986). However, unravelling the tectonic setting of the deposition of metamorphosed sedimentary sequences should rely on immobile trace elements. Therefore, we first applied the ternary plots Sc-Th-Zr, Th-Co-Zr and Th-La-Sc of Bhatia and Crook (1986). These plots show that the samples analysed have a typical trace element composition of sediments derived from erosion of the continental arc or active continental margin (Fig. 11e–g). However, as shown by Verma and Armstrong-Altrin (2013), major elements can also provide reliable information on the tectonic setting of the sedimentary basin. They proposed two new discriminant functions based on major elements for the tectonic discrimination of siliciclastic sediments and suggested that the functions are insensitive to element mobility. Indeed, the studied metasedimentary rocks have the chemical composition of the major element typical of arc-related sandstones demonstrating the usefulness of this technique even for metamorphosed rock suites (Fig. 11h).

In summary, the chemical composition of the mica schists and paragneisses from the KMB and DMC, in terms of main and trace elements, is typical of sediments derived from erosion of suprasubduction complexes.

4.d. Age of deposition of the KMB and DMC volcano-sedimentary succession

The youngest prominent density peaks defined by detrital zircon grains in the mica schists of the KMB (samples PK007 and PK023) range from 610 to 600 Ma (Fig. 12a, b). However, both samples reveal less prominent density peaks at 540 (sample PK007) and 520 Ma (sample PK023) (Fig. 12a, b). On the other hand, paragneiss samples from the DMC (samples MD01-32 and MD04-01) have the youngest prominent density peaks at 480–470 Ma (Fig. 12c, d). Consequently, these peaks represent the youngest graphical age peaks controlled by more than one grain and could therefore be interpreted as MDAs for these samples (Dickinson & Gehrels, 2009) (Fig. 12a–d). However, we additionally calculated MDA using the mean age of the youngest two or more grains that overlap in age at 1σ (Dickinson & Gehrels, 2009). Using this approach, the MDA for sample PK007 is 528.8 ± 8.8 Ma (MSWD = 1.02), 529 ± 19 Ma (MSWD = 1.4) for sample PK023, 468 ± 27 (MSWD 2.3) for sample MD04 and 455.7 ± 7.4 (MSWD = 0.27) for sample MD01. The only prominent peak documented in the metarhyolite sample from the KMB has an age of 510 Ma and is interpreted as a magmatic age (Fig. 12e). Considering the differences between the MDAs calculated by the two methods, we finally decided to use the ages calculated using the

https://doi.org/10.1017/S0016756823000523 Published online by Cambridge University Press

Table 6. Laser ablation ICP-MS U–Pb isotopic data of detrital zircons from sample MD04-01

		Isotopic ratios							Ages [Ma]						Approximate	
Sample	^{238}U cps*1000	^{206}Pb/^{238}U	2SE	^{207}Pb/^{235}U	2SE	Rho	^{207}Pb/^{206}Pb	2SE	^{206}Pb/^{238}U	2SE	^{207}Pb/^{235}U	2SE	^{207}Pb/^{206}Pb	2SE	Th/U	Disc.%
MD04-1 – 1	148	0.07658	0.0022	0.623	0.033	0.22	0.0585	0.0023	476	13	490	21	504	86	0.4	2.9
MD04-1 – 2	276	0.0762	0.0021	0.609	0.030	0.06	0.0574	0.0021	474	13	482	19	470	80	0.7	1.6
MD04-1 – 3	88	0.102	0.003	0.804	0.045	0.10	0.0573	0.0027	626	17	596	26	430	99	1.1	5.0
MD04-1 – 4	316	0.08571	0.0024	0.678	0.029	0.17	0.0573	0.0014	530	14	526	17	489	55	0.6	0.8
MD04-1 – 5	134	0.07399	0.0021	0.605	0.033	0.17	0.0591	0.0026	460	13	476	21	510	95	0.1	3.3
MD04-1 – 6	109	0.1042	0.003	0.933	0.048	0.23	0.0638	0.0025	639	18	664	25	670	87	0.7	3.8
MD04-1 – 7	107	0.1018	0.0037	0.833	0.044	0.19	0.0591	0.0025	625	22	609	27	490	89	1.1	2.6
MD04-1 – 8	212	0.0651	0.002	0.721	0.036	0.07	0.0796	0.0028	407	12	549	22	1163	72	0.2	25.9
MD04-1 – 9	65	0.3491	0.0098	5.990	0.250	0.36	0.1232	0.0028	1930	47	1966	37	1985	41	0.7	1.8
MD04-1 – 10	57	0.4123	0.012	7.880	0.320	0.25	0.1368	0.0031	2224	53	2212	37	2172	40	0.7	0.5
MD04-1 – 11	508	0.05417	0.0016	0.617	0.027	0.10	0.0818	0.0025	340	10	486	17	1208	69	0.2	30.0
MD04-1 – 12	61	0.0807	0.0025	0.612	0.044	0.16	0.0553	0.0037	500	15	476	30	320	140	0.4	5.1
MD04-1 – 13	169	0.1087	0.003	0.969	0.043	0.16	0.0631	0.0020	665	17	682	23	640	76	0.5	2.5
MD04-1 – 14	201	0.05632	0.0016	0.406	0.022	0.21	0.0514	0.0024	353	10	343	17	210	94	0.3	3.0
MD04-1 – 15	52	0.3365	0.0097	5.690	0.230	0.24	0.1222	0.0029	1869	47	1924	35	1970	43	0.8	2.9
MD04-1 – 16	134	0.0827	0.0024	0.650	0.034	0.08	0.0570	0.0023	512	14	504	20	420	84	0.1	1.6
MD04-1 – 17	97	0.0841	0.0025	0.657	0.039	0.21	0.0563	0.0027	521	15	507	24	390	100	0.2	2.7
MD04-1 – 18	114	0.0935	0.0027	0.764	0.038	0.16	0.0590	0.0022	576	16	572	22	512	81	0.7	0.7
MD04-1 – 19	114	0.0762	0.0023	0.621	0.038	0.05	0.0590	0.0031	473	13	485	23	490	110	0.2	2.4
MD04-1 – 20	166	0.0846	0.0027	0.676	0.039	0.05	0.0572	0.0023	524	16	520	23	440	85	0.1	0.7
MD04-1 – 21	136	0.0926	0.0027	0.769	0.038	0.05	0.0604	0.0023	571	16	575	22	557	82	1.3	0.7
MD04-1 – 22	138	0.07947	0.0023	0.624	0.033	0.08	0.0568	0.0024	493	14	488	21	420	93	0.4	1.0
MD04-1 – 23	109	0.0979	0.0029	0.805	0.043	0.11	0.0595	0.0025	602	17	594	24	516	91	1.2	1.4
MD04-1 – 24	43	0.1531	0.0046	1.460	0.089	0.07	0.0691	0.0036	918	26	899	37	810	110	0.5	2.1
MD04-1 – 25	110	0.0858	0.0026	0.711	0.043	0.04	0.0605	0.0030	531	15	546	26	550	110	0.6	2.8
MD04-1 – 26	82	0.1591	0.0046	1.780	0.088	0.21	0.0818	0.0030	952	26	1033	32	1170	76	0.8	7.8
MD04-1 – 27	413	0.0863	0.0024	0.721	0.033	0.32	0.0589	0.0020	534	14	549	20	530	70	0.5	2.8
MD04-1 – 28	107	0.079	0.0023	0.589	0.033	0.11	0.0538	0.0025	490	14	468	20	312	99	0.1	4.7
MD04-1 – 29	62	0.4097	0.012	8.970	0.350	0.35	0.1579	0.0030	2215	55	2330	36	2422	33	1.0	4.9
MD04-1 – 30	196	0.1304	0.0036	1.206	0.047	0.06	0.0672	0.0014	790	21	801	22	815	42	0.5	1.4

(*Continued*)

Table 6. (*Continued*)

		Isotopic ratios							Ages [Ma]						Approximate	
Sample	^{238}U cps*1000	^{206}Pb/^{238}U	2SE	^{207}Pb/^{235}U	2SE	Rho	^{207}Pb/^{206}Pb	2SE	^{206}Pb/^{238}U	2SE	^{207}Pb/^{235}U	2SE	^{207}Pb/^{206}Pb	2SE	Th/U	Disc.%
MD04-1 – 31	50	0.2982	0.0092	4.380	0.190	0.05	0.1070	0.0031	1682	47	1700	38	1720	54	0.9	1.1
MD04-1 – 32	152	0.1267	0.0035	1.169	0.052	0.06	0.0666	0.0020	769	20	782	24	787	63	1.5	1.7
MD04-1 – 33	360	0.09146	0.0026	0.728	0.030	0.11	0.0575	0.0014	564	15	555	18	493	55	0.8	1.6
MD04-1 – 34	256	0.0923	0.0028	0.862	0.043	0.10	0.0670	0.0024	569	16	628	23	789	80	1.1	9.4
MD04-1 – 35	64	0.097	0.0032	0.813	0.054	0.11	0.0602	0.0037	597	19	594	31	500	130	0.6	0.5
MD04-1 – 36	121	0.1002	0.0029	1.010	0.071	0.05	0.0730	0.0047	616	17	696	35	880	120	0.4	11.5
MD04-1 – 37	175	0.1596	0.0043	1.643	0.065	0.31	0.0728	0.0018	955	24	983	27	983	54	1.1	2.8
MD04-1 – 38	106	0.1424	0.004	1.322	0.063	0.08	0.0675	0.0024	858	23	852	28	799	75	0.9	0.7
MD04-1 – 39	414	0.09859	0.0027	0.820	0.033	0.27	0.0599	0.0013	606	16	607	19	579	49	1.0	0.1
MD04-1 – 40	53	0.1049	0.0032	0.905	0.054	0.03	0.0629	0.0033	643	18	646	28	610	110	0.3	0.5
MD04-1 – 41	39	0.078	0.0025	0.655	0.061	0.00	0.0613	0.0055	484	15	493	38	420	180	0.9	1.8
MD04-1 – 42	177	0.2789	0.0079	4.259	0.160	0.22	0.1086	0.0017	1585	40	1682	32	1773	29	0.5	5.8
MD04-1 – 43	30	0.0779	0.0029	0.653	0.065	0.03	0.0603	0.0054	483	18	490	41	430	190	1.6	1.4
MD04-1 – 44	735	0.05989	0.0016	0.610	0.023	0.21	0.0733	0.0014	375	10	483.1	15	1012	38	0.1	22.4
MD04-1 – 45	35	0.0981	0.0033	1.490	0.130	0.02	0.1110	0.0086	603	19	892	59	1530	190	0.5	32.4
MD04-1 – 46	139	0.1358	0.0038	1.259	0.056	0.04	0.0673	0.0021	821	22	825	26	802	68	0.2	0.5
MD04-1 – 47	167	0.0868	0.0026	0.714	0.098	0.09	0.0593	0.0071	537	15	543	45	522	160	0.5	1.2
MD04-1 – 48	199	0.1831	0.0057	2.249	0.091	0.47	0.0891	0.0016	1084	32	1194	32	1395	37	0.1	9.2
MD04-1 – 49	62	0.1403	0.0042	1.290	0.070	0.23	0.0665	0.0028	846	24	832	31	762	87	0.7	1.7
MD04-1 – 50	99	0.0794	0.0024	0.606	0.038	0.07	0.0554	0.0030	493	14	475	24	340	110	0.3	3.7
MD04-1 – 51	73	0.3592	0.011	6.120	0.250	0.12	0.1221	0.0028	1978	53	1989	37	1973	41	1.2	0.6
MD04-1 – 52	193	0.07359	0.0021	0.580	0.029	0.20	0.0572	0.0021	458	13	462	19	447	81	0.4	0.9
MD04-1 – 53	92	0.3114	0.009	5.050	0.200	0.28	0.1167	0.0023	1747	44	1823	34	1891	36	0.6	4.2
MD04-1 – 54	66	0.0902	0.0028	0.731	0.048	0.08	0.0595	0.0036	556	16	555	30	480	130	0.1	0.3
MD04-1 – 55	391	0.0958	0.0026	0.980	0.047	0.39	0.0738	0.0026	590	15	692	23	1035	58	0.4	14.8
MD04-1 – 56	122	0.0944	0.0029	0.786	0.039	0.01	0.0606	0.0026	582	17	583	22	590	83	0.8	0.2
MD04-1 – 57	41	0.1761	0.0053	1.853	0.100	0.00	0.0761	0.0035	1045	29	1051	37	1020	100	0.7	0.6
MD04-1 – 58	77	0.2257	0.0067	2.600	0.130	0.11	0.0841	0.0028	1311	35	1299	35	1252	65	0.5	0.9
MD04-1 – 59	82	0.1031	0.003	1.083	0.066	0.15	0.0763	0.0039	632	18	738	32	1010	110	0.6	14.3
MD04-1 – 60	238	0.0871	0.0024	0.716	0.035	0.02	0.0594	0.0022	538	15	545	21	531	81	0.6	1.3
MD04-1 – 61	221	0.0895	0.0026	0.719	0.031	0.17	0.0582	0.0016	553	15	550	19	513	62	0.6	0.5

(*Continued*)

Table 6. (*Continued*)

MD04-1 – 62	226	0.0987	0.0031	0.903	0.039	0.00	0.0662	0.0027	607	19	651	21	779	73	0.2	6.8
MD04-1 – 63	124	0.0983	0.003	0.847	0.040	0.12	0.0626	0.0020	605	17	617	22	630	67	0.7	2.0
MD04-1 – 64	169	0.0798	0.0023	0.657	0.031	0.11	0.0586	0.0022	495	14	509	20	500	88	0.4	2.7
MD04-1 – 65	55	0.0941	0.0029	0.747	0.048	0.04	0.0588	0.0035	580	17	568	31	460	130	0.5	2.1
MD04-1 – 66	165	0.1018	0.0029	0.952	0.044	0.05	0.0677	0.0024	625	17	674	24	801	75	0.6	7.3
MD04-1 – 67	50	0.0983	0.003	0.862	0.061	0.07	0.0637	0.0040	604	17	617	34	590	140	0.5	2.0
MD04-1 – 68	635	0.0619	0.0017	0.728	0.030	0.12	0.0845	0.0023	387	10	554.6	19	1298	50	0.4	30.2
MD04-1 – 69	771	0.07542	0.0027	0.973	0.054	0.32	0.0914	0.0022	469	16	689	25	1440	40	0.1	32.0
MD04-1 – 70	218	0.0871	0.0025	0.831	0.033	0.09	0.0680	0.0020	538	15	610	20	810	65	0.8	11.8
MD04-1 – 71	2151	0.04829	0.0014	2.043	0.080	0.52	0.3044	0.0032	304	9	1129.1	25	3490	16	0.1	73.1
MD04-1 – 72	491	0.08029	0.003	0.747	0.034	0.31	0.0648	0.0014	498	18	565	19	771	52	0.1	11.9
MD04-1 – 73	27	0.5162	0.018	13.900	0.630	0.22	0.1962	0.0045	2681	80	2736	49	2777	39	0.4	2.0
MD04-1 – 74	668	0.0554	0.0018	0.802	0.031	0.29	0.1027	0.0027	348	11	597	18	1658	54	0.3	41.8
MD04-1 – 75	219	0.0765	0.0022	0.614	0.031	0.01	0.0572	0.0028	475	13	483	19	450	92	0.3	1.7
MD04-1 – 76	139	0.0961	0.0027	0.794	0.040	0.09	0.0598	0.0023	592	16	589	23	535	82	0.6	0.4
MD04-1 – 77	53	0.2858	0.0082	4.910	0.210	0.26	0.1225	0.0033	1620	41	1794	38	1977	51	1.1	9.7
MD04-1 – 78	583	0.08679	0.0024	0.794	0.033	0.12	0.0661	0.0017	537	14	591	19	776	55	0.5	9.2
MD04-1 – 79	27	0.1747	0.0051	1.550	0.095	0.07	0.0650	0.0035	1037	28	929	36	630	110	0.6	11.6
MD04-1 – 80	52	0.0769	0.0026	0.594	0.044	0.07	0.0563	0.0038	477	15	464	28	360	140	0.7	2.8
MD04-1 – 81	268	0.06638	0.0019	0.953	0.047	0.05	0.1037	0.0037	414	11	675	25	1662	67	0.2	38.6
MD04-1 – 82	320	0.1135	0.0032	1.201	0.049	0.23	0.0762	0.0018	693	19	798	23	1077	47	0.2	13.1
MD04-1 – 83	262	0.1204	0.0039	1.147	0.056	0.00	0.0679	0.0020	733	22	773	26	828	61	0.5	5.2
MD04-1 – 84	420	0.05476	0.0015	0.410	0.019	0.15	0.0542	0.0016	344	9	347.9	14	344	67	0.0	1.2
MD04-1 – 85	106	0.104	0.0031	0.867	0.045	0.21	0.0601	0.0023	638	18	632	24	570	77	0.6	0.9
MD04-1 – 86	40	0.0823	0.0028	0.882	0.067	0.17	0.0761	0.0051	510	16	627	35	970	140	0.7	18.7
MD04-1 – 87	382	0.0937	0.0028	0.911	0.040	0.23	0.0700	0.0019	577	16	656	23	908	58	0.9	12.0
MD04-1 – 88	104	0.0987	0.003	0.873	0.047	0.16	0.0643	0.0031	607	17	631	26	660	100	1.7	3.8
MD04-1 – 89	167	0.09231	0.0026	0.740	0.036	0.11	0.0580	0.0020	569	15	559	21	480	74	1.0	1.8
MD04-1 – 90	195	0.4307	0.012	9.680	0.360	0.32	0.1632	0.0018	2309	57	2403	37	2485	19	0.1	3.9
MD04-1 – 91	31	0.3266	0.0098	5.750	0.260	0.19	0.1264	0.0041	1821	48	1936	41	2045	55	3.1	5.9
MD04-1 – 92	48	0.0762	0.0024	0.663	0.048	0.08	0.0624	0.0042	473	14	504	30	540	140	1.8	6.2
MD04-1 – 93	60	0.0924	0.0027	0.811	0.055	0.13	0.0634	0.0037	569	16	596	30	600	130	0.6	4.5
MD04-1 – 94	193	0.0797	0.0024	1.538	0.077	0.23	0.1405	0.0051	494	15	943	37	2219	86	0.0	47.6

(*Continued*)

Table 6. (*Continued*)

		Isotopic ratios							Ages [Ma]						Approximate	
Sample	^{238}U cps*1000	^{206}Pb/^{238}U	2SE	^{207}Pb/^{235}U	2SE	Rho	^{207}Pb/^{206}Pb	2SE	^{206}Pb/^{238}U	2SE	^{207}Pb/^{235}U	2SE	^{207}Pb/^{206}Pb	2SE	Th/U	Disc.%
MD04-1 – 95	146	0.0872	0.008	0.711	0.130	0.23	0.0566	0.0037	539	45	541	53	450	100	0.0	0.4
MD04-1 – 96	88	0.0763	0.0026	0.567	0.039	0.18	0.0542	0.0027	474	15	462	25	310	110	0.8	2.6
MD04-1 – 97	664	0.07347	0.002	0.607	0.024	0.17	0.0590	0.0014	457	12	481	16	558	53	0.1	5.0
MD04-1 – 98	324	0.0944	0.0026	0.797	0.037	0.12	0.0603	0.0019	582	15	593	21	581	66	1.9	1.9
MD04-1 – 99	275	0.0711	0.0022	0.576	0.027	0.37	0.0586	0.0018	443	13	461	18	520	70	0.1	4.0
MD04-1 – 100	135	0.1014	0.003	0.872	0.041	0.09	0.0622	0.0020	622	18	633	22	647	72	1.4	1.7
MD04-1 – 101	38	0.0971	0.0031	0.815	0.062	0.12	0.0616	0.0045	597	18	595	35	510	160	1.1	0.3
MD04-1 – 102	149	0.078	0.0023	0.644	0.033	0.19	0.0597	0.0023	484	14	501	20	529	84	0.2	3.4
MD04-1 – 103	430	0.0985	0.0028	1.192	0.049	0.18	0.0867	0.0020	606	17	795	24	1346	47	0.1	23.8
MD04-1 – 104	433	0.0684	0.0021	0.603	0.028	0.69	0.0632	0.0014	426	13	477	17	699	50	0.1	10.6
MD04-1 – 105	290	0.0669	0.002	1.334	0.074	0.13	0.1432	0.0061	418	12	858	38	2244	100	0.3	51.3
MD04-1 – 106	82	0.0912	0.0027	0.798	0.046	0.02	0.0636	0.0031	563	16	589	26	655	98	0.4	4.5
MD04-1 – 107	13	0.1238	0.0061	1.140	0.099	0.13	0.0668	0.0055	751	35	731	52	590	180	0.4	2.7
MD04-1 – 108	125	0.0691	0.0022	0.872	0.063	0.03	0.0915	0.0049	431	13	631	32	1380	97	0.7	31.8
MD04-1 – 109	310	0.07004	0.0021	0.558	0.037	0.15	0.0580	0.0023	436	12	452	22	515	78	0.6	3.5
MD04-1 – 110	114	0.308	0.014	6.520	0.360	0.45	0.1529	0.0026	1730	66	2051	40	2372	30	0.3	15.7
MD04-1 – 111	56	0.1061	0.0032	0.856	0.055	0.26	0.0581	0.0031	650	19	618	31	440	120	0.7	5.1
MD04-1 – 112	136	0.1105	0.0031	1.020	0.048	0.13	0.0667	0.0022	676	18	712	23	793	67	0.6	5.1
MD04-1 – 113	212	0.1007	0.0028	0.858	0.046	0.12	0.0610	0.0027	618	17	625	25	580	87	1.4	1.1
MD04-1 – 114	330	0.0694	0.0019	0.702	0.035	0.22	0.0725	0.0032	433	12	538	21	993	77	0.7	19.6
MD04-1 – 115	328	0.08199	0.0024	0.641	0.029	0.27	0.0560	0.0017	508	14	501	18	431	67	0.2	1.4
MD04-1 – 116	386	0.0636	0.0034	0.542	0.045	0.13	0.0600	0.0026	397	20	438	27	630	99	0.2	9.3
MD04-1 – 117	498	0.05509	0.0015	0.500	0.022	0.28	0.0659	0.0019	346	9	410.5	15	781	63	0.0	15.8
MD04-1 – 118	446	0.06681	0.0018	0.613	0.026	0.24	0.0663	0.0018	417	11	484	16	798	61	0.1	13.9
MD04-1 – 119	95	0.0818	0.0026	0.780	0.042	0.00	0.0696	0.0030	507	15	580	24	850	93	0.7	12.6
MD04-1 – 120	502	0.05999	0.0016	0.579	0.027	0.17	0.0697	0.0021	376	10	462	17	891	63	0.0	18.7
MD04-1 – 121	34	0.3641	0.011	7.940	0.340	0.16	0.1586	0.0043	2000	51	2216	40	2419	47	0.4	9.7
MD04-1 – 122	265	0.1016	0.0028	0.903	0.039	0.31	0.0629	0.0020	624	16	651	22	701	62	0.8	4.2
MD04-1 – 123	153	0.0772	0.0022	0.853	0.099	0.07	0.0797	0.0098	480	13	619	45	1100	150	0.1	22.5
MD04-1 – 124	119	0.0892	0.0026	0.919	0.049	0.05	0.0747	0.0033	551	15	656	26	980	94	1.2	16.1
MD04-1 – 125	390	0.0873	0.0024	0.728	0.029	0.40	0.0594	0.0014	539	14	554	17	578	49	0.4	2.7
MD04-1 – 126	258	0.0843	0.0025	0.720	0.029	0.15	0.0622	0.0018	522	15	549	18	652	56	0.4	5.0
MD04-1 – 127	42	0.0973	0.003	0.825	0.065	0.08	0.0615	0.0044	598	18	608	34	570	140	1.2	1.6
MD04-1 – 128	146	0.1038	0.0039	1.012	0.080	0.26	0.0697	0.0068	636	23	707	36	860	130	1.2	10.0

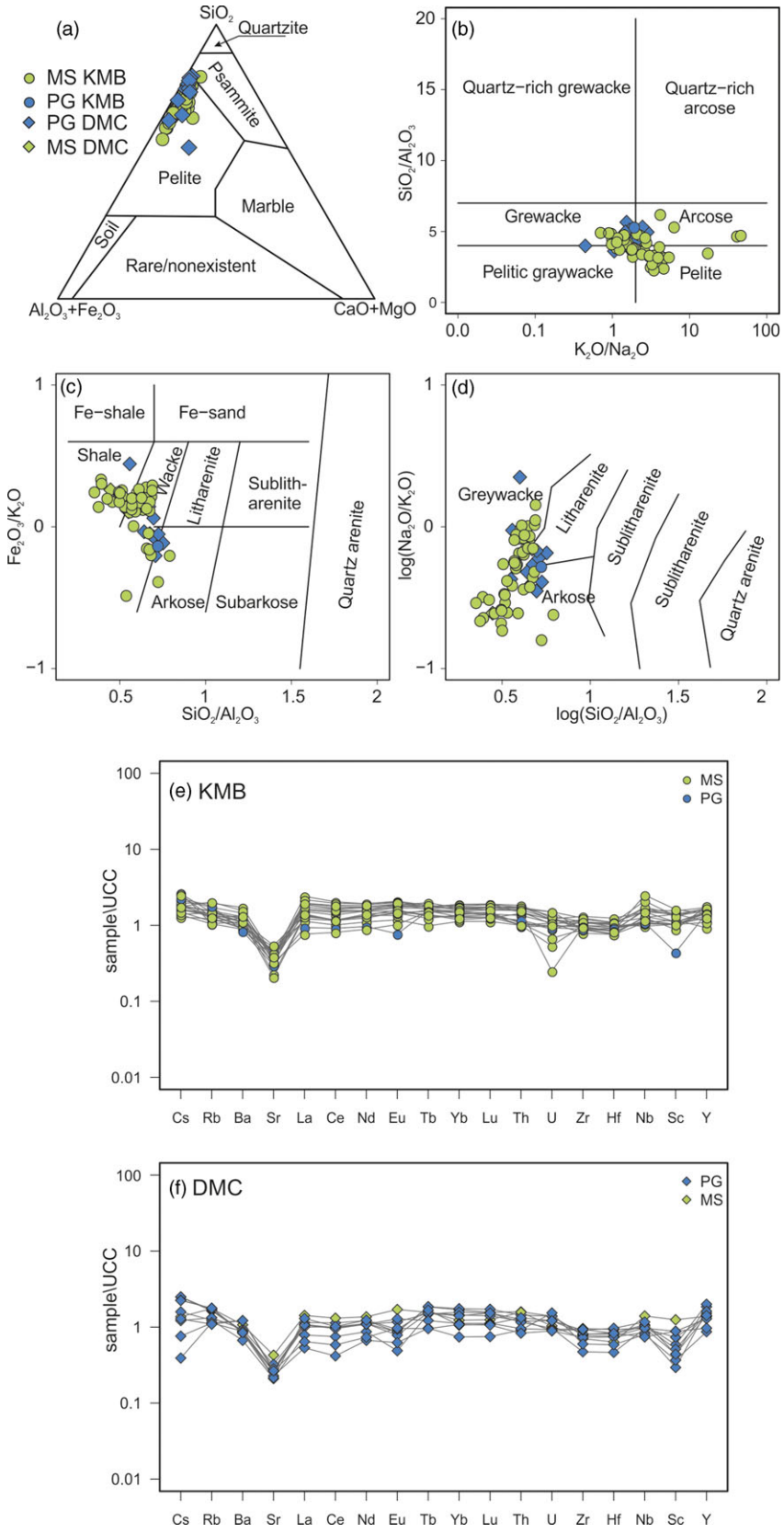

Figure 5. (Colour online) Geochemical characteristics of the studied metasedimentary rocks from the Kamieniec Metamorphic Belt and the Doboszowice Metamorphic Complex. (a–d) Classification diagrams after (a) Hasterok *et al.* (2018), (b) Wimmenauer (1984), (c) Herron (1988) and (d) Pettijohn *et al.* (1987). (c, d) Upper continental crust (UCC)-normalized major element pattern for investigated samples from the Kamieniec Metamorphic Belt and the Doboszowice Metamorphic Complex. Normalization factors after Taylor and McLennan (1995). MS – mica schists, PG – paragneisses.

mean age of the youngest two or more grains that overlap in age at 1σ. Consequently, the results presented suggest that the studied volcano-sedimentary successions exposed in the eastern part of the Fore-Sudetic Block may represent two different rock sequences in terms of MDA. The mica schists exposed in the KMB show an early Cambrian MDA at c. 529 Ma, whereas the paragneiss of the DMC

https://doi.org/10.1017/S0016756823000523 Published online by Cambridge University Press

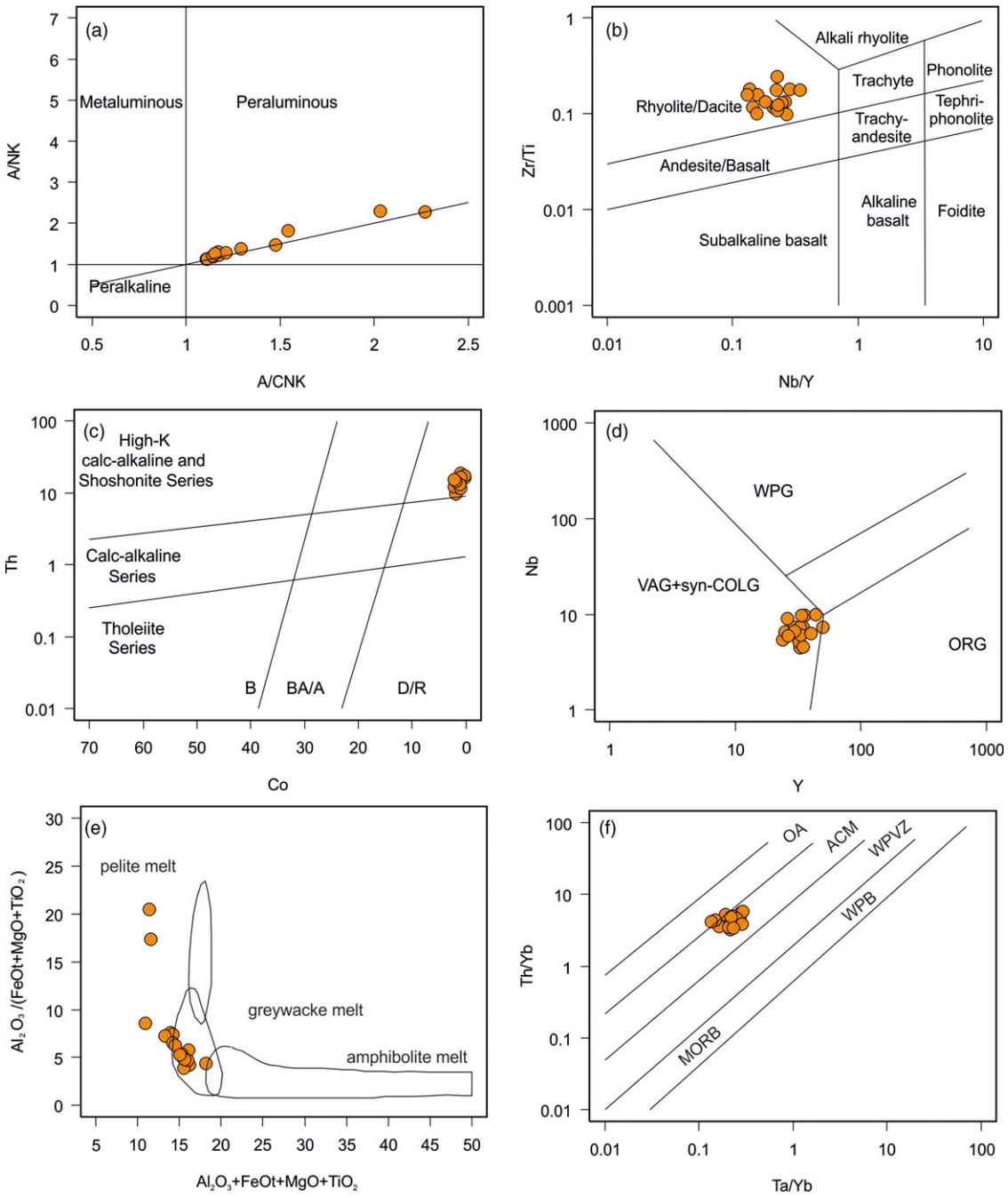

Figure 6. (Colour online) Geochemical data for the meta-rhyolites of the Kamieniec Metamorphic Belt. (a) Aluminousity diagram of Shand (1943) with divisions after Maniar and Piccoli (1989). (b) Zr/Ti–Nb/Y classification diagram of Winchester and Floyd (1977). (c) Th–Co classification diagram of Hastie *et al.* (2007). (d) Nb–Y discrimination diagram of Pearce *et al.* (1984). ORG – orogenic granites, syn-COLG – syn-collisional granites, VAG – volcanic arc granites, WPG – within-plate granites. (e) Meta-rhyolites plotted against fields for granitic liquids experimentally derived from pelites, greywackes and amphibolites (data from Patiño Douce (1999) compiled by Jung *et al.* 2009). (f) Th/Yb–Ta/Yb geotectonic classification diagram of Gorton and Schandl (2000). OA – oceanic arcs, ACM – active continental margins, WPVZ – within-plate volcanic zones, WPB – within-plate basalts, MORB – mid-ocean ridge basalts. See text.

represent an Upper Ordovician sequence with a MDA of c. 456 Ma. In addition, an early Cambrian sequence of the KMB was injected by several rhyolitic sills at c. 510 Ma. Our interpretation of the studied metarhyolites as sills is supported by their very consistent chemical composition and consistent textural features, with no evidence of, for example, degassing. This allows us to reject the suggestion that the metarhyolites represent tuffs or lava flows as suggested by Dziedzicowa (1966). Moreover, it should be emphasized that younger age peaks documented for samples PK023 and MD04 are mostly defined by dark grains or thin dark rims formed due to metamorphism (Fig. 12b, c, see section 4.h.).

Our estimate of MDA of the mica schists from the KMB and Chałupki paragneiss form the DMC is c. 30 Ma younger compared to previously published maximum depositional ages (Oberc-Dziedzic *et al.* 2018; Jastrzębski *et al.* 2020; Jastrzębski *et al.* 2023). Consequently, in terms of a MDA, we interpret the volcano-sedimentary successions exposed in the KMB equivalent to the early Cambrian sedimentary sequences exposed in other parts of

https://doi.org/10.1017/S0016756823000523 Published online by Cambridge University Press

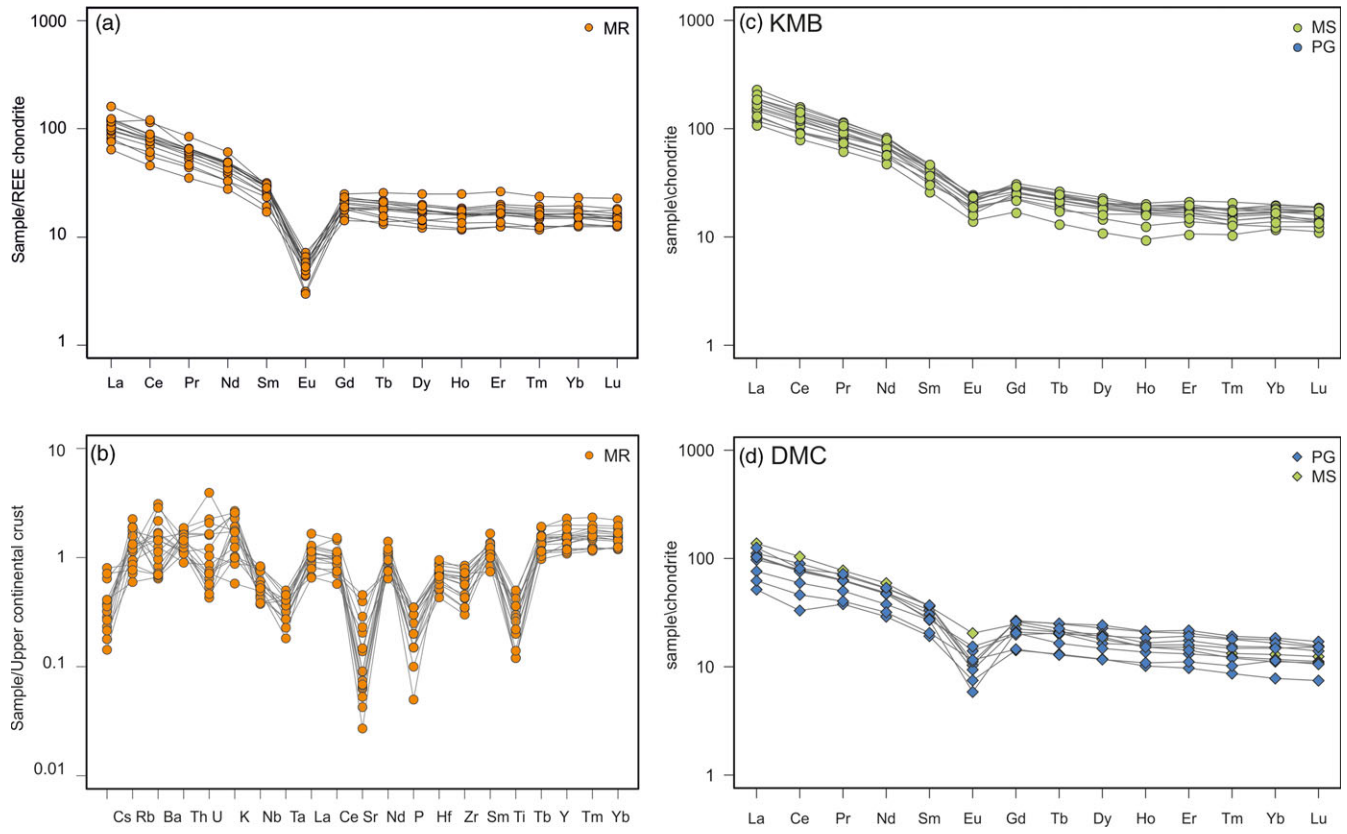

Figure 7. (Colour online) Trace element diagrams for the studied samples of meta-rhyolite and metasediments from the Kamieniec Metamorphic Belt: (a) REE patterns normalized to chondrite, (b) immobile incompatible elements normalized to primitive mantle. Normalization factor after Sun and McDonough (1989). Dark shaded area is for mica schists form the KMB, while light shaded area is for the Doboszowice paragneiss for the DMC, (c) chondrite-normalized REE patterns for investigated samples from (c) the Kamieniec Metamorphic Belt and (d) the Doboszowice Metamorphic Complex. Normalization factors after Sun and McDonough (1989). Symbols for metasedimentary rocks as in Fig. 5.

the Variscan belt of Europe. The early Cambrian succession exposed in the Central Sudetes is represented by metamorphosed pelites with supra-subduction geochemical signature (e.g. Szczepański & Ilnicki, 2014). On the other hand, the Upper Ordovician sequence exposed in the DMC has no equivalent in the Sudetes, but it was documented in the Teplá-Barrandian Unit (Drost *et al.* 2011). The only Ordovician sequence known from the Sudetes is of Early Ordovician in age and is often represented by metamorphosed quartzarenites showing geochemical signature typical of sediments deposited on a passive continental margin (e.g. Žáčková *et al.* 2010; Mazur *et al.* 2012; Szczepański & Ilnicki, 2014; Szczepański *et al.* 2020). However, similar to described from the DMC Ordovician paragneiss and mica schist lithologies with geochemical signature indicating erosion of supra-subduction rock complexes have recently been documented from the Teplá-Barrandian of the Bohemian Massif (Hajná *et al.* 2017; Soejono *et al.* 2020).

In conclusion, we suggest that the volcano-sedimentary successions of the KMB and DMC represent fragment of the early Palaeozoic siliciclastic cover deposited on the Gondwana margin.

4.e. Provenance constraints

Figure 13 compares the age spectra from the KMB and DMC with those from various cratonic areas of Gondwana.

The youngest age spectra defined by detrital grains recognized in the investigated rocks are typical of the Cambro-Ordovician sedimentary cover of the Cadomian crust exposed in the Sudetes and other parts of the Variscan belt of Europe (Figs. 12–14; e.g. Fernández-Suárez *et al.* 2002; Linnemann, 2007; Linnemann *et al.* 2008; Žáčková *et al.* 2010; Drost *et al.* 2011; Mazur *et al.* 2012; Košler *et al.* 2014; Strachan *et al.* 2014; Soejono *et al.* 2020). The youngest population of zircon grains recognized in the metasedimentary succession analysed from the DMC was probably derived from the erosion of Cambro-Ordovician granites widely exposed in the Saxothuringian (Zieger *et al.* 2018 and references therein), Teplá-Barradian (e.g. Žák *et al.* 2013) and Moldanubian zones (Žák *et al.* 2023). An example of such intrusion is the Doboszowice orthogneiss dated at 488 ± 6 Ma, which is exposed in the DMC (Mazur *et al.* 2010). Furthermore, zircon grains ranging in age from ca. 490 to 520 Ma were most likely supplied by Cambrian granites known from the Sudetes exemplified by, for example, Śnieżnik or Izera orthogneiss (e.g. Turniak *et al.* 2000; Lange *et al.* 2005; Mazur *et al.* 2010; Zieger *et al.* 2018). Neoproterozoic grains could have been derived from granitoid intrusions dated at c. 540 Ma that were reported from several fragments of Cadomian basement exposed in the Bohemian Massif (Linnemann & Heuse, 2001; Tichomirowa *et al.* 2001; Mingram *et al.* 2004; Żelaźniewicz *et al.* 2004; Jastrzębski *et al.* 2021; Tabaud *et al.* 2021; Śliwiński *et al.et al.* 2022; Soejono *et al.* 2022). However, several detrital zircons were most probably supplied by volcano-sedimentary successions represented by, for example, the Stronie and Młynowiec formations in the Orlica-Śnieżnik dome (Jastrzębski *et al.* 2010; Mazur *et al.* 2012; Mazur *et al.* 2015), the Zwethau and

https://doi.org/10.1017/S0016756823000523 Published online by Cambridge University Press

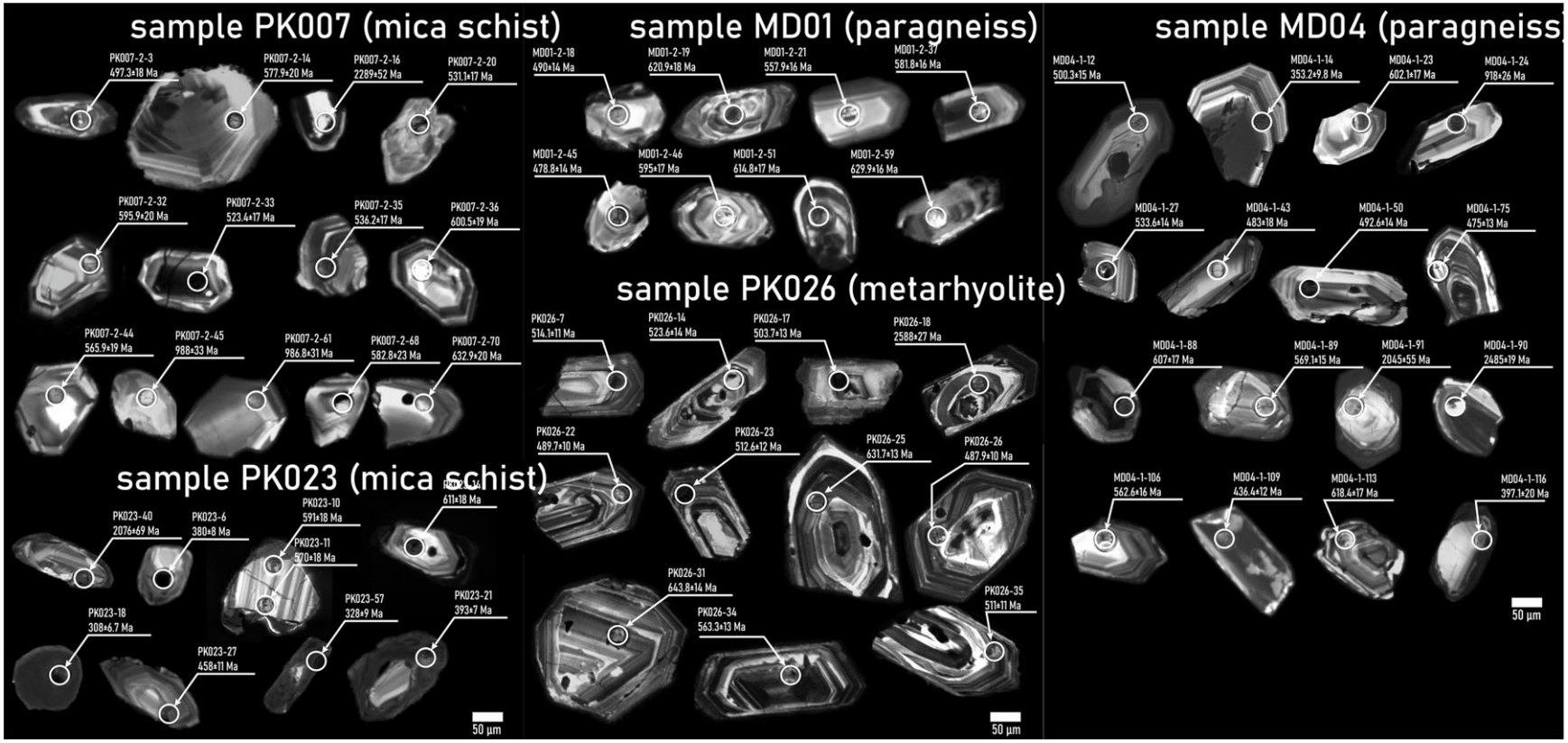

Figure 8. (Colour online) Examples of cathodo luminescence images of zircon grains from: (a) mica schists PK007 and PK023, (b) paragneiss MD01 and metarhyolite PK026 and (c) paragneiss MD04. Grain numbers and ages (Ma) refer to Tables 2–6; Uncertainties are 1σ.

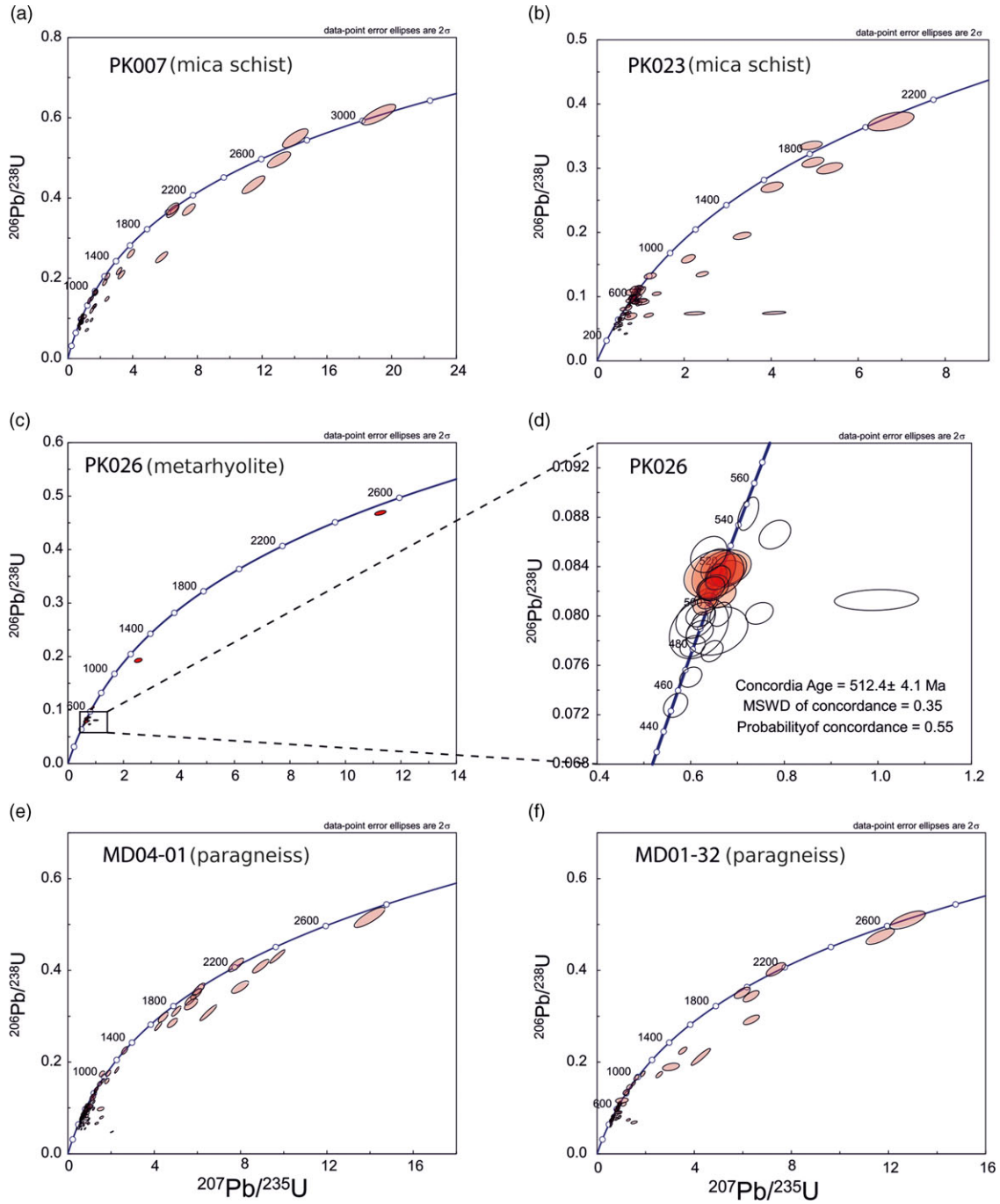

Figure 9. (Colour online) U–Pb Concordia diagrams for samples from the DMC and KMB. Concordia plots were done using the Isoplot/Ex 4.15 Excel add-in (Ludwig, 2008). (a) micaschist PK007, (b) micaschist PK023, (c, d) metarhyolite PK026, (e) paragneiss MD04-01 and (f) paragneiss MD01-32.

the Rothstein formations in the Saxohuringian zone (e.g. Elicki, 1997; Linnemann, 2007) or from glaciomarine sedimentary rocks documented in the Elbe zone and the North Saxon antiform in the southeastern part of the Saxothuringian zone (Linnemann *et al.* 2018). Consequently, the anhedral Neoproterozoic zircons documented in the studied rocks may represent recycled material supplied by local sedimentary successions. This may explain the low abundance of the oldest, Paleoproterozoic or Archean zircons, in the studied samples.

The detrital zircon age spectra clearly show the paucity of Mesoproterozic zircons pointing to a period of magmatic and volcanic inactivity in the source area, as there are only a few zircon grains of this age documented in the investigated rocks (Figs. 10 and 13). This Mesoproterozoic age gap in zircon age spectra is commonly reported from the West African Craton and from the Trans-Saharan Belt (e.g. Tuareg Shield) (Fig. 13). Interestingly, the Saharan Metacraton, Amazonia and Baltica can be excluded as a potential source of detritus, since these cratonic areas are characterized by the presence of Mesoproterozoic zircons (Fig. 13).

In summary, we suggest that the data presented here advocate for the West African provenance for the studied volcano-sedimentary

https://doi.org/10.1017/S0016756823000523 Published online by Cambridge University Press

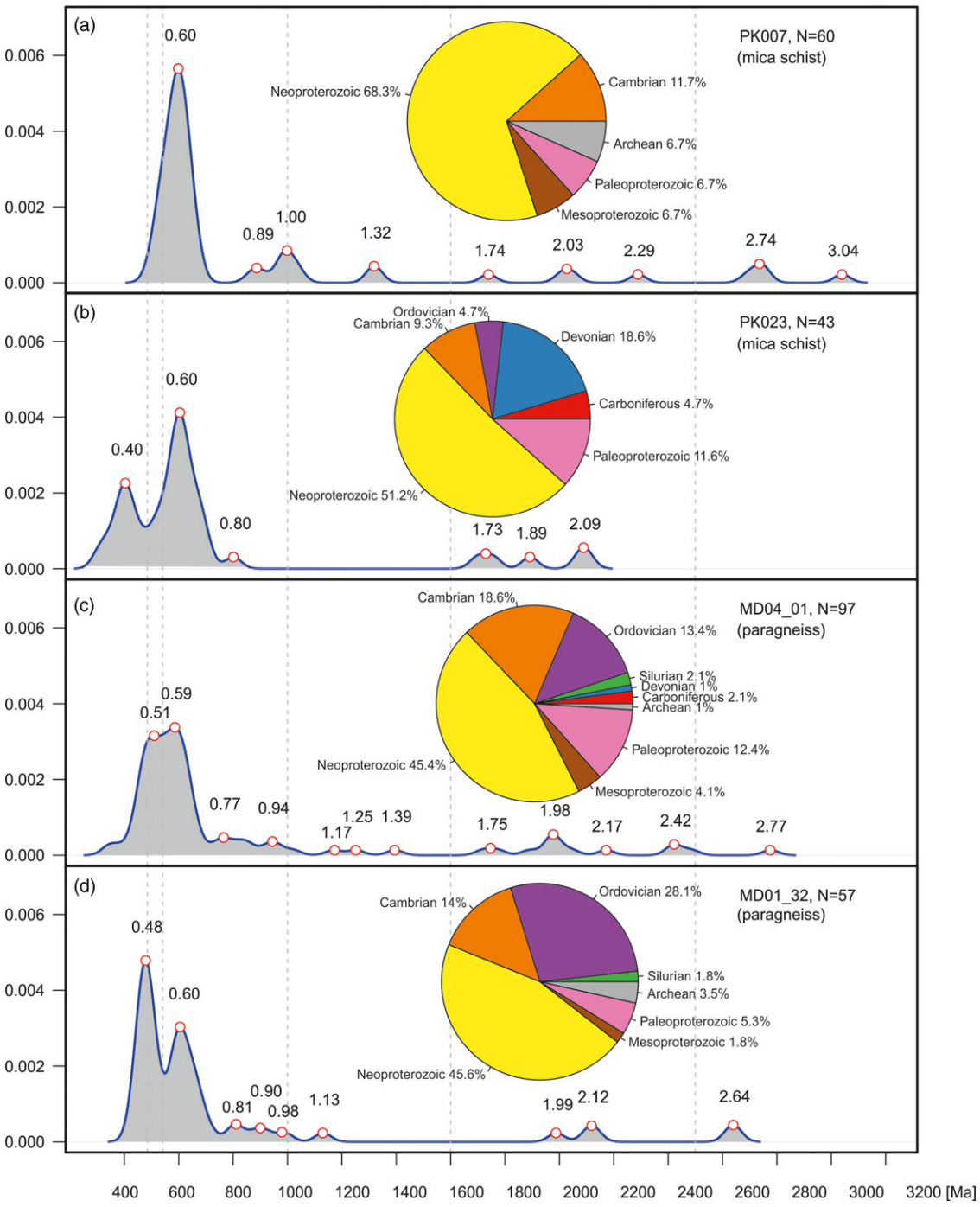

Figure 10. (Colour online) Binned frequency-density plots of detrital zircons from: (a–d) analysed samples (N = number of analyses). For zircons older than, 1 Ga ^{207}Pb/^{206}Pb ages were taken for interpretation and the ^{206}Pb/^{238}U ages for younger grains. Frequency-density plots were designed via the R software environment (R Core Team, 2021). KDE bandwidth is 30 Ma.

succession. Available detrital zircon ages from Cambro-Ordovician sedimentary successions covering the Saxothuringian, Teplá-Barrandian and Moldanubian zones as well as the Armorican Massif clearly indicate that all these Neoproterozoic crustal fragments were derived from the same cratonic areas and Cadomian arc-related basement located at the northern periphery of Gondwana (Figs. 13 and 14; corresponding references are given in Fig. 14). Consequently, we support suggestions that during the Cambro-Ordovician time, Cadomian crustal fragments were dispersed along the northern periphery of Gondwana, most probably forming an extended shelf that developed on a passive continental margin (e.g. Drost *et al.* 2011; Žák & Sláma 2018; Soejono *et al.* 2020; Collett *et al.* 2021; Tabaud *et al.* 2021; Tabaud *et al.* 2021; Collett *et al.* 2022).

4.f. Petrogenetic interpretation of the KMB volcanism

The zircons from metarhyolite sample are dominated by an age peak of 510 Ma that we correlate with the time of magmatic emplacement (Figs. 9c, d and 12e). Rare Neoproterozoic and

https://doi.org/10.1017/S0016756823000523 Published online by Cambridge University Press

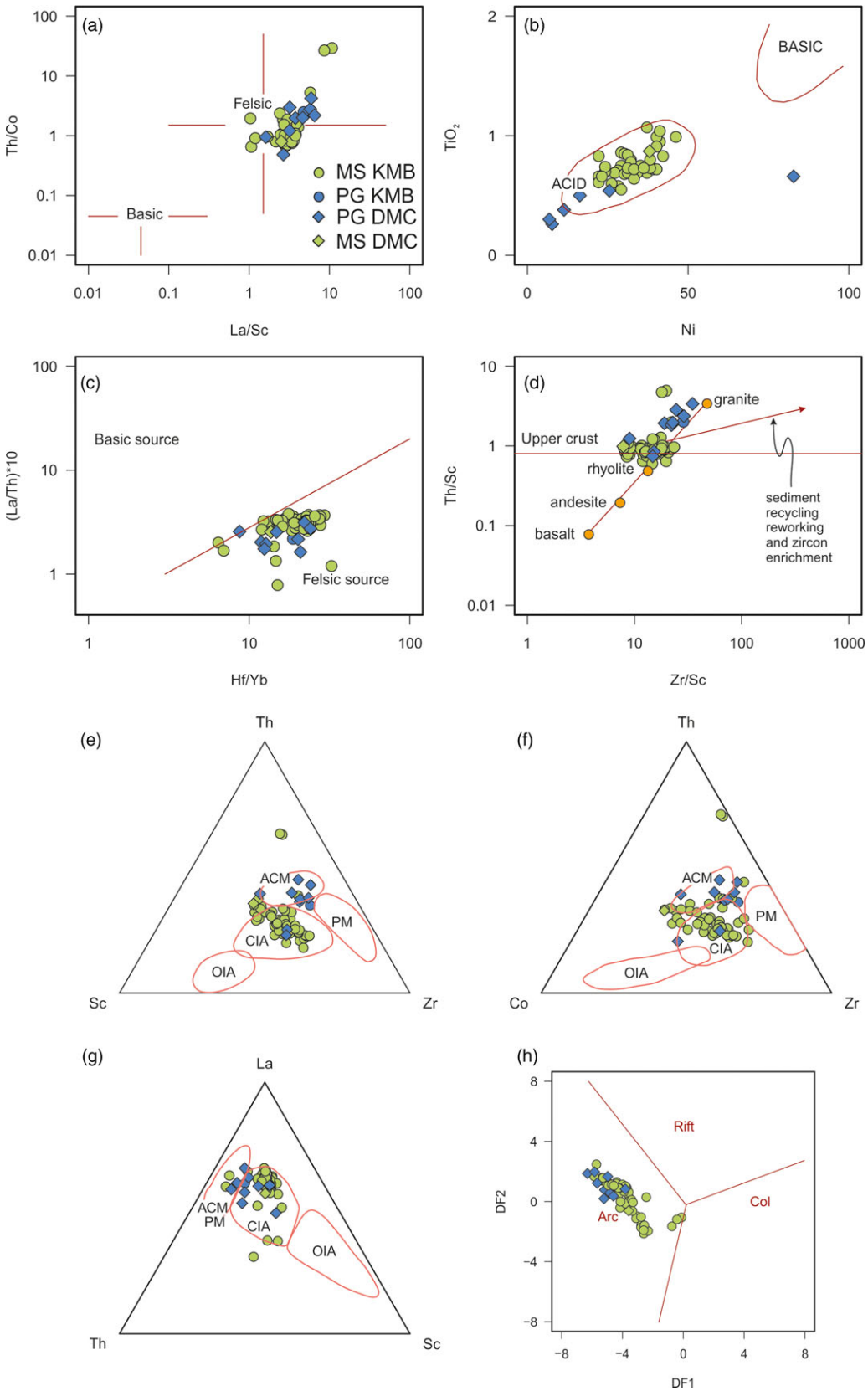

Figure 11. (Colour online) Diagrams illustrating lithology of the source area after (a) Cullers (2002), (b) Floyd *et al.* (1989), (c) Hladil *et al.* (2003) and (d) the influence of sediment recycling and zircon enrichment on chemical composition of the investigated quartzites after McLennan *et al.* (1993). (e, f) Discrimination diagrams showing tectonic setting of deposition of the protolith to the mica schists and paragneisses of the Kamieniec Metamorphic Belt and the Doboszowice Metamorphic Complex. (after Bhatia & Crook, 1986). Abbreviations: PM – passive margin, CIA – continental island arc, ACM – Active continental margin, OIA – oceanic island arc. d) Discriminant-function multi-dimensional diagram after Verma and Armstrong-Altrin (2013). Samples fall in the field typical of arc-related sediments. Symbols as in Fig. 5.

https://doi.org/10.1017/S0016756823000523 Published online by Cambridge University Press

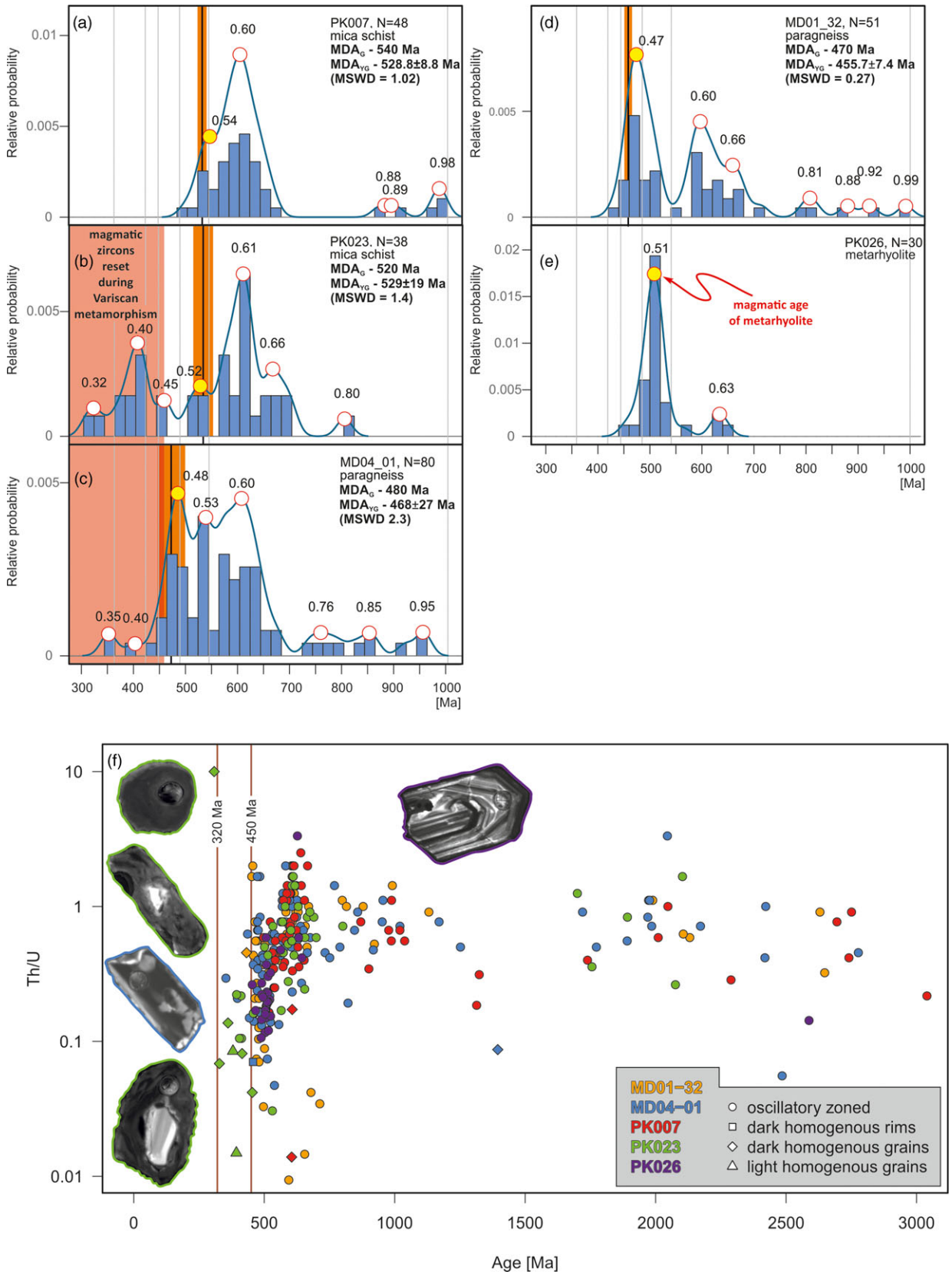

Figure 12. (Colour online) (a–e) Histograms with kernel density estimates of the Phanerozoic and Neoproterozoic zircon age populations from the dated mica schists and paragneisses of the Kamieniec Metamorphic Belt and the Doboszowice Metamorphic Complex. Bin width for histogram is 20 Ma, and bandwidth for KDE is 15 Ma. Orange rectangles and black lines are for MDA calculated using the mean age of the youngest two or more grains that overlap in age at 1σ (MDA$_G$). Yellow dots are for MDA calculated using the youngest graphical age peaks controlled by more than one grain (MDA$_{YG}$). Vertical axis is relative age probability. (f) Diagram showing Th/U zircon ratios versus the age showing the chemical variation of magmatic and metamorphic zircon domains for the studied samples. The colour code refers to the investigated samples, while the different dot shapes refer to the different types of zircons.

https://doi.org/10.1017/S0016756823000523 Published online by Cambridge University Press

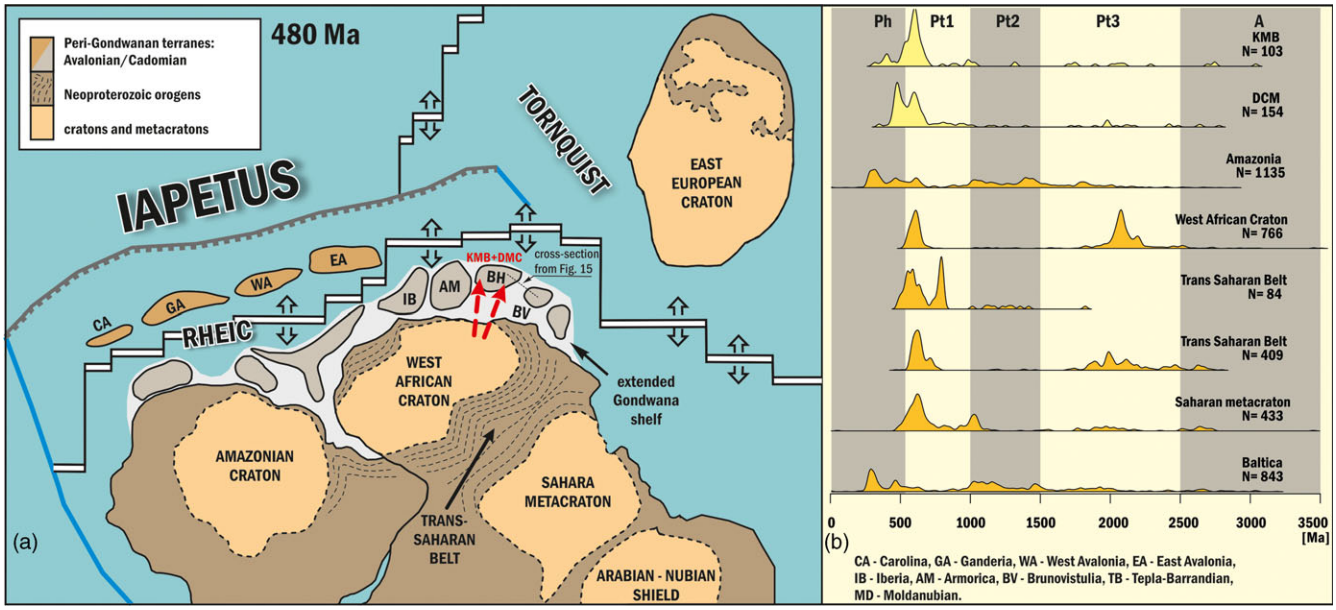

Figure 13. (Colour online) (a) Tentative simplified reconstruction of Western Gondwana extended passive margin during the Early Ordovician, modified after Domeier (2016) and Torsvik (2017). Abbreviations: CA – Carolina, GA – Ganderia, WA – West Avalonia, EA – East Avalonia, IB – Iberia, AM – Armorica, BV – Brunovistulia, BH – Saxothuringia, Tepla-Barrandian and – Moldanubia, KMB – Kamieniec Metamorphic Belt, DMC – Doboszowice Metamorphic Complex. Red arrows indicate the main directon of sedimentary transport. Types of lithospheric boundaries: black-white – spreading ridge, grey – subduction, blue – transform. (b) Kernel density plots for detrital zircons from: Kamieniec Metamorphic Belt (this study), Doboszowice Metamorphic Complex (this study), Amazonian Craton (Gaucher *et al.* 2008; Geraldes *et al.* 2014; Pankhurst *et al.* 2016), West African Craton (Abati *et al.* 2010), Trans-Saharan Belt – Tuareg Shield (Henry *et al.* 2009), Trans-Saharan Belt (Peucat *et al.* 2003; Abdallah *et al.* 2007; Bendaoud *et al.* 2008; Bosch *et al.* 2016), Saharan Metacraton (Meinhold *et al.* 2011) and Baltica (Valverde-Vaquero *et al.* 2000; Kristoffersen *et al.* 2014; Kuznetsov *et al.* 2014). Kernel density plots were designed via the R software environment (R Core Team, 2021). Abreviations: Ph – Phanerozoic, Pt1 – Neoproterozoic, Pt2 – Mesoproterozoic, Pt2 – Paleoproterozoic, A – Archean.

Archaean inheritance points to the involvement of an older crustal component in magma genesis (Fig. 9c, d).

The derivation of metarhyolites protolith from continental crust material is implied by the peraluminous and corundum-normative composition, depletion in HFSE (Figs. 6 and 7) and by low Zr/Nb (8.2–23) and Nb/Th (0.23–0.69) (Supplementary Table 1). Depletion in HFSE together with enrichment in LREE, a flat MREE-HREE profile, elevated Th content and high Th/Nb are also consistent with a subduction-related environment of magma origin (e.g. Pearce *et al.* 1984; Pearce & Peate, 1995, Schandl & Gorton, 2002).

Jung *et al.* (2009) through compilation of experimentally derived liquids devised a diagram for discrimination of granitoid sources (Fig. 6e). The plot shows that the KMB metarhyolites are related to a greywacke precursor (with no input from mantle-derived sources). This inference is consistent with their peraluminous affinity, whilst the plagioclase-bearing residue in the source possibly explains the negative Eu and Sr anomalies. Furthermore, immature, quartz-feldspathic-rich sources (e.g. psammites, paragneisses, etc.) that are able to supply peraluminous, cordierite-crystallizing liquids, require higher melting temperatures (>850–875°C; Sylvester, 1998, Moyen *et al.* 2017). Sylvester (1998) showed that low to moderate values of Al_2O_3/TiO_2 in strongly peraluminous granitic rocks may serve as a proxy of hot, melt-forming conditions. Moderate values of Al_2O_3/TiO_2 (52–228, av. 108 ± 48) of the studied metarhyolites seem to confirm these premises.

Although some of the discrimination diagrams support an active continental margin as a possible tectonic environment (Fig. 6f), we interpret this as a signature of inherited geochemical features pertinent to the tectonic setting of sedimentary precursor to the KMB meta-rhyolites. Additionally, collisional or post-collisional affinity is suggested (Fig. 6d and S04a). Furthermore, the discrimination diagram of Verma *et al.* (2013) with probability of 65% points to the collisional setting of the KMB meta-rhyolites. However, within-plate environment is also apparent (probability of 34%; Fig. S04b). Given no affinity to alkaline, A-type granitoid magmas, the latter indication possibly echoes the progression of tectonic setting from post-collisional towards anorogenic, presumably extensional regime (Fig. S04c and d).

The Cambrian age (ca. 510 Ma) and geochemical features of the KMB meta-rhyolites (S-type, peraluminous magmas from post-collisional, transitional setting) emphasize their similarities to post-orogenic (meta-)granites from the Saxothuringian domain in the West Sudetes, notably, ca. 504 Ma Rumburk granites and ca. 500–511 Ma Izera-Kowary gneisses (Oberc-Dziedzic *et al.* 2005, Pin *et al.* 2007, Oberc-Dziedzic *et al.* 2009) and those from the Moldanubian and Tepla-Barandian domains (e.g. Žák, Kraft & Hajná, 2013; Žák *et al.* 2023), but not the Brunovistulian domain. Thus, we consider the origin of the meta-rhyolites as another facet of magmatic pulses concurrent with the gradual change of tectonic environment marking the end of the Cadomian orogeny (arc-Gondwana continent collision) and the onset of Cambro-Ordovician rifting. These genetic links are highlighted by sparse inherited zircon ages of meta-rhyolites (ca. 560, 630 and 2590 Ma, Fig. 9c, d). They are close to the age peaks reported from the Rumburk granites and Izera-Kowary gneisses, and resemble those of Lusatian greywackes (1.1–2.6 Ma and 540–730 Ma; Kröner *et al.* 1994, Linnemann *et al.* 2004) considered as their sedimentary precursors formed in the Cadomian arc.

The lack of HP conditions during Cadomian arc-continent collision and limited crustal thickening (e.g. Dörr *et al.* 2002) are

https://doi.org/10.1017/S0016756823000523 Published online by Cambridge University Press

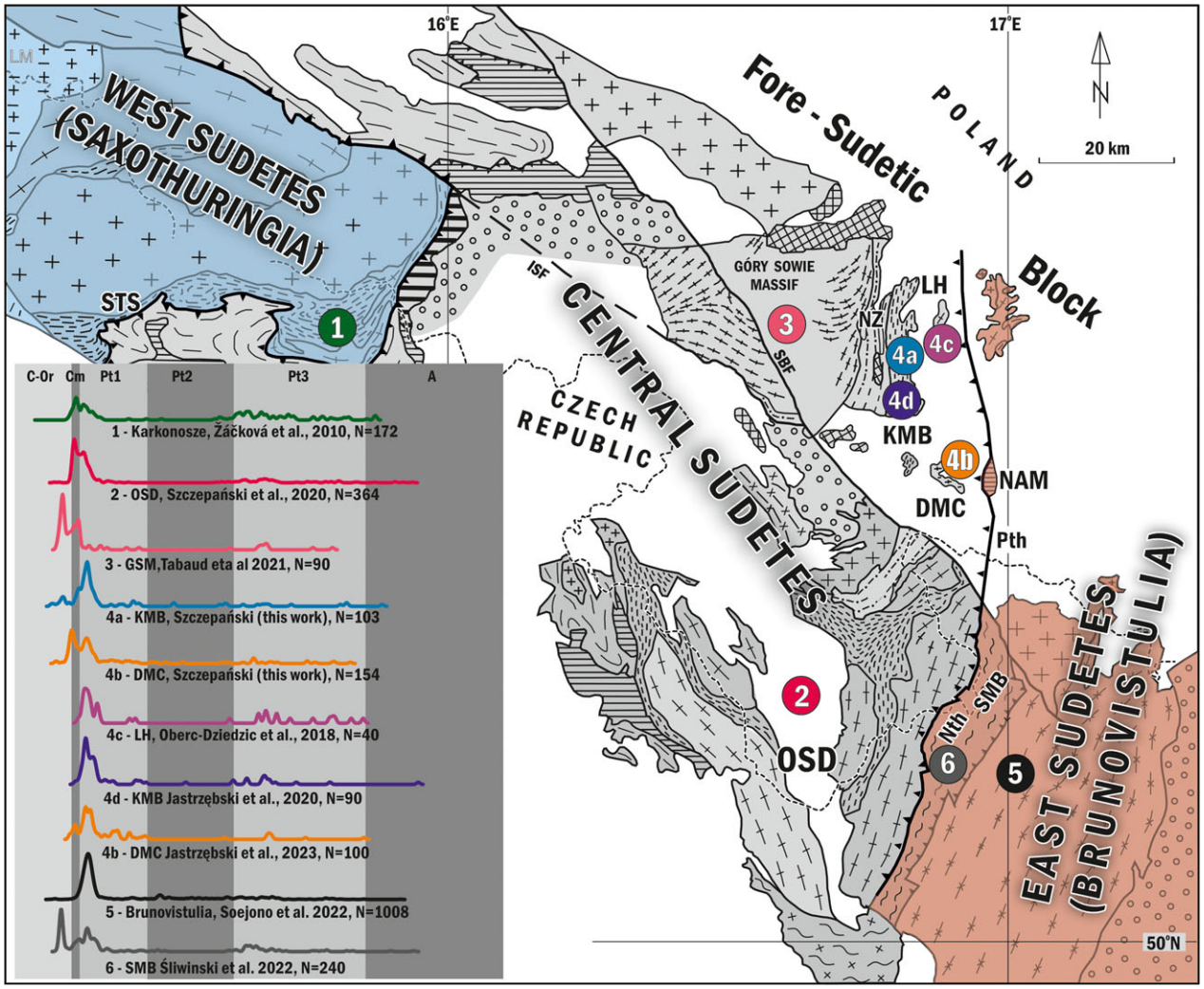

Fig. 14

Figure 14. (Colour online) Comparison of zircon age spectra obtained for various crustal domains from the Sudetes shown on the geological sketch map of the Sudetes after Mazur *et al.* (2006). Kernel density plots for detrital zircons from: 1. Karkonosze (Žáčková *et al.* 2010), 2. Orlica-Śnieżnik Dome (Szczepański *et al.* 2020); 3. Góry Sowie Massif (Tabaud *et al.* 2021); 4a. Kamieniec Metamorphic Belt (this work), 4b. Doboszowice Crystalline Massif (this work and Jastrzębski *et al.* 2023), 4c – Lipowe Hills (Oberc-Dziedzic *et al.* 2018); 4d. Kamieniec Metamorphic Belt (Jastrzębski *et al.* 2020); 5. Brunovistulia (Friedl *et al.* 2004; Mazur *et al.* 2010), 6. Staré Město Belt (Śliwiński *et al.* 2022). Abbreviations: STS – Saxothuringian suture, OSD – Orlica-Śnieżnik Dome, DMC – Doboszowice Crystalline Massif, KMB – Kamieniec Metamorphic Belt, NZ – Niemcza Zone, LH – Lipowe Hills, NAM – Niedźwiedź amphibolite Massif, Pth – Paczków thrust, Nth – Nyznerov thrust, SMB – Staré Město Belt. Abbreviations in inset: C-Or – Carboniferous-Ordovician, Cm – Cambrian, Pt1 – Neoproterozoic, Pt2 – Mesoproterozoic, Pt2 – Paleoproterozoic, A – Archean.

consistent with the inferred hot conditions of the KMB rhyolitic magma generation and correlate with intrusions into transitional crust at the peripheries of Gondwana that were postulated by tectonic model of Linnemann (2007) for the late Cambrian in the Saxothuringia (e.g. Zieger *et al.* 2018).

4.g. Is the Rheic suture exposed on the Fore-Sudetic Block?

The presented zircon age spectra demonstrate that the volcano-sedimentary successions of the KMB and DMC are typical of the Gondwana-derived terranes now exposed in the Bohemian Massif and exemplified by the Saxothuringian, Teplá-Barrandian and Moldanubian zones (see Žák & Sláma, 2018). It is worth noting that some volcano-sedimentary successions exposed in the Brunovistulian zone also show similar detrital zircon signature (Soejono *et al.* 2022). However, this domain is characterized by a paucity of magmatic and volcanic rocks of c. 500 Ma that are commonly exposed in the KMB and DMC. Furthermore, the existence of extensive Ordovician cover seems to be rather typical for such Gondwana-derived terranes like Saxothuringia, Moldanubia or Teplá-Barrandia. The only Ordovician strata documented in the Brunovistulian domain includes light green clay-rich siliceous rocks, interbedded with fine-grained quartz sandstones that has only been encountered in a restricted area in the northern part of Upper Silesia (see Kalvoda *et al.* 2008). It is worth noting that an affinity to the Saxothuringian domain was previously suggested by Jastrzębski *et al.* (2020, 2023) and Oberc-Dziedzic *et al.* (2018) for rocks of the DMC, Lipowe Hills and KMB (sites 4b, 4c and 4d in Fig. 14, respectively). Furthermore, similar age spectra were also reported by Tabaud *et al.* (2021) for the Góry Sowie Massif (site 3 in Fig. 14). On the other hand, Tabaud *et al.* (2021) suggested that the rocks exposed to the east of the Góry Sowie Massif and to the west of the Strzelin Massif represent the Moldanubian zone. However, it is worth noting that Chopin *et al.*

https://doi.org/10.1017/S0016756823000523 Published online by Cambridge University Press

(2012) defined the Moldanubian zone as a recycled passive margin of the Saxothuringian zone. Therefore, the results of our study combined with existing data allow us to identify the volcano-sedimentary successions now exposed in the longitudinal belt between the Góry Sowie massif in the west and the Lipowe Hills in the east as part of the Gondwana-derived terranes now exposed in the Bohemian Massif including Saxothuringia, its recycled part described as Moldanubia or Teplá-Barrandia (Fig. 14). Furthermore, similar detrital zircon age spectra of the late Neoproterozoic (Ediacaran) and Cambro-Ordovician volcano-sedimentary sequences were recently documented from the Stare Město Belt and the Bunovistulian terrane (sites 6 and 5 on Fig. 14, respectively, Collett *et al.* 2021; Śliwiński *et al.* 2022; Soejono *et al.* 2022). This implies that mentioned Gondwana-derived terranes and Brunovistulia were located within the extended Gondwana shelf at that time and were sourced from the same cratonic area (e.g. Collett *et al.* 2021; Śliwiński *et al.* 2022; Soejono *et al.* 2022). Furthermore, early Cambrian–Early Ordovician metabasalts of the Staré Město Belt and the Letovice ophiolite as well as the NAM (considered as the northern continuation of the Staré Město Belt on the Fore-Sudetic Block at the western tectonic boundary of the Brunovistulia; Fig. 14) all show intra-continental geochemical signatures (Awdankiewicz, 2008; Soejono *et al.* 2010; Collett *et al.* 2021). Therefore, by combining the geochemical signal of the aforementioned metaigneous complexes with the provenance signature of the associated metasedimentary successions, we support the previous assumptions that the Saxoturingia–Brunovistulia boundary is a remnant of the initial intracontinental rift that developed on the extended Gondwana shelf that was later closed during the Variscan orogeny (see, e.g. Collett *et al.* 2021; Soejono *et al.* 2022). Consequently, we are inclined to support the hypothesis that the Rheic suture is not exposed in the eastern part of the Bohemian Massif (e.g. Mazur *et al.* 2020; Collett *et al.* 2021; Soejono *et al.* 2022).

4.h. Variscan thermal event recorded by the volcano-sedimentary succession

The youngest zircons documented in the studied metasedimentary samples (PK023 and MD04-01, Fig. 12b, c) reach ages of c. 330–320 Ma. We interpret all ages in the range between 450 and 320 Ma as reflecting lead loss due to the Variscan metamorphism. Several such young grains have been documented in samples PK023, MD04-01 and MD01-32 and are characterized by the appearance of thin dark rims or patchy zonation (Fig. 8). These features are characteristic of crystals that have experienced fluid interaction, for example, as a result of metamorphism (e.g. Spandler *et al.* 2004). Furthermore, dark zircon rims or dark homogeneous grains are mostly characterized by a low Th/U ratio, which is typical for metamorphic zircons (Fig. 12f). We would like to emphasize that many such dark and thin zircon rims were documented in the samples examined but could not be dated due to their small dimensions. (Fig. S03). We suggest that the youngest zircons in our collection, with ages ranging between 330 and 320 Ma, most likely represent the age of the Variscan thermal overprint that caused Pb loss in some of the examined zircon grains.

4.i. From the Gondwana active margin to the Variscan collision of Cadomian terranes

Several early-middle Cambrian to Lower Ordovician sedimentary successions have been documented in the Variscan basement of the Bohemian Massif including the Münchberg Massif as well as the Teplá-Barrandian, the Saxothurignian and the Moldanubian domains (e.g. Linnemann *et al.* 2000; Drost *et al.* 2011; Košler *et al.* 2014; Hajná *et al.* 2018; Koglin *et al.* 2018; Tabaud *et al.* 2021). These volcano-sedimentary successions are mainly characterized by immature graywacke protoliths with chemical composition indicating deposition in a supra-subduction environment (Drost *et al.* 2011; Koglin *et al.* 2018; Tabaud *et al.* 2021).

The data presented here indicate that the early-middle Cambrian and Ordovician sediments exposed in the KMB and DMC were deposited in a sedimentary basin sourced by a Cadomian orogen and their geochemical signal point to detritus derivation from a magmatic arc system. Therefore, in terms of provenance signature, it was the same or very similar detritus that fed the volcano-sedimentary successions exposed in the Saxoturingian domain including the neighbouring Orlica-Śnieżnik dome, the south-eastern part of the Karkonosze-Izera Block, the Góry Sowie massif, the Staré Město Belt and also the Brunovistulia in the East Sudetes (Fig. 14, and references therein). The most interesting is that in some of these areas the Early Ordovician rock successions represent light quartzites interpreted as mature quartzitic sandstones deposited on a passive continental margin (e.g. the Goszów Quartzites from the Orlica-Śnieżnik dome, Mazur *et al.* 2012; Szczepański *et al.* 2020). This suggests that the sedimentary basin that developed along the northern margin of Gondwana was active during the whole Ordovician and was fed by detritus characterized by varying proportions of mature cratonic material and immature arc detritus. Therefore, we support the idea that the Cambro-Ordovician basin at the northern margin of Gondwana developed above a retreating subducting oceanic slab represented by the Iapetus Ocean (e.g. Arenas *et al.* 2007; Díez Fernández *et al.* 2012; Hajná *et al.* 2018; Soejono *et al.* 2020). The retreat of a subducting oceanic slab was responsible for the continental extension and the formation of a passive Gondwana margin. This process led to lithospheric thinning and asteno-spheric mantle upwelling responsible for crustal anatexis and the formation of granitoid intrusions at c. 520–480 Ma as proposed earlier by, for example, Soejono *et al.* (2020). Postulated lithospheric thinning and extension was also responsible for the separation of Cadomian crustal fragments that formed the extended Gondwana shelf and the development of local intra-continental rifts, remnants of which are now exemplified by the NAM metabasalts on the Fore-Sudetic Block (Fig. 15a).

The Cambro-Ordovician extension is well documented in the post-Cadomian successions within the Variscan belt of Europe due to the occurrence of 517–480 Ma granitoid intrusions exposed, for example, throughout the Saxothuringian zone (e.g. the Izera-Karkonosze Massif), but also widely exposed in the Teplá-Barrandian and Moldanubian zones. Although metagranitoids from the Izera-Karkonosze Massif have a chemical composition typical of volcanic arc granites (e.g. Turniak *et al.* 2000; Zieger *et al.* 2018), Oberc-Dziedzic *et al.* (2005) and Pin *et al.* (2007) interpreted them on the basis of Sm-Nd isotopic data and bulk rock geochemistry as either typical S-type post-collisional or anorogenic and related to continental break-up. The latter idea and the relationship of the metagranitoids to continental break-up was recently supported by Jastrzębski *et al.* (2017).

The final stage in the evolution of the rock successions exposed in the KMB and DMC was the closure of the intracontinental rift, remnants of which are found in the NAM on the Fore-Sudetic Block, followed by subduction of fragments of Gondwana continental shelf below Brunovistulia during the Variscan Orogeny (Fig. 15b). The results of classical geothermobarometry,

https://doi.org/10.1017/S0016756823000523 Published online by Cambridge University Press

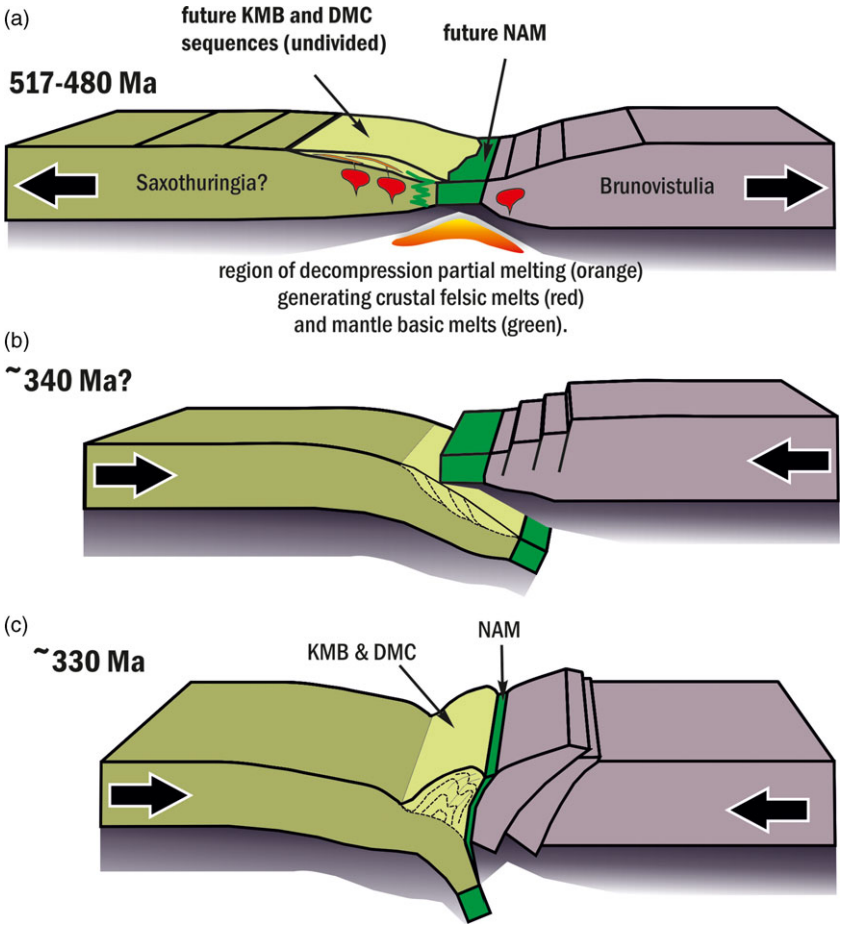

Figure 15. (Colour online) Simplified tectonic model for early Palaeozoic–Carboniferous evolution of the KMB and DMC. See text for explanation.

thermodynamic calculations and quartz in garnet elastobarometry point to burial of the KMB volcano-sedimentary succession to depths of ~65–70 km, which was followed by its imbrication, exhumation and folding (Szczepański *et al.* 2022; Szczepański & Goleń, 2022; Fig. 15b, c). The age of maximum burial of the rock complexes within the postulated subduction zone is unknown and requires further investigation. The data presented in this study and previously published isotopic dating of monazite grains suggest that the last stages of exhumation occurred c. 320–330 Ma (Jastrzębski *et al.* 2020). However, more recently published U-Th-Pb monazite data indicate that DMC experienced metamorphic episode at ca. 346–340 Ma (Jastrzębski *et al.* 2023). This is confirmed by Lu-Hf and Sm-Nd garnet dating of the Chałupki paragneiss, which shows that these rocks were metamorphosed between 347 ± 3.6 Ma and 337.3 ± 6.6 Ma (Szczepański *et al.* 2022). A scenario proposed here involving Cambro-Ordovician rifting followed by Variscan collision of terranes is consistent with previously proposed models for the development of the Cadomian and Cambro-Ordovician successions exposed in the Bohemian Massif (Martínez Catalán *et al.* 2020; Collett *et al.* 2021; Martínez Catalán *et al.* 2021; Tabaud *et al.* 2021; Soejono *et al.* 2022).

5. Conclusions

The volcano-sedimentary successions from the eastern part of the Fore-Sudetic Block (the KMB and the DMC) provide new input to understand the pre-Variscan and Varciscan history of the Cambro-Ordovician rocks outcropping in the eastern part of the Central Sudetes. Bulk rock chemistry and detrital zircon age spectra obtained using LA–ICP–MS U–Pb show that the mica schists of the KMB represent a succession equivalent to the Stronie Formation of the Orlica-Śnieżnik dome, while there is no exact time equivalent in the Sudetes for the Chałupki paragneisses now exposed in the DMC. The only Ordovician rock succession exposed in the Sudetes is represented by the Goszów quartzites of the Orlica-Śnieżnik dome. The data presented indicate that the volcano-sedimentary successions exposed in the eastern part of the Fore-Sudetic Block were sourced from the West African Craton or, more probably, from part of the Trans-Saharan Belt of Gondwana. Bulk rock geochemistry suggests that the studied volcano-sedimentary successions were deposited on the Gondwana margin during their transformation from an active to a passive setting within the back-arc environment. The youngest single zircon grains documented in the metasediment samples show ages of c. 330–320 Ma that we interpret as reflecting lead loss owing to the Variscan thermal overprint. Our data, combined with published results, suggest that the suture separating the Brunovistulian and Saxothuringian terranes is an intracontinental rift closed during the Variscan Orogeny, rather than a continuation of the Rheic suture.

Supplementary material. To view supplementary material for this article, please visit https://doi.org/10.1017/S0016756823000523

Acknowledgements. We thank Ulf Linnemann, Stanislaw Mazur, José R. Martínez Catalán and four anonymous reviewers for their constructive comments that led to substantial improvement of the manuscript, as well as

Laura Bracciali and Peter Clift for editorial handling. The study was supported from NCN research grant UMO-2015/17/B/ST10/02212. Dariusz Marciniak and Marcin Goleń are thanked for help during preparation of zircon concentrates.

Competing interests. The author(s) declare none.

References

Abati J, Aghzer AM, Gerdes A and Ennih N (2010) Detrital zircon ages of Neoproterozoic sequences of the Moroccan Anti-Atlas belt. *Precambrian Research* **181**, 115–28.

Abdallah N, Liégeois J-P, De Waele B, Fezaa N and Ouabadi A (2007) The Temaguessine Fe-cordierite orbicular granite (Central Hoggar, Algeria): U–Pb SHRIMP age, petrology, origin and geodynamical consequences for the late Pan-African magmatism of the Tuareg shield. *Journal of African Earth Sciences* **49**, 153–78.

Arenas R, Martínez Catalán JR, Sánchez Martínez S, Fernández-Suárez J, Andonaegui P, Pearce JA and Corfu F (2007) The Vila de Cruces Ophiolite: a Remnant of the early Rheic Ocean in the Variscan Suture of Galicia (Northwest Iberian Massif). *The Journal of Geology* **115**, 129–48.

Awdankiewicz H (2008) The petrology and geochemistryof the metabasites of the Niedzwiedz Massifin the Fore-Sudetic Block. *Prace Państwowego Instytutu Geologicznego* **189**, 5–56.

Bendaoud A, Ouzegane K, Godard G, Liégeois J-P, Kienast J-R, Bruguier O and Drareni A (2008) Geochronology and metamorphic P – T – X evolution of the Eburnean granulite-facies metapelites of Tidjenouine (Central Hoggar, Algeria): witness of the LATEA metacratonic evolution. *Geological Society, London, Special Publications* **297**, 111–46.

Bhatia MR (1983) Plate tectonics and geochemical composition of sandstones. *Journal of Geology* **91**, 611–27.

Bhatia MR and Crook KAW (1986) Trace element characteristics of graywackes and tectonic setting discrimination of sedimentary basins. *Contributions to Mineralogy and Petrology* **92**, 181–93.

Boris R, Domeier M and Jakob J (2021) On the origins of the Iapetus Ocean. *Earth-Science Reviews* **221**, 103791.

Bosch D, Bruguier O, Caby R, Buscail F and Hammor D (2016) Orogenic development of the Adrar des Iforas (Tuareg Shield, NE Mali): new geochemical and geochronological data and geodynamic implications. *Journal of Geodynamics* **96**, 104–30.

Chopin F, Schulmann K, Skrzypek E, Lehmann J, Dujardin JR, Martelat JE, Lexa O, Corsini M, Edel JB, Štípská P and Pitra P (2012) Crustal influx, indentation, ductile thinning and gravity redistribution in a continental wedge: building a Moldanubian mantled gneiss dome with underthrust Saxothuringian material (European Variscan belt). *Tectonics* **31**, TC1013.

Collett S, Schulmann K, Deiller P, Štípská P, Peřestý V, Ulrich M, Jiang Y, de Hoÿm de Marien L and Míková J (2022) Reconstruction of the mid-Devonian HP-HT metamorphic event in the Bohemian Massif (European Variscan belt). *Geoscience Frontiers* **13**, 101374.

Collett S, Schulmann K, Štípská P and Míková J (2020) Chronological and geochemical constraints on the pre-variscan tectonic history of the Erzgebirge, Saxothuringian Zone. *Gondwana Research* **79**, 27–48.

Collett S, Štípská P, Schulmann K, Míková J and Kröner A (2021) Tectonic significance of the Variscan suture between Brunovistulia and the Bohemian Massif. *Journal of the Geological Society* **178**. doi: 10.1144/jgs2020-176jgs2020176.

Cullers RL (1994) The controls on the major and trace element variation of shales, siltstones, and sandstones of Pennsylvanian-Permian age from uplifted continental blocks in Colorado to platform sediment in Kansas, USA. *Geochimica et Cosmochimica Acta* **58**, 4955–72.

Cullers RL (2000) The geochemistry of shales, siltstones and sandstones of Pennsylvanian–Permian age, Colorado, USA: implications for provenance and metamorphic studies. *Lithos* **51**, 181–203.

Cullers RL (2002) Implications of elemental concentrations for provenance, redox conditions, and metamorphic studies of shales and limestones near Pueblo, CO, USA. *Chemical Geology* **191**, 305–27.

Dickinson WR and Gehrels GE (2009) Use of U–Pb ages of detrital zircons to infer maximum depositional ages of strata: a test against a Colorado Plateau Mesozoic database. *Earth and Planetary Science Letters* **288**, 115–25.

Díez Fernández R, Castiñeiras P and Gómez Barreiro J (2012) Age constraints on lower Paleozoic convection system: magmatic events in the NW Iberian Gondwana margin. *Gondwana Research* **21**, 1066–79.

Domeier M (2016) A plate tectonic scenario for the Iapetus and Rheic oceans. *Gondwana Research* **36**, 275–95.

Dörr W, Zulauf G, Fiala J, Franke W and Vejnar Z (2002) Neoproterozoic to early Cambrian history of an active plate margin in the Teplá–Barrandian unit—a correlation of U–Pb isotopic-dilution-TIMS ages (Bohemia, Czech Republic). *Tectonophysics* **352**, 65–85.

Drost K, Gerdes A, Jeffries T, Linnemann U and Storey C (2011) Provenance of Neoproterozoic and early Paleozoic siliciclastic rocks of the Teplá-Barrandian unit (Bohemian Massif): Evidence from U–Pb detrital zircon ages. *Gondwana Research* **19**, 213–31.

Dziedzicowa H (1966) Seria łupków krystalicznych na wschód od strefy Niemczy w świetle nowych badań. The schists series east of the Niemcza Zone in the light of new investigations, (in Polish, English summary). *Z geologii Ziem Zachodnich*, Scientific Session of the 20th Anniversary of Polish Research 1945-1965, Wroclaw. 101–18.

Elicki O (1997) Biostratigraphic data of the German Cambrian—present state of knowledge. *Freiberger Forschungshefte* **C466**, 155–65.

Fernández-Suárez J, Alonso GG, Cox R and Jenner GA (2002) Assembly of the Armorica Microplate: a strike-slip Terrane delivery? Evidence from U-Pb ages of detrital zircons. *The Journal of Geology* **110**, 619–26.

Floyd PA, Leveridge BE, Franke W, Shail R and Doerr W (1990) Provenance and depositional environment of Rhenohercynian synorogenic greywackes from the Giessen Nappe, Germany. *Geologische Rundschau* **79**, 611–26.

Floyd PA, Winchester JA and Park RG (1989) Geochemistry and tectonic setting of Lewisian clastic metasediments of the early Proterozoic Loch Maree Group of Gairloch, NW Scotland. *Precambrian Research* **45**, 203–14.

Franke W (1989) Tectonostratigraphic units in the Variscan Belt of Central Europe. *Terranes in the Circum-Atlantic Paleozoic orogens* **230**, 67–90.

Friedl G, Finger F, Paquette J-L, von Quadt A, McNaughton NJ and Fletcher IR (2004) Pre-Variscan geological events in the Austrian part of the Bohemian Massif deduced from U-Pb zircon ages. *The Avalonian-Cadomian Belt and related peri-Gondwanan terranes* **93**, 802–23.

Gaucher C, Finney S, Poire D, Valencia V, Grove M, Blanco G, Pamoukaghlian K and Peral L (2008) Detrital zircon ages of Neoproterozoic sedimentary successions in Uruguay and Argentina: insights into the geological evolution of the Río de la Plata Craton. *Precambrian Research* **167**, 150–70.

Geraldes MC, Nogueira C, Vargas-Mattos G, Matos R, Teixeira W, Valencia V and Ruiz J (2014) U–Pb detrital zircon ages from the Aguapeí Group (Brazil): implications for the geological evolution of the SW border of the Amazonian Craton. *Precambrian Research* **244**, 306–16.

Gorton MP and Schandl ES (2000) From continents to island arcs: a geochemical index of tectonic setting for arc-related and within-plate felsic to intermediate volcanic rocks. *The Canadian Mineralogist* **38**, 1065–73.

Hajná J, Žák J and Dörr W (2017) Time scales and mechanisms of growth of active margins of Gondwana: a model based on detrital zircon ages from the Neoproterozoic to Cambrian Blovice accretionary complex, Bohemian Massif. *Gondwana Research* **42**, 63–83.

Hajná J, Žák J, Dörr W, Kachlík V and Sláma J (2018) New constraints from detrital zircon ages on prolonged, multiphase transition from the Cadomian accretionary orogen to a passive margin of Gondwana. *Precambrian Research* **317**, 159–78.

Hasterok D, Gard M and Webb J (2018) On the radiogenic heat production of metamorphic, igneous, and sedimentary rocks. *Geoscience Frontiers* **9**, 1777–94.

Hastie AR, Kerr AC, Pearce JA and Mitchell SF (2007) Classification of altered Volcanic Island Arc rocks using immobile trace elements: development of the Th–Co discrimination diagram. *Journal of Petrology* **48**, 2341–57.

Henry B, Liégeois JP, Nouar O, Derder MEM, Bayou B, Bruguier O, Ouabadi A, Belhai D, Amenna M, Hemmi A and Ayache M (2009) Repeated granitoid intrusions during the Neoproterozoic along the western

boundary of the Saharan metacraton, Eastern Hoggar, Tuareg shield, Algeria: an AMS and U–Pb zircon age study. *Tectonophysics* **474**, 417–34.

Herron MM (1988) Geochemical classification of terrigenous sands and shales from core or log data. *Journal of Sedimentary Research* **58**, 820–9.

Hladil J, Patocka F, Kachlik V, Melichar R and Hubacik M (2003) Metamorphosed carbonates of Krkonose mountains and Paleozoic evolution of Sudetic terranes (NE Bohemia, Czech Republic). *Geologica Carpathica* **54**, 281–97.

Jackson SE, Pearson NJ, Griffin WL and Belousova EA (2004) The application of laser ablation-inductively coupled plasma-mass spectrometry to in situ U–Pb zircon geochronology. *Chemical Geology* **211**, 47–69.

Jastrzębski M, Budzyń B and Stawikowski W (2017) Cambro-Ordovician vs Devono-Carboniferous geodynamic evolution of the Bohemian Massif: evidence from *P–T–t* studies in the Orlica–Śnieżnik Dome, SW Poland. *Geological Magazine* **156**, 447–70.

Jastrzębski M, Żelaźniewcz A, Sláma J, Machowiak K, Śliwiński M, Jaźwa A and Kocjan I (2021) Provenance of Precambrian basement of the Brunovistulian Terrane: new data from its Silesian part (Czech Republic, Poland), central Europe, and implications for Gondwana break-up. *Precambrian Research* **355**, 106108.

Jastrzębski M, Żelaźniewicz A, Budzyń B, Sláma J and Konečny P (2020) Age constraints on the Pre-Variscan and Variscan thermal events in the Kamieniec Ząbkowicki Metamorphic belt (the Fore-Sudetic Block, SW Poland). *Annales Societatis Geologorum Poloniae* **90**, 27–49.

Jastrzębski M, Żelaźniewicz A, Majka J, Murtezi M, Bazarnik J and Kapitonov I (2013) Constraints on the Devonian–Carboniferous closure of the Rheic Ocean from a multi-method geochronology study of the Staré Město Belt in the Sudetes (Poland and the Czech Republic). *Lithos* **170–171**, 54–72.

Jastrzębski M, Żelaźniewicz A, Murtezi M, Larionov AN and Sergeev S (2015) The Moldanubian Thrust Zone — a terrane boundary in the Central European Variscides refined based on lithostratigraphy and U–Pb zircon geochronology. *Lithos* **220–223**, 116–32.

Jastrzębski M, Żelaźniewicz A, Nowak I, Murtezi M and Larionov AN (2010) Protolith age and provenance of metasedimentary rocks in Variscan allochthon units: U/Pb SHRIMP zircon data from the Orlica-Śnieżnik Dome, West Sudetes. *Geological Magazine* **147**, 416–33.

Jastrzębski M, Żelaźniewicz A, Stawikowski W, Budzyń B, Krzemińska E, Machowiak K, Madej S, Białek D, Sláma J, Czupyt Z and Jaźwa A (2023) The eastern part of the Saxothuringian Terrane characterized by zircon and monazite data from the Doboszowice Metamorphic Complex in the Sudetes (SW Poland). *Annales Societatis Geologorum Poloniae* **93** (in print).

Jung S, Masberg P, Mihm D and Hoernes S (2009) Partial melting of diverse crustal sources — constraints from Sr–Nd–O isotope compositions of quartz diorite–granodiorite–leucogranite associations (Kaoko Belt, Namibia). *Lithos* **111**, 236–51.

Kalvoda J, Babek O, Fatka O, Leichmann J, Melichar R, Nehyba S and Spacek P (2008) Brunovistulian terrane (Bohemian Massif, Central Europe) from late Proterozoic to late Paleozoic: a review. *International Journal of Earth Sciences* **97**, 497–518.

Kirchner F and Albert R (2020) New detrital zircon age data reveal the location of the Rheic suture in the Mid-German Crystalline Zone (Spessart and Odenwald Crystalline Complexes). *International Journal of Earth Sciences* **109**, 2287–305.

Koglin N, Zeh A, Franz G, Schüssler U, Glodny J, Gerdes A and Brätz H (2018) From Cadomian magmatic arc to Rheic ocean closure: the geochronological-geochemical record of nappe protoliths of the Münchberg Massif, NE Bavaria (Germany). *Gondwana Research* **55**, 135–52.

Košler J, Konopásek J, Sláma J and Vrána S (2014) U–Pb zircon provenance of Moldanubian metasediments in the Bohemian Massif. *Journal of the Geological Society* **171**, 83–95.

Kristoffersen M, Andersen T and Andresen A (2014) U–Pb age and Lu–Hf signatures of detrital zircon from Palaeozoic sandstones in the Oslo Rift, Norway. *Geological Magazine* **151**, 816–29.

Kröner A, Jaeckel P and Opletal M (1994) Pb-Pb and U-Pb zircon ages for orthogneisses from eastern Bohemia; further evidence for a major Cambro-Ordovician magmatic event. *Evolution of Variscan (Hercynian) and Comparable Palaeozoic Orogenic Belts; Joint Meeting of Geologische Vereinigung e.V. and Ceska Geologicka Spolecnost* **39**, 61.

Kuznetsov NB, Meert JG and Romanyuk TV (2014) Ages of detrital zircons (U/Pb, LA-ICP-MS) from the Latest Neoproterozoic–Middle Cambrian(?) Asha Group and early Devonian Takaty Formation, the Southwestern Urals: a test of an Australia-Baltica connection within Rodinia. *Precambrian Research* **244**, 288–305.

Lange U, Bröcker M, Armstrong R, Żelaźniewicz A, Trapp E and Mezger K (2005) The orthogneisses of the Orlica-Śnieżnik complex (West Sudetes, Poland): geochemical characteristics, the importance of pre-Variscan migmatization and constraints on the cooling history. *Journal of the Geological Society* **162**, 973–84.

Linnemann U (2007) Ediacaran rocks from the Cadomian basement of the Saxo-Thuringian Zone (NE Bohemian Massif, Germany); age constraints, geotectonic setting and basin development. *The Rise and Fall of the Ediacaran Biota* **286**, 35–51.

Linnemann U, Gehmlich M, Tichomirowa M, Buschmann B, Nasdala L, Jonas P, Luetzner H and Bombach K (2000) From Cadomian subduction to early Paleozoic rifting; the evolution of Saxo-Thuringia at the margin of Gondwana in the light of single zircon geochronology and basin development (Central European Variscides, Germany). *Orogenic Processes; Quantification and Modelling in the Variscan Belt* **179**, 131–53.

Linnemann U, Gerdes A, Drost K and Buschmann B (2007) The continuum between Cadomian orogenesis and opening of the Rheic Ocean: constraints from LA-ICP-MS U-Pb zircon dating and analysis of plate-tectonic setting (Saxo-Thuringian zone, northeastern Bohemian Massif, Germany). *Special Paper 423: The Evolution of the Rheic Ocean: From Avalonian-Cadomian Active Margin to Alleghenian-Variscan Collision* **423**, 61–96.

Linnemann U and Heuse T (2001) The Ordovician of the Schwarzburg Anticline: geotectonic setting, biostratigraphy and sequence stratigraphy (Saxo-Thuringian Terrane, Germany). *Zeitschrift der Deutschen Geologischen Gesellschaft* **151**, 471–91.

Linnemann U, McNaughton NJ, Romer RL, Gehmlich M, Drost K and Tonk C (2004) West African provenance for Saxo-Thuringia (Bohemian Massif); Did Armorica ever leave pre-Pangean Gondwana? U/Pb-SHRIMP zircon evidence and the Nd-isotopic record. *The Avalonian-Cadomian Belt and related peri-Gondwanan terranes* **93**, 683–705.

Linnemann U, Pereira F, Jeffries TE, Drost K and Gerdes A (2008) The Cadomian Orogeny and the opening of the Rheic Ocean; the diacrony of geotectonic processes constrained by LA-ICP-MS U/Pb zircon dating (Ossa-Morena and Saxo-Thuringian zones, Iberian and Bohemian massifs). *The Foundations and Birth of the Rheic Ocean; Avalonian-Cadomian Orogenic Processes and Early Paleozoic Rifting at the Northern Gondwana Margin* **461**, 21–43.

Linnemann U, Pidal AP, Hofmann M, Drost K, Quesada C, Gerdes A, Marko L, Gärtner A, Zieger J, Ulrich J, Krause R, Vickers-Rich P and Horak J (2018) A ~565 Ma old glaciation in the Ediacaran of peri-Gondwanan West Africa. *International Journal of Earth Sciences* **107**, 885–911.

Ludwig KR (2008) Isoplot/Ex 3.70. A Geochronological Toolkit for Microsoft Excel. Berkeley: Geochronological Center.

Maniar PD and Piccoli PM (1989) Tectonic discrimination of granitoids. *Geological Society of America Bulletin* **101**, 635–43.

Martínez Catalán JR, Collett S, Schulmann K, Aleksandrowski P and Mazur S (2020) Correlation of allochthonous terranes and major tectonostratigraphic domains between NW Iberia and the Bohemian Massif, European Variscan belt. *International Journal of Earth Sciences* **109**, 1105–31.

Martínez Catalán JR, Schulmann K and Ghienne J-F (2021) The Mid-Variscan Allochthon: keys from correlation, partial retrodeformation and plate-tectonic reconstruction to unlock the geometry of a non-cylindrical belt. *Earth-Science Reviews* **220**, 103700.

Mazur S, Aleksandrowski P, Gągała Ł, Krzywiec P, Żaba J, Gaidzik K and Sikora R (2020) Late Palaeozoic strike-slip tectonics versus oroclinal bending at the SW outskirts of Baltica: case of the Variscan belt's eastern end in Poland. *International Journal of Earth Sciences* **109**, 1133–60.

Mazur S, Aleksandrowski P, Kryza R and Oberc-Dziedzic T (2006) The Variscan Orogen in Poland. *Geological Quarterly* **50**, 89–118.

Mazur S, Kröner A, Szczepański J, Turniak K, Hanžl P, Melichar R, Rodionov NV, Paderin I and Sergeev SA (2010) Single zircon U/Pb ages

and geochemistry of granitoid gneisses from SW Poland: evidence for an Avalonian affinity of the Brunian microcontinent. *Geological Magazine* **147**, 508–26.

Mazur S, Szczepański J, Turniak K and McNaughton NJ (2012) Location of the Rheic suture in the eastern Bohemian Massif: evidence from detrital zircon data. *Terra Nova* **24**, 199–206.

Mazur S, Turniak K, Szczepański J and McNaughton NJ (2015) Vestiges of Saxothuringian crust in the Central Sudetes, Bohemian Massif: zircon evidence of a recycled subducted slab provenance. *Gondwana Research* **27**, 825–39.

McLennan SM (1989) Rare earth elements in sedimentary rocks; influence of provenance and sedimentary processes. *Reviews in Mineralogy and Geochemistry* **21**, 169–200.

McLennan SM, Hemming S, McDaniel DK and Hanson GN (1993) Geochemical approaches to sedimentation, provenance, and tectonics. *Processes Controlling the Composition of Clastic Sediments* **284**, 21–40.

Meinhold G, Morton AC, Fanning CM, Frei D, Howard JP, Phillips RJ, Strogen D and Whitham AG (2011) Evidence from detrital zircons for recycling of Mesoproterozoic and Neoproterozoic crust recorded in Paleozoic and Mesozoic sandstones of southern Libya. *Earth and Planetary Science Letters* **312**, 164–75.

Merdith AS, Williams SE, Collins AS, Tetley MG, Mulder JA, Blades ML, Young A, Armistead SE, Cannon J, Zahirovic S and Müller RD (2021) Extending full-plate tectonic models into deep time: linking the Neoproterozoic and the Phanerozoic. *Earth-Science Reviews* **214**, 103477.

Mingram B, Kröner A, Hegner E and Krentz O (2004) Zircon ages, geochemistry, and Nd isotopic systematics of pre-Variscan orthogneisses from the Erzgebirge, Saxony (Germany), and geodynamic interpretation. *International Journal of Earth Sciences* **93**, 706–27.

Moyen J-F, Laurent O, Chelle-Michou C, Couzinié S, Vanderhaeghe O, Zeh A, Villaros A and Gardien V (2017) Collision vs. subduction-related magmatism: Two contrasting ways of granite formation and implications for crustal growth. *Lithos* **277**, 154–77.

Nance RD, Gutiérrez-Alonso G, Keppie JD, Linnemann U, Murphy JB, Quesada C, Strachan RA and Woodcock NH (2010) Evolution of the Rheic Ocean. *Gondwana Research* **17**, 194–222.

Nance RD, Gutiérrez-Alonso G, Keppie JD, Linnemann U, Murphy JB, Quesada C, Strachan RA and Woodcock NH (2012) A brief history of the Rheic Ocean. *Geoscience Frontiers* **3**, 125–35.

Nance RD and Linnemann U (2008) The Rheic Ocean: origin, evolution, and significance. *GSA Today* **18**, 4.

Nance RD, Murphy JB, Strachan RA, Keppie JD, Gutierrez Alonso G, Fernandez Suarez J, Quesada C, Linnemann U, d'Lemos R and Pisarevsky SA (2008) Neoproterozoic-early Palaeozoic tectonostratigraphy and palaeogeography of the peri-Gondwanan terranes; Amazonian v. West African connections. The Boundaries of the West African Craton 297, 345–83.

Oberc-Dziedzic T, Kryza R, Madej S and Pin C (2018) The Saxothuringian Terrane affinity of the metamorphic Stachów Complex (Strzelin Massif, Fore-Sudetic Block, Poland) inferred from zircon ages. *Geological Quarterly* **62**, 237–256.

Oberc-Dziedzic T, Kryza R, Pin Ch, Mochnacka K and Larionov A (2009) The Orthogneiss and Schist complex of the Karkonosze–Izera Mas sif (Sudetes, SW Poland): U-Pb SHRIMP zircon ages, Nd-iso tope systematics and protoliths. *Geologia Sudetica* **41**, 3–24.

Oberc-Dziedzic T, Pin C and Kryza R (2005) Early Palaeozoic crustal melting in an extensional setting: petrological and Sm-Nd evidence from the Izera granite-gneisses, Polish Sudetes. *International Journal of Earth Sciences* **94**, 354–68.

Oriolo S, Schulz B, Geuna S, González PD, Otamendi JE, Sláma J, Druguet E and Siegesmund S (2021) Early Paleozoic accretionary orogens along the Western Gondwana margin. *Geoscience Frontiers* **12**, 109–30.

Pankhurst RJ, Hervé F, Fanning CM, Calderón M, Niemeyer H, Griem-Klee S and Soto F (2016) The pre-Mesozoic rocks of northern Chile: U–Pb ages, and Hf and O isotopes. *Earth-Science Reviews* **152**, 88–105.

Patiño Douce AE (1999) What do experiments tell us about the relative contributions of crust and mantle to the origin of granitic magmas? *Geological Society, London, Special Publications* **168**, 55–75.

Paton C, Hellstrom J, Paul B, Woodhead J and Hergt J (2011) Iolite: freeware for the visualisation and processing of mass spectrometric data. *Journal of Analytical Atomic Spectrometry* **26**, 2508.

Paton C, Woodhead JD, Hellstrom JC, Hergt JM, Greig A and Maas R (2010) Improved laser ablation U-Pb zircon geochronology through robust downhole fractionation correction: improved laser ablation U-Pb geochronology. *Geochemistry, Geophysics, Geosystems* **11**, n/a–n/a.

Pearce JA, Harris NBW and Tindle AG (1984) Trace element discrimination diagrams for the tectonic interpretation of granitic rocks. *Journal of Petrology* **25**, 956–83.

Pearce JA and Peate DW (1995) Tectonic implications of the composition of volcanic arc magmas. *Annual Review of Earth and Planetary Sciences* **23**, 251–85.

Pérez-Cáceres I, Martínez Poyatos D, Simancas JF and Azor A (2015) The elusive nature of the Rheic Ocean suture in SW Iberia. *Tectonics* **34**, 2429–50.

Pettijohn FJ, Potter PE and Siever R (1987) *Sand and Sandstone*. New York, NY: Springer New York.

Peucat JJ, Drareni A, Latouche L, Deloule E and Vidal P (2003) U–Pb zircon (TIMS and SIMS) and Sm–Nd whole-rock geochronology of the Gour Oumelalen granulitic basement, Hoggar massif, Tuareg shield, Algeria. *Journal of African Earth Sciences* **37**, 229–39.

Pin C, Kryza R, Oberc-Dziedzic T, Mazur S, Turniak K and Waldhausrová J (2007) The diversity and geodynamic significance of Late Cambrian (ca. 500 Ma) felsic anorogenic magmatism in the northern part of the Bohemian Massif: A review based on Sm-Nd isotope and geochemical data. In *The Evolution of the Rheic Ocean: From Avalonian-Cadomian Active Margin to Alleghenian-Variscan Collision* (eds U Linnemann, RD Nance, P Kraft & G Zulauf), pp. 209–229, Geological Society of America.

Puziewicz J, Mazur S and Papiewska C (1999) Petrography and origin of two-mica paragneisses and amphibolites of the Doboszowice Metamorphic Unit (Sudetes, SW Poland). *Archiwum Mineralogiczne* **52**, 35–70.

R Core Team (2021) *R: A language and environment for statistical computing*. R Foundation for Statistical Computing, Vienna, Austria. https://www.R-project.org/.

Roser BP and Korsch RJ (1986) Determination of tectonic setting of sandstone – mudstone suits using SiO2 content and K2O/Na2O ratio. *Journal of Geology* **94**, 635–50.

Schandl ES and Gorton MP (2002) Application of high field strength elements to discriminate tectonic settings in VMS environments. *Economic Geology* **97**, 629–42.

Schulmann K, Konopásek J, Janousek V, Lexa O, Lardeaux J-M, Edel J-B, Stípská P and Ulrich S (2009) An Andean type Palaeozoic convergence in the Bohemian Massif. *Comptes Rendus Geosciences* **341**, 266–86.

Shand JS (1943) *Eruptive Rocks. Their Genesis Composition. Classification, and Their Relation to Ore-Deposits with a Chapter on Meteorite*. New York: John Wiley & Sons, 444p.

Sláma J, Dunkley DJ, Kachlík V and Kusiak MA (2008b) Transition from island-arc to passive setting on the continental margin of Gondwana: U–Pb zircon dating of Neoproterozoic metaconglomerates from the SE margin of the Teplá–Barrandian Unit, Bohemian Massif. *Tectonophysics* **461**, 44–59.

Sláma J, Košler J, Condon DJ, Crowley JL, Gerdes A, Hanchar JM, Horstwood MSA, Morris GA, Nasdala L, Norberg N, Schaltegger U, Schoene B, Tubrett MN and Whitehouse MJ (2008a) Plešovice zircon — a new natural reference material for U–Pb and Hf isotopic microanalysis. *Chemical Geology* **249**, 1–35.

Śliwiński M, Jastrzębski M and Sláma J (2022) Detrital zircon analysis of metasedimentary rocks of the Staré Mìsto Belt, Sudetes: implications for the provenance and evolution of the eastern margin of the Saxothuringian terrane, NE Bohemian Massif. *Geological Quarterly* **66**, 1–21.

Soejono I, Machek M, Sláma J, Janoušek V and Kohút M (2020) Cambro-Ordovician anatexis and magmatic recycling at the thinned Gondwana margin: new constraints from the Kouřim Unit, Bohemian Massif. *Journal of the Geological Society* **177**, 325–41.

Soejono I, Schulmann K, Sláma J, Hrdličková K, Hanžl P, Konopásek J, Collett S and Míková J (2022) Pre-collisional crustal evolution of the European Variscan periphery: constraints from detrital zircon U–Pb ages

https://doi.org/10.1017/S0016756823000523 Published online by Cambridge University Press

and Hf isotopic record in the Precambrian metasedimentary basement of the Brunovistulian Domain. *Precambrian Research* **372**, 106606.

Soejono I, Žáčková E, Janoušek V, Machek M and Košler J (2010) Vestige of an Early Cambrian incipient oceanic crust incorporated in the Variscan orogen: Letovice Complex, Bohemian Massif. *Journal of the Geological Society* **167**, 1113–30.

Spandler C, Hermann J and Rubatto D (2004) Exsolution of thortveitite, yttrialite, and xenotime during low-temperature recrystallization of zircon from New Caledonia, and their significance for trace element incorporation in zircon. *American Mineralogist* **89**, 1795–806.

Strachan RA, Linnemann U, Jeffries T, Drost K and Ulrich J (2014) Armorican provenance for the mélange deposits below the Lizard ophiolite (Cornwall, UK): evidence for Devonian obduction of Cadomian and Lower Palaeozoic crust onto the southern margin of Avalonia. *International Journal of Earth Sciences* **103**, 1359–83.

Sun SS and McDonough WF (1989) Chemical and isotopic systematics of oceanic basalts; implications for mantle composition and processes. *Magmatism in the ocean basins* **42**, 313–45.

Sylvester PJ (1998) Post-Collisional strongly peraluminous granites. *Lithos* **45**, 29–44.

Szczepanski J, Anczkiewicz R and Marciniak D (2022) P-T conditions and chronology of the Variscan collision in the easternmost part of the Saxothuringian crust (Bohemian Massif, Fore-Sudetic Block, Poland). *Mineralogia – Special Papers* **50**, 88.

Szczepański J and Goleń M (2022) Tracing exhumation record in high-pressure micaschists: a new tectonometamorphic model of the evolution of the eastern part of the Fore Sudetic Block, Kamieniec Metamorphic Belt, NE Bohemian Massif, SW Poland. *Geochemistry* **82**, 125859.

Szczepański J and Ilnicki S (2014) From Cadomian arc to Ordovician passive margin: geochemical records preserved in metasedimentary successions of the Orlica-Śnieżnik Dome in SW Poland. *International Journal of Earth Sciences* **103**, 627–47.

Szczepański J and Marciniak D (2018) PT history preserved in mica schists from the Doboszowice Metamorphic Complex (Bohemian Massif, Fore-Sudetic Block). *Mineralogia – Special Papers* **48**, 86.

Szczepański J, Turniak K, Anczkiewicz R and Gleichner P (2020) Dating of detrital zircons and tracing the provenance of quartzites from the Bystrzyckie Mts: implications for the tectonic setting of the Early Palaeozoic sedimentary basin developed on the Gondwana margin. *International Journal of Earth Sciences* **109**, 2049–79.

Szczepański J, Zhong X, Dąbrowski M, Wang H and Goleń M (2022) Combined phase diagram modelling and quartz-in-garnet barometry of *HP* metapelites from the Kamieniec Metamorphic Belt (NE Bohemian Massif). *Journal of Metamorphic Geology* **40**, 3–37.

Tabaud AS, Štípská P, Mazur S, Schulmann K, Míková J, Wong J and Sun M (2021) Evolution of a Cambro-Ordovician active margin in northern Gondwana: geochemical and zircon geochronological evidence from the Góry Sowie metasedimentary rocks, Poland. *Gondwana Research* **90**, 1–26.

Taylor SR and McLennan SM (1985) *The Continental Crust; Its Composition and Evolution; An Examination of the Geochemical Record Preserved in Sedimentary Rocks*. Oxford: Blackwell Science Publications, 312p.

Taylor SR and McLennan SM (1995) The geochemical evolution of the continental crust. *Reviews of Geophysics* **33**, 241–65.

Tichomirowa M, Berger H-J, Koch EA, Belyatski BV, Götze J, Kempe U, Nasdala L and Schaltegger U (2001) Zircon ages of high-grade gneisses in the Eastern Erzgebirge (Central European Variscides)—constraints on origin of the rocks and Precambrian to Ordovician magmatic events in the Variscan foldbelt. *Lithos* **56**, 303–32.

Torsvik TH (2017) *Earth History and Palaeogeography: Trond H. Torsvik, University of Oslo, and L. Robin M. Cocks*. London: The Natural History Museum.

Turniak K, Mazur S and Wysoczański R (2000) SHRIMP zircon geochronology and geochemistry of the Orlica-Śnieżnik gneisses (Variscan belt of Central Europe) and their tectonic implications. *Geodinamica Acta* **13**, 293–312.

Valverde-Vaquero P, Dörr W, Belka Z, Franke W, Wiszniewska J and Schastok J (2000) U–Pb single-grain dating of detrital zircon in the Cambrian of central Poland: implications for Gondwana versus Baltica provenance studies. *Earth and Planetary Science Letters* **184**, 225–40.

Verma SP and Armstrong-Altrin JS (2013) New multi-dimensional diagrams for tectonic discrimination of siliciclastic sediments and their application to Precambrian basins. *Chemical Geology* **355**, 117–33.

Verma SP, Pandarinath K, Verma SK and Agrawal S (2013) Fifteen new discriminant-function-based multi-dimensional robust diagrams for acid rocks and their application to Precambrian rocks. *Lithos* **168–169**, 113–23.

Whitney DL and Evans BW (2010) Abbreviations for names of rock-forming minerals. *American Mineralogist* **95**, 185–7.

Wiedenbeck M, Allé P, Corfu F, Griffin WL, Meier M, Oberli F, Quadt AV, Roddick JC and Spiegel W (1995) Three natural zircon standards for U-TH-PB, LU-HF, trace element and ree analyses. *Geostandards and Geoanalytical Research* **19**, 1–23.

Wimmenauer W (1984) Das pravariskische Kristallin im Schwarzwald. *Fortschritt der Mineralogie* **62**, 69–86.

Winchester JA and Floyd PA (1977) Geochemical discrimination of different magma series and their differentiation products using immobile elements. *Chemical Geology* **20**, 325–43.

Winchester JA, Pharaoh TC, Verniers J, Ioane D and Seghedi A (2006) Palaeozoic accretion of Gondwana-derived terranes to the East European Craton: recognition of detached terrane fragments dispersed after collision with promontories. *Geological Society, London, Memoirs* **32**, 323–32.

Žáčková E, Konopásek J, Košler J and Jeřábek P (2010) Detrital zircon populations in quartzites of the Krkonoše–Jizera Massif: implications for pre-collisional history of the Saxothuringian Domain in the Bohemian Massif. *Geological Magazine* **149**, 443–58.

Žák J, Kraft P and Hajná J (2013) Timing, styles, and kinematics of Cambro–Ordovician extension in the Teplá–Barrandian Unit, Bohemian Massif, and its bearing on the opening of the Rheic Ocean. *International Journal of Earth Sciences* **102**, 415–33.

Žák J and Sláma J (2018) How far did the Cadomian 'terranes' travel from Gondwana during early Palaeozoic? A critical reappraisal based on detrital zircon geochronology. *International Geology Review* **60**, 319–38.

Žák J, Sláma J, Syahputra R and Nance RD (2023) Dynamics of Cambro–Ordovician rifting of the northern margin of Gondwana as revealed by the timing of subsidence and magmatism in rift-related basins. *International Geology Review*, 1–24.

Żelaźniewicz A, Dörr W, Bylina P, Franke W, Haack U, Heinisch H, Schastok J, Grandmontagne K and Kulicki C (2004) The eastern continuation of the Cadomian orogen: U–Pb zircon evidence from Saxo-Thuringian granitoids in south-western Poland and the northern Czech Republic. *International Journal of Earth Sciences* **93**, 773–81.

Zieger J, Linnemann U, Hofmann M, Gärtner A, Marko L and Gerdes A (2018) A new U–Pb LA-ICP-MS age of the Rumburk granite (Lausitz Block, Saxo-Thuringian Zone): constraints for a magmatic event in the Upper Cambrian. *International Journal of Earth Sciences* **107**, 933–53.